A power management system for isolated operation of microbial fuel cells with voltage protection

by

Alireza KAZEMMANESH

THESIS PRESENTED TO ÉCOLE DE TECHNOLOGIE SUPÉRIEURE
IN PARTIAL FULFILLEMENT FOR A MASTER DEGREE
WITH THESIS IN ELECTRICAL ENGINEERING
M.A.SC.

MONTREAL, DECEMBER 16, 2022

ÉCOLE DE TECHNOLOGIE SUPÉRIEURE
UNIVERSITÉ DU QUÉBEC

BOARD OF EXAMINERS

THIS THESIS HAS BEEN EVALUATED

BY THE FOLLOWING BOARD OF EXAMINERS

Mr. Ghyslain Gagnon, Thesis Supervisor
Department of Electrical Engineering, École de technologie supérieure

Ms. Lyne Woodward, Thesis Co-supervisor
Department of Electrical Engineering, École de technologie supérieure

Mr. Ricardo Izquierdo, President of the Board of Examiners
Department of Electrical Engineering, École de technologie supérieure

Ms. Rachel Bouserhal, Member of the jury
Department of Electrical Engineering, École de technologie supérieure

THIS THESIS WAS PRENSENTED AND DEFENDED

IN THE PRESENCE OF A BOARD OF EXAMINERS AND PUBLIC

ON DECEMBER 2, 2022

AT ÉCOLE DE TECHNOLOGIE SUPÉRIEURE

ACKNOWLEDGMENT

Foremost, I would like to express my sincerest gratitude to my supervisor, Professor Ghyslain Gagnon, for providing me a chance to work at École de technologie supérieure and made this work possible through his guidance, advice, patience, enthusiasm, and immense knowledge.

I would also like to give my deepest thanks to my co-supervisor, Professor Lyne Woodward, for her guidance, encouragement, insights, and patience throughout the research period. She has taught me to present the research works and reports as clearly as possible. Her support and intelligence carried me through the stage of writing my thesis.

I would like to thank Professors Ricardo Izquierdo and Rachel Bouserhal for taking the time to assess this thesis.

I am incredibly grateful to my parents for their unconditional love, prayers, caring, and sacrifices for educating and preparing me for my future. I am very thankful to my sister for her understanding, infinite kindness, and love toward me. Her Continued support made this research possible.

My special thanks to my friend and colleague in the lab, Mr. Amirreza Azimi, for sharing his knowledge and experience. He provided a positive atmosphere and joyful moments during the long days and nights in the lab. I would also like to thank him for his friendship and empathy toward me. I would like to thank my girlfriend, Victoria, for her silent support and countless sacrifices during my research.

Système de gestion d'alimentation pour le fonctionnement isolé de piles à combustible microbiennes avec protection de tension

Alireza KAZEMIMANESH

RÉSUMÉ

Les sources d'énergie renouvelables se développent rapidement dans le monde. En 2020, elles représentaient 29% de toute l'énergie électrique produite. La pile à combustible microbienne (PCM) est une source d'énergie à fort potentiel dans cette catégorie. Elle aide à éliminer les contaminants environnementaux tels que ceux présents dans les eaux usées, à réduire le dioxyde de carbone dans l'atmosphère et à convertir les substrats organiques en électricité par une réaction bioélectrochimique.

Cependant, en raison d'une faible densité de puissance, une seule PCM ne suffit pas pour alimenter la plupart des applications électroniques courantes. Une solution pour augmenter la puissance consiste à utiliser plusieurs PCM et à les connecter en parallèle ou en série. Toutefois, ces types de configurations de circuit peuvent engendrer une perte générale d'efficacité de puissance dû à l'instabilité et l'imprévisibilité des PCM.

Cette étude vise à concevoir un système de gestion de l'alimentation (PMS) conçu pour récupérer le maximum d'énergie de chaque PCM dans la pile. Le PMS contrôle la connexion et la déconnexion des PCM de manière à ce que chaque PCM fonctionne indépendamment. Par conséquent, en cas de déconnexion d'une PCM en raison d'une défaillance, le processus de récupération d'énergie à partir des autres PCM se poursuit sans interruption. Le PMS est développé pour tenir compte de la limitation biochimique des micro-organismes afin d'étendre leur durée de vie. Ceci a été accompli en utilisant un algorithme de protection de la santé du PCM. Cet algorithme empêche une faible PCM de participer au processus de récupération d'énergie. Des techniques de commande telles que le contrôle de l'hystérésis et le suivi du point de puissance maximale (MPPT) sont mises en œuvre pour obtenir ces contributions.

Un convertisseur CC-CC à haut rendement est sélectionné comme convertisseur élévateur principal pour augmenter la sortie de tension à un niveau désiré. Le contrôleur à mode glissant (SMC), qui est une technique de régulation de tension (VReg), est appliqué au contrôle de la commutation du convertisseur. Le contrôleur proposé maintient la tension de sortie du convertisseur dans des limites appropriées, quelque soient les volatilités de la tension d'entrée causées par la non-linéarité du système. Une référence de tension à deux niveaux a été appliquée à la technique de régulation de tension pour obtenir un niveau de tension et de puissance plus élevé à la charge.

Une procédure de test a été élaborée pour évaluer les performances du PMS en fonction des caractéristiques réelles des PCM. Pour ce faire, de nombreuses expériences en laboratoire sur quatre PCM réelles ont été menées et les données extraites ont été classées en trois points de référence. Chaque benchmark reproduit les caractéristiques électriques des PCM basés sur un modèle en fonction de leur large gamme de conditions ambiantes et opérationnelles. Ces repères ont été appliqués à une approche comparable d'une étude précédente et ses avantages et inconvénients ont été comparés au PMS proposé.

La puissance de charge moyenne ($Pload_{ave}$) de 5.16 mW a été obtenue en utilisant le VReg à deux niveaux, soit 3.44 fois de plus qu'en utilisant le VReg à un niveau (1.5 mW). Selon les

résultats de la comparaison des PMS, le PMS proposé pourrait alimenter avec succès la charge résistive sans interruption alors que de multiples perturbations de l'alimentation de la charge ont été observées dans une étude précédente. Par conséquent, il a été rapporté que le PMS proposé avait une $Pload_{ave}$ supérieure de 41% dans cette comparaison en cas de défaillance multiple de PCM.
Une amélioration supplémentaire de cette étude peut consister à inclure un circuit de démarrage au convertisseur pour un fonctionnement autonome du système, une caractéristique nécessaire pour l'utilisation du PCM dans des zones éloignées.

Mots-clés : sources d’énergie renouvelable, pile à combustible microbienne (PCM), système de gestion de l'énergie (PMS), suivi du point de puissance maximale (MPPT), commande en mode glissant (SMC)

A power management system for isolated operation of microbial fuel cells with voltage protection

Alireza KAZEMIMANESH

ABSTRACT

Renewable energy sources are growing rapidly in the world. In 2020, they made up 29% of all the electric power generated. Microbial fuel cell (MFC) is a high-potential energy source in this category. It helps remove environmental contaminants such those in wastewater, decrease carbon dioxide in the atmosphere, and convert organic substrates to electricity through a bioelectrochemical reaction.

However, due to its low power density, a single MFC cannot power most of common electronic applications. One solution to increase the power is to use multiple MFCs and connect them in parallel or series. However, these types of circuit configurations can result in overall lower power efficiency due to the unpredictable and unstable nature of MFCs.

This study aims to design a power management system (PMS) for harvesting the maximum energy from the MFCs in the stack. The PMS controls the connection and disconnection of the MFCs such that each MFC operates independently. Consequently, should there be an MFC failure leading to unwanted MFC disconnection, the energy harvesting process from the other MFC(s) continues without interruption. The PMS is developed to consider the biochemical limitation of microorganism in order to expand their lifetime. This was accomplished by employing an MFC health protection algorithm. This algorithm prevents the weak MFC to participate in the energy harvesting process. Control techniques such as hysteresis control and the maximum power point tracking (MPPT) are executed to achieve these contributions.

A high-efficiency DC-DC converter is selected as the back-end upconverter to boost the output voltage to a desirable level. The sliding mode controller (SMC), which is a voltage regulation (VReg) technique, is applied to the control of converter switching. The proposed controller maintains the output voltage of the converter within acceptable limits, regardless of the input voltage volatilities caused by the system nonlinearity. A two-level voltage reference was applied to the VReg technic to obtain higher levels of voltage and power at the load.

A testing procedure was constructed to evaluate the PMS performance based on the real-world MFCs characteristics. To make this happen, numerous lab experiments on four real MFCs were conducted and the extracted data was classified into three benchmarks. Each benchmark replicates the electrical characteristics of model-based MFCs according to their wide range of ambient and operational conditions. These benchmarks were applied to a comparable approach from a previous study and its pros and cons were compared to the proposed PMS.

The average load power ($P_{load_{ave}}$) of 5.16 mW was obtained using the two-level VReg, which is 3.44 times more than utilizing the single-level VReg (1.5 mW). According to the PMS's comparison results, the proposed PMS could successfully power the resistive load without interruption while multiple load power disruptions were observed in the previous study. Hence, the proposed PMS was reported to have a 41% higher $P_{load_{ave}}$ in this comparison in the case of multiple MFC failure.

Further improvement upon this study can be including a start-up circuit to the converter for autonomous operation of the system, a necessary feature for using MFCs in remote areas.

Keywords: renewable energy sources, microbial fuel cell (MFC), power management system (PMS), maximum power point tracking (MPPT), sliding mode control (SMC)

TABLE OF CONTENTS

Page

LIST OF TABLES

Page

LIST OF FIGURES

Page

LIST OF ABREVIATIONS

ACD	Alternate Charging and Discharging
ANN	Artificial Neural Network
BES	Bioelectrochemical System
COD	Chemical Oxygen Demand
CSTR	Continued Stirred Tank Reactors
IEH	Intermittent Energy Harvesting
MFC	Microbial Fuel Cell
MGGP	Multi-gene Genetic Programming
MMSE	Minimum Mean-Squared Error
MPPT	Maximum Power Point Tracking
MU	Multiunit Optimization
OCV	Open Circuit Voltage
PEM	Power Exchange Membrane
PI	Proportional-Integral
PMS	Power Management System
PWM	Pulse Width Modulation
SMC	Sliding Mode Control
SMFC	Sediment Microbial Fuel Cell
SPST	Single Pole Single throw
SVM	Support Vector Regression
TDS	Total Dissolved Solid

LIST OF SYMBOLES

T_{d_max}	Maximum discharge time of C_i
C_i	Capacitor of the MFC_i
VcL_i	Lower threshold for the C_i voltage
VcH_i	Higher threshold for the C_i voltage
V_{Low}	lower limit of VcL_i
V_{High}	Higher limit of VcL_i
$Pload_{ave}$	Average load power
$PMFC_{ave}$	Average power obtained from the stack of MFCs
$P_{IN\text{-}ave}$	Average input power of DC-DC boost converter
S_M	Switch between MFC_i and C_i
S_S	Switch between C_i and supercapacitor
SC	Supercapacitor of the circuit
S_B	DC-DC boost Converter switch
R_1, R_2, C_{int}	Internal Parameters of MFC based on its equivalent electrical model
λ	Interval between voltage measurements of online V_{OC} estimation
M	Offset between $V_{OC}/2$ and V_H or V_L which is a percentage of V_{OC}
α	The incrementally increases of the V_CH_i of the waiting C_i to discharge into SC
α_{max}	Maximum increase of VcH_i in a few increments
σ	A linear combination of the state variables called sliding function in SMC
KI, KV	The sliding coefficient that adjusts the SMC's response speed

D	Duty cycle of the boost converter
V_{in}	Input voltage of the boost converter
V_{out}	Output voltage of the boost converter
C_O	Output capacitor of the boost converter
R_L	Resistive load connected to the system circuit
L	Dc-Dc converter Inductor
f	Switching frequency of the boost converter

INTRODUCTION

Biomass energy is a type of renewable energy produced by living or once-living organisms. Wood, plants, and waste are the most common biomass materials used for generating energy. This energy can be used in multiple ways such as heat through burning, electricity through energy conversion and biofuel through processing. Among them, electricity through energy conversion from biomass attracted more attention due to its wide aspects of usage in life and industry. As an approach for biomass conversion to electricity, microbial fuel cell (MFC) has been highly regarded for its high theoretical energy efficiency and moderate operating condition requirements (Mathuriya & Yakhmi, 2016).

MFC is a promising bioelectrochemical emerging source that employs the catalytic activity of microorganisms to produce electricity by converting the chemical energy of the organic compounds (Moradian et al., 2021). MFCs have a unique application in remote sensing for hard-to-reach areas with rich organic material, such as sewage water and ocean floors (Donovan et al., 2008), where the usage and replacement of batteries could be costly and even unfeasible in some circumstances.

In spite of these opportunities, one of the main limitations of energy harvesting from MFC technology is the low output power provided by a single MFC. The power levels can typically vary from microwatts to a few milliwatts per litre with an open circuit voltage (OCV) of 0.4 – 0.8 V (Khaled et al., 2014). As a result, most electrical loads cannot be directly powered by an MFC because of its low output parameters. For instance, pHTemp2000 and Level1000 are wireless sensors with a power consumption between of 1 to 2 mW and a supply voltage near 3 V which is impossible to power them directly by an MFC. The pHTemp2000 sensor measures the temperature and water pH and the Level1000 sensor records the water level (Khaled et al., 2016).

The low power density of the MFC has been the subject of several studies in the literature, which can mainly be divided into three categories: biological, architectural, and electrical aspects. The first category is focused on improving the design of the reactor by altering the

shape, size and the materials to observe these changes and their effects on the power density of the MFC. The second category investigates the effects of utilizing various substrates, different microorganisms in mixed and single culture, concentration, etc. Contrary to the first two categories, the third category does not apply changes to the MFC's structure such as biological parameters or the reactor design. The studies in this category treat the MFC as an electrical source and try to maximize the energy generated by the MFC and delivering this energy to the load with the lowest loss possible.

In this category, a promising approach is utilizing power management systems (PMS) in order to maximize the power conversion efficiency of the MFC. Several studies tried to improve the efficiency of energy harvesting from a single MFC system by implementing different PMSs (Donovan et al., 2008). Yet, a single MFC cannot produce enough power to supply a typical electronic load continuously. As a solution, multiple MFCs connected in series or parallel can provide sufficient output power with a practical output voltage level. However, Voltage reversal is one of the drawbacks for MFCs in series (Khaled et al., 2014). The voltage reversal can potentially reduce the overall voltage and efficiency which contradicts the main goal of using MFCs in the stack, maximizing energy harvesting (An et al., 2019). In addition, it can drastically damage bio-anode by deforming the biofilms, which is a serious threat for the health of the MFC and its lifetime (Li et al., 2017). The parallel connection of MFCs is recommended as the solution of voltage reversal problem in some studies (Liu et al., 2008). However, the reversal current in parallel connection of MFCs reduces the power density of MFCs in the stack (Wu et al., 2016).

Another challenge is boosting and regulating the output voltage to meet the electrical load’s requirements. As the MFCs are stacked, differences in the voltage of each MFC can result in the voltage volatility at the converter’s input (Khaled et al., 2014). In this case, the regulated converter's output voltage can experience disturbances or even interruptions, which might induce load damage. Furthermore, incompatible voltage regulation methods applied to nonlinear systems such as MFCs can result in slow responses to the converter’s input voltage volatilities. Consequently, it can impede the PMS to harvest maximum energy from the stack.

Therefore, this study has the following objectives:

1. Building a new PMS for a stack of MFCs that enhances MFCs' maximum energy harvesting and minimizes the total power losses while ensuring MFCs' viability and output power continuity;
2. Obtaining a smooth regulated voltage at the load immune to the volatilities;
3. Developing a procedure to quantify the performance of PMSs and test its efficacy in various conditions, which will consequently make comparisons between different PMS approaches possible.

In this study, to address the stated challenges, a novel PMS was proposed alongside an effective output voltage regulation method. The MFCs are connected to the system through the PMS without being connected in series or parallel, avoiding the voltage, and current reversal phenomenon. A testing procedure, based on the MFCs' real-world conditions, was constructed to quantify the effectiveness of the PMS through simulations.

The contributions of this study are listed below:

1. A PMS approach is proposed that achieves maximum power output while:
    a) Ensuring that MFCs' voltage do not drop below a certain threshold to prevent power over-depletion from the weak MFC(s), causing damage to the biofilm;
    b) Continuously powering the load in case of MFC failure.
2. A two-level voltage regulation approach has been utilized which employs sliding mode control (SMC) in the control of boost converter switching. This approach successfully regulates voltage despite boost converter input voltage volatility;
3. A testing framework was constructed to quantify the efficacy of the PMS under predefined real-world scenarios. Since these scenarios show a wide range of possible ambient and internal MFC conditions and are repeatable in the simulation, the collected data (i.e., mean output power, output voltage, efficiency, etc.) of each PMS can be a reliable measure of that PMS's performance. This data can be used to compare different PMSs from an objective perspective.

The outcome of this study can have tangible effect on real-world applications like small electronic applications. As an instance, a small robot running on MFCs (like waste gathering robots) can utilize this PMS to do more energy intensive tasks given the higher power at its disposal, can function for longer thanks to the PMS health protection feature, and perform the tasks with minimal interruptions.

Thesis outline

The following brief provides a better understanding of the thesis overview. *CHAPTER 1* presents the principle of operation of an MFC and some of its important applications. Based on two classifications, several MFC models are discussed in more details. Next, the PMS including its techniques such as maximum power point tracking (MPPT) and power management system (PWM), as well as its configurations were described. Finally, the DC-DC boost converter topologies and voltage regulation methods were analyzed according to their cons and pros. In *CHAPTER 2,* the contributions of the proposed study such as the PMS algorithm and the voltage regulation technique are explained. Finally, *CHAPTER 3* is divided into two main parts. The first part includes the data acquisition processes from laboratory experiments to sorting the data, as well as conducting the simulations in MATLAB Simulink. Then, the second part showcases the results and analyses from the proposed and previous studies.

CHAPTER 1

LITERATURE REVIEW

Our predecessors depended on extremely basic types of energy such as human and animal muscle, as well as the combustion of biomass like wood and crops. However, after the industrial revolution, the discovery of fossil fuels as a new source of energy opened the door to technological, economical and societal enhancements. Coil, oil, and gas like fossil fuels have played a major role in our energy systems during the last centuries.

Nevertheless, using fossil fuels has had several negative repercussions, including climate change, air and water pollution, which are deemed to be responsible for millions of early deaths annually. In order to understand how the use of fossil fuels has had an increasing impact on the growth of our planet's atmospheric carbon dioxide, it would be helpful to take a closer look at the graph provided by the NASA climate change website (Figure 1.1). It is shown that the CO_2 concentrations in the atmosphere peaked on May 9th, 2013, at 400 parts per million (ppm). For the first time in human history, we have reached this significant milestone. These concerns have facilitated the establishment of alternate energy sources, such as nuclear-and other widely accessible low-carbon renewable energies including fuel cells (Hannah Ritchie, 2020).

Water pollution, on the other hand, requires a considerable deal of attention owing to the complexities of pollutant retention in wastewater (Li et al., 2014). The conventional wastewater treatment technologies such as aerobic activated sludge treatment, ion exchange, chemical precipitation, and adsorption (Wang et al., 2003) demand high energy and cost for the treatment process. However, bio-electrochemical systems are seen as a viable alternative for both removing wastewater pollutants and generating power through microbial metabolisms (Gude, 2016).

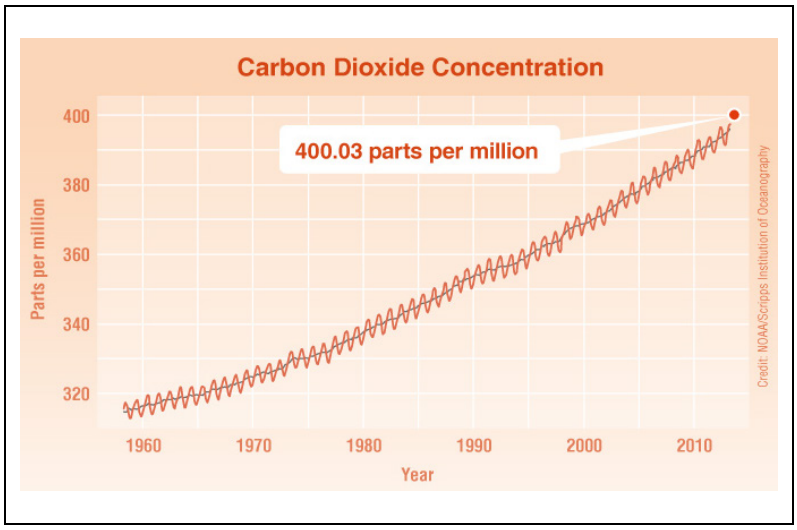

Figure 1.1 Carbon dioxide concentration graph starting 1960 which reached 400 PPM in 2013
Taken from NASA (2013)

1.1 Microbial fuel cell (MFC)

Employing metallic catalysts in conventional fuel cells to facilitate the oxidation fuels such as hydrogen and low molecular weight alcohols is considered as advanced technology. Nonetheless, the expenses involved using this technology are still unaffordable, which would limit their widespread use despite their strong scientific background (Trapero et al., 2017). It wasn't until the late 90s that Microbial Fuel Cells (MFCs) emerged as a viable alternative. Their beginnings trace all the way back to 1912, when Potter (1911) highlighted the concept of generating power from biological degradation of organic matter. However, poor results hindered further studies until the previous two decades particularly, when the demand for energy sources with low CO2 emissions has increased substantially (Trapero et al., 2017). The inexpensive cost of organic compounds (Pant et al., 2010), safe exhibition, and quiet performance (Rabaey & Verstraete, 2005) have made the MFC an intriguing renewable energy alternative for further investigation. Another advantage of the MFC technology is its high conversion efficiency rate. The MFC can gather up to 90 percent of electrons from the bacterial electron transportation system, compared to approximately 50 percent for a conventional fossil power planet (Mathuriya & Yakhmi, 2016).

1.2 Design and operating principles of an MFC

Various configurations are available for MFCs. The operating principle of a dual chamber MFC, which is widely used, is shown in Figure 1.2. The MFC is a bioelectrochemical device consisting of an anodic and a cathodic chamber that are separated by a proton exchange membrane (PEM). The anode chamber is anaerobic which includes an electrode, microorganisms and an anolyte. The cathode chamber can be aerobic or anaerobic (depends on its architecture) and includes an electrode, an electron acceptor and a catalyst. In the anode chamber, microorganisms are utilized as biocatalysts to oxidize the substrate. Through an electrical connection, electrons are transmitted to the anodic (electrode) surface and subsequently directed to the cathode chamber (Yong et al., 2014). Electrons combine with protons and oxygen to generate water in the cathode. Typically, a catalyst, like as platinum, is employed to catalyze the reduction reaction in the cathode (Kumar et al., 2016).

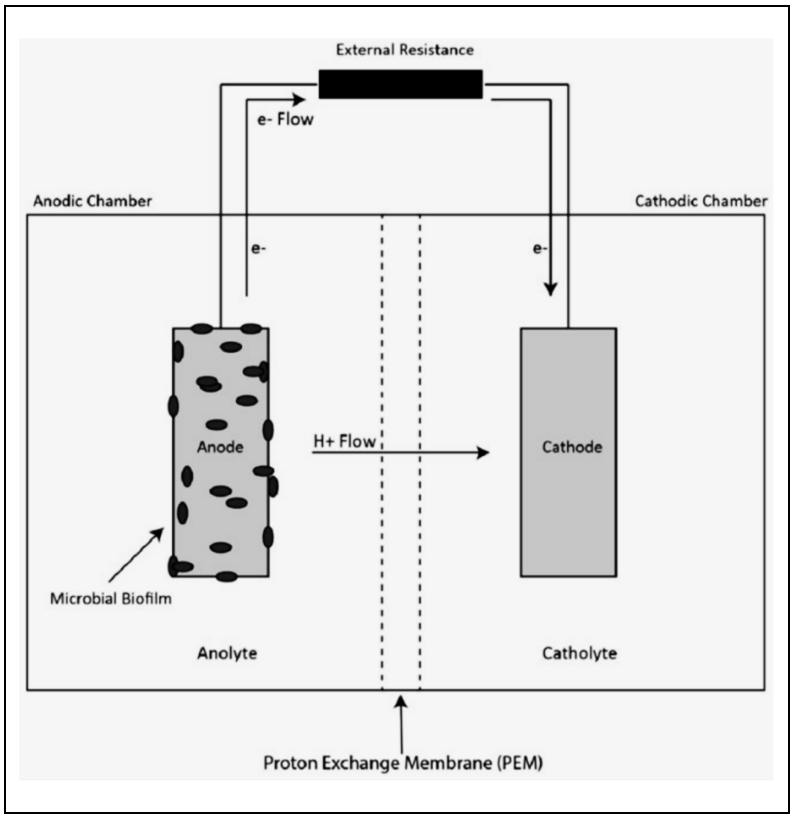

Figure 1.2 General structure of a dual chamber MFC
Taken from Breheny et al. (2019)

1.2.1 Anode

The anodic chamber contains organic substances that microorganisms digest for energy production and growth. In other words, organic substances serve as the MFC's fuel, and they are degraded by the microorganisms through oxidation of biodegradable substrates and production of protons, electrons, and carbon dioxide. Next, cytochromes or redox-active proteins transport the generated electron to the anode's electrode surface, where it is then passed on to the cathode (Kumar et al., 2015).

The anode material must be highly electrically conductive, non-corrosive, and highly porous. Copper, graphite fiber, carbon cloth, carbon paper, carbon felt, and carbon foam can be used as the anode conductive material with an average linear resistance of 1.2 Ω/cm. The conductive polymer sheet with a linear resistance of 130 Ω/cm can be also used as the anode conductive material (Logan, 2008). At the point where the electrons are produced by the bacteria and travel through the anodic material to reach the collecting point (a copper wire shown in Figure 2), few ohms from the anode material may significantly diminish the power. In addition, the bacteria need to be attached properly to the material in order to obtain a good electrical connection (Logan et al., 2006).

Flowing water through the anode material is one technique for increasing power. Cheng et al. (2006) reported that by lowering the electrode spacing from 2 to 1 cm and enabling the water to flow through the carbon cloth toward the anode, power densities in an air cathode MFC improved by 90%, from 811 to 1,540 mW/m2. It was thought that the increase was due to reduced oxygen diffusion into the anode chamber, but advective flow may have also aided in proton transportation toward the cathode.

Park and Zeikus (2003) employed Mn (IV) graphite and covalently linked neutral red (NR-graphite) felt as the anode electrodes to facilitate the electron transportation to the anode and to improve its performance. It was reported that Mn (IV) and NR have superior performance than normal graphite electrodes while Mn (IV) performs as the best. Furthermore,

Electrocatalytic materials including polyanilins/Pt composites help the microbial metabolite oxidation to enhance the current generation (Niessen et al., 2004).

1.2.2 Cathode

Cathode chamber is required to close the circuit and complete the cycle of electricity generation. It includes a high-potential electron acceptor. Since microorganisms are highly vulnerable to toxic effects, it is essential to choose a sustainable electron acceptor to preserve their community and to maximize power density. Ferricyanide and oxygen are both effective oxidizers and electron acceptors (Ucar et al., 2017). In one experiment (Oh et al., 2004), by substituting ferricyanide for dissolved oxygen, the maximum power is increased by 50-80%. This outcome was essentially the result of enhanced mass transfer efficiencies and a greater cathode potential of ferricyanide than that of dissolved oxygen. However, several concerns would restrict the use of ferricyanide to mainly laboratory studies. For instance, in terms of cost-effectivity, ferricyanide is not an economical choice. Also, it needs to be chemically regenerated, therefore it is not sustainable (Flimban et al., 2019).

The aqueous cathode is used in most two-chamber MFCs, with the water being bubbled with air to give dissolved oxygen to the electrodes. However, in single chamber MFCs (air cathode MFC), the cathode can be exposed directly to the oxygen regardless of the presence or absence of the membrane (Liu & Logan, 2004). Oxygen is an outstanding example of an electron acceptor considering the wide availability at no cost, lack of toxicity, high oxidation potential, and absence of chemical waste (water is the sole byproduct), which facilitates the operation of MFCs. The electrons reaching the cathode interact with protons diffused from the anode via a separator and oxygen received from the air. As a result, the final product obtained is water (Kim et al., 2002).

1.2.3 Membrane

Anode and cathode chambers are often split by a tube containing a cation exchange membrane separator (CEM). CEM is also known as the proton exchange membrane (PEM). The membrane material should enable the protons to travel across the anode and cathode chambers

while blocking the transfer of the substrate and electron acceptor (Logan et al., 2006). Nafion (Bond et al., 2002), Ultrex (Min et al., 2005) and plain salt bridge (Rabaey et al., 2003) are used as the membrane material. While the primary task defined for the membrane is to prevent water from penetrating the cathode chamber from the anode side, it also blocks oxygen diffusion in the anode chamber. Given the fact that oxygen used by bacteria on the anode side results in the Coulombic efficiency reduction. However, this is not a plausible scenario. As shown in Figure 1.3A, a typical architecture for the dual chamber MFC configurations is an H-shaped design where two bottles, representing the anode and cathode chambers, are connected via a tube as a separator. As illustrated in this figure, the membrane is clamped inside the tube. If the membrane is directly and securely clamped between the anode and cathode chambers, then the tube can be removed (Figure 1.3B).

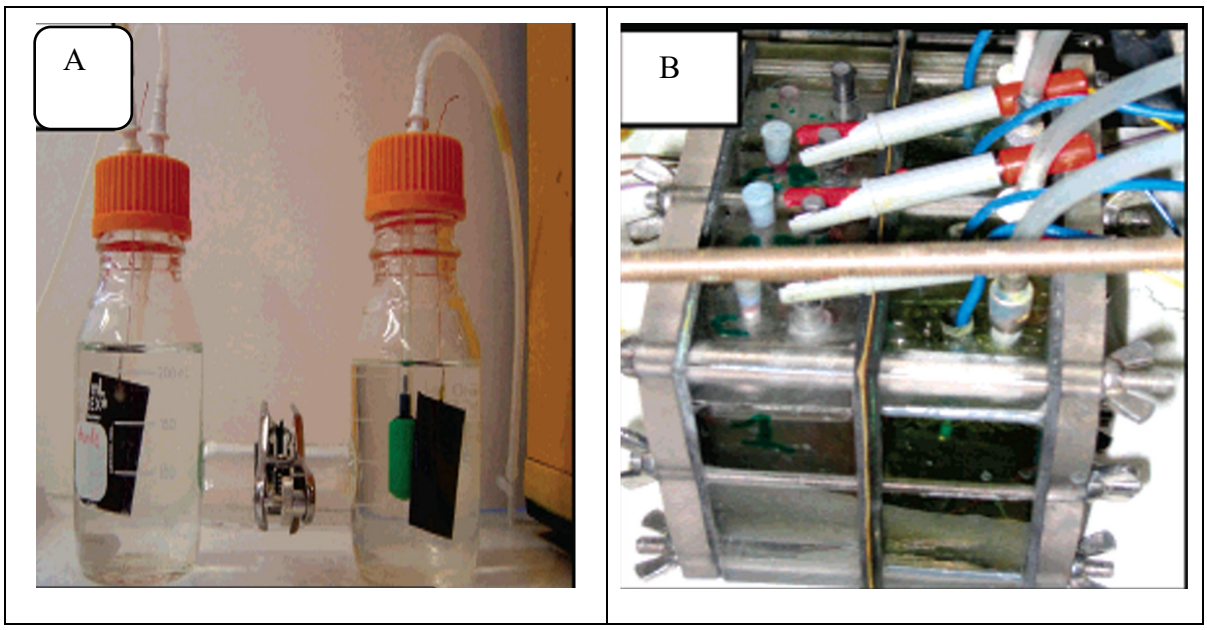

Figure 1.3 (A) H-type two chamber MFC configuration using a tube as a separator (B) four batch-type MFCs, chambers separated by the membrane but without employing a tube
Taken From Logan et al. (2006)

1.3 Microbial operational modes

Microbial cultures contain living microbial cells. In regard to chemical and biochemical reactions, these cultures are operated in three modes: batch, continuous, and semi-batch or semi-continuous modes.

1.3.1 Batch mode

In batch mode, all essential medium parts are added to the cells at the outset, and it is not possible to add or control medium components once the setup phase is completed. However, basic controls can be applied on temperature and oxygen dissolving (Lim & Shin, 2013). In batch culture mode, nutrient availability will deplete with time, resulting in reduction of overall bioelectricity production (Rabaey et al., 2004).

1.3.2 Continuous mode

In continuous mode, the MFC is continually fed with the main nutrients through one or more feed streams while the effluent stream is also extracted continuously (Lim & Shin, 2013). The continuous operation has the advantage of maintaining consistent cell density, substrate, and product concentrations. By establishing a steady state, the flow rates of the feed and effluent streams are equalized. As a result, the culture is diluted with fresh media (Rahimnejad et al., 2011).

1.3.3 Fed-batch mode

Fed-batch mode, also called semi-batch culture is defined as the biotechnological process in which at least one main nutrient is fed to the bioreactor intermittently. When microorganisms consume the nutrients, it is replenished. The primary substrate will remain within the cell until the end of the operating time. As long as the cells remain alive and prolific, the feeding procedure may be repeated. During this process, there are one or more feed streams but no effluent stream (Lim & Shin, 2013).

1.4 Applications

The MFC performance is determined by the reactor's architecture, design, and materials used for each component. Nonetheless, as MFC technology has become gradually applicable and drifted away from laboratory experiments only, a further aspect has influenced the design decisions of the MFC: application-specific requirements (Gajda et al., 2018). The main application envisaged for the MFC is electrical power generation. In general, the MFC can be used in pilot applications, sensing and treatment. Wastewater treatment (Watanabe, 2008), heavy metal recovery (Fu & Wang, 2011), bioremediation (Hong et al., 2010), dye decolorization (Cao et al., 2010), biohydrogen (Booth, 2005), robotics (Ieropoulos et al., 2012), biosensors (Kim et al., 2009), in situ power source using sediment MFC (Logan & Regan, 2006), body implanted MFC (Franks & Nevin, 2010), and a number of other applications would not be viable without ongoing efforts in the MFC architectural modification, such as the optimization of the MFC configurations, biochemical operating conditions, and selection of biocatalyst. In the following sections, some MFC applications are discussed.

1.4.1 Wastewater treatment

Population growth has contributed to the development of smaller cities and their industrialization, which is one of the primary reasons for the increase of wastewater. Existing wastewater treatments are neither sustainable technologies nor energy-efficient or cost-effective (Gude, 2016). MFC technology might be a sustainable and eco-friendly solution that may address the water sanitation demands. Wastewater is a source of enormous microorganisms that can thrive in severe environments, called Flora. Using the microbial flora for degrading the wastewater to produce energy is the motivation for developing many recent MFCs (Mathuriya & Yakhmi, 2016).

The advantages of using MFC in wastewater treatment is described as follows:

- Low energy consumption compared to activated sludge process (Watanabe, 2008);

- Simple regulated distribution system in comparison with hydrogen-based fuel cells (Mathuriya & Yakhmi, 2016);
- Treating low-strength and volatile fatty acids wastewater which are not appropriate for anaerobic digestion operations (Rittmann, 2008);
- The sludge produced by the MFC is more durable than the one produced via aerobic treatment approach (Kim et al., 2007).

Skeptics may choose not to take into consideration MFC as a viable option for the treatment of wastewater for the time being. However, throughout the course of the last decades, its potential has drawn a significant number of studies. The MFC technology is the only one now that can convert organic waste into power directly. In addition, it has the potential of supplying the energy required to treat wastewater by itself, which could significantly lower the cost of wastewater treatment systems worldwide, especially in underdeveloped countries with the lowest access to electricity.

1.4.2 Desalination

Another valuable application of MFC is for desalination in distant areas, which may be a challenging task for other bioenergy choices. Merging microbial desalination cells (MDCs) with microbial fuel cells creates a distinguished approach that produces both fresh water and power from salt water simultaneously (Borjas et al., 2017). A continuously operating upflow MDC for salt removal was proposed by Jacobson (Jacobson et al., 2011). During four months of continuous operation, a power density of 30.8 W/m3 was produced, and over 99% of the sodium chloride was removed from the salt solution (the initial salt concentration was 30 g/l). This desalinated water fulfilled the drinking water requirement for the total dissolved solids (TDS) content, which was 7.50 g/l d (salt solution volume) or 5.25 g/l d (wastewater volume). The total dissolved solids (TDS) concentration of the desalinated water was within acceptable parameters for use as drinking water. In another study, Brastad and He (2013) constructed an MDC made up of three different compartments: the anode, the cathode, and a salt compartment that was located in between the anode and cathode. The purpose of this work was to soften the hard water by generating electricity through the MDC as heavy metal contamination in

drinking water, including arsenic, cadmium, nickel, mercury, chromium, zinc, and lead, is becoming a serious public and professional health concern (Rehman et al., 2018). The hard water used in this MDC was softened with the successful rate of more than 90% from several hard water samples gathered across the United States. In a synthetic solution, the MDC was successful in removing 89%, 97%, 99% and 95% of the arsenic, copper, mercury, and nickel respectively at the testing concentrations. The excellent results approved the concept of using the MFC in water desalination and hard water softening.

1.4.3 Robotics

When discussing MFC applications in robotics, the objective is often to provide energy sustainability, meaning the robot is capable of doing its tasks while self-powering itself. While using renewable energy sources like wind, hydropower, sun, and biomass, a robot can operate autonomously in a variety of environments (Ieropoulos et al., 2012). The first attempt of utilizing organic matter in an autonomous robot was carried out by Kelly et al. (2000). The “Slugbot” project was the first attempt to harvest energy from organic foods within the robot’s environment. Wilkinson (2000) introduced the "Gastrobot" project the same year, which used sugar for the first time as its food supply and Escherichia coli bacteria to break down the food in order to generate power. The robot, which was officially named “Gastronome”, consists of three wagons with a 6-cells stacked-plate MFC located in the middle wagon as pictured in Figure 1.4. Sugar cubes, the MFC nutrient, were manually positioned into its “stomach” tank. This tank was located in the first wagon through a unique esophagus design. The electricity generated by the robot powered the NiCd rechargeable battery pack which was placed in the third wagon.

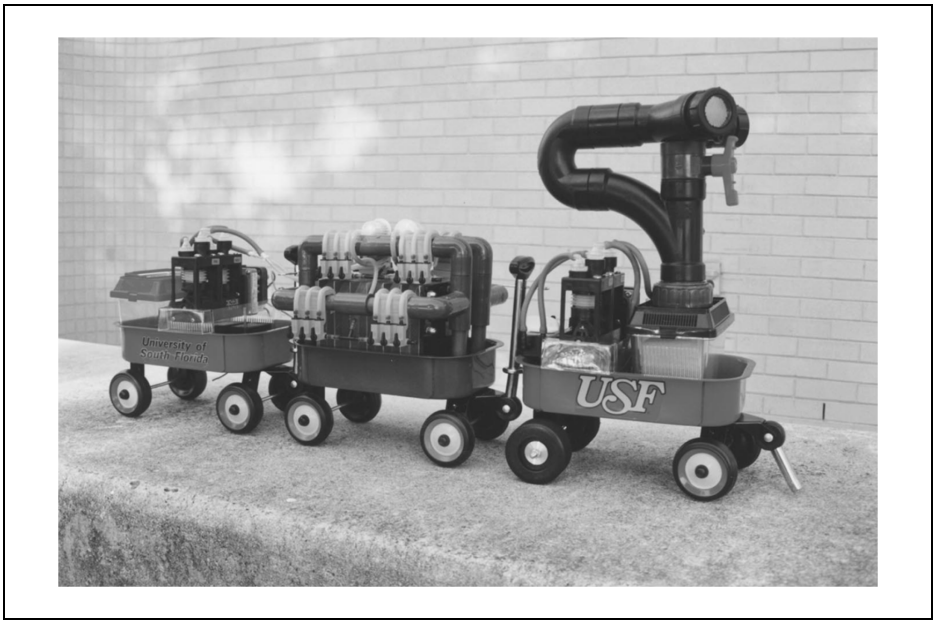

Figure 1.4 Gastronome, a robot powered by MFC
Taken from Wilkinson (2000)

In another project, the stack of eight MFCs were connected in series to generate the overall power of a robot called “EcoBot” (Ieropoulos et al., 2012). This robot was the initial iteration of a prolonged project, EcoBot I, II, and III. EcoBot-I employed Escherichia coli, the same microorganism utilized in Gastronome, to digest food and produce electrons. In the cathode chamber, ferricyanide was used, and methylene blue was applied in the anode chamber. The power generated by the MFC stack was stored in a bank of six electrolytic capacitors with 28.2 mF in total. EcoBot1’s task was to move towards the light for 3 seconds. Afterward, EcoBot-II was developed to multitask for the first time. It was equipped with an embedded system, a microcontroller for the processing, a sensor used for detecting the ambient temperature, and a communication system to wirelessly transmit the data collected by the sensor. Eight membrane-less MFCs along with the mixed sludge culture anode and an air cathode powered the robot to do its defined task for 3 seconds for 12 days intermittently. Each charge cycle took 14 minutes to restore the onboard capacitor (28.2 mF). Finally, EcoBot-III was developed based on EcoBot I and II. The MFCs’ two tires, each consisting of 24 MFCs stacked on top of one another are used to power the robot (Figure 1.5). A unique artificial digestion system including ingestion, digestion, and egestion was designed for EcoBot-III, which made it

feasible to collect food and water from the environment. Then, the food was digested and distributed throughout the MFCs with the help of mechatronic units. In the last step, the robot was capable of evacuating the produced waste from the MFCs along with its digester unit (Ieropoulos et al., 2010).

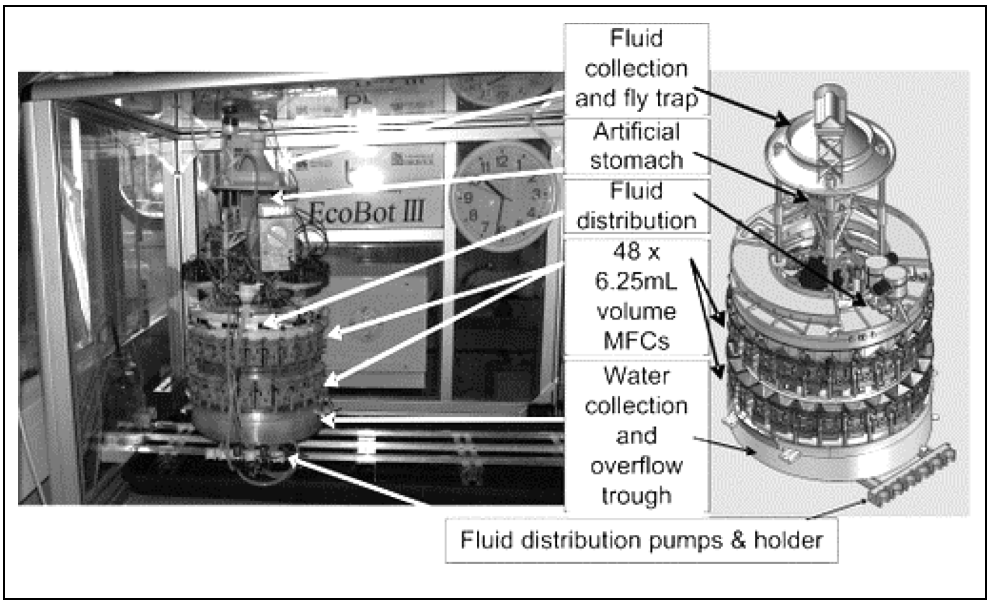

Figure 1.5 EcoBot III with an artificial digestion system with two tires of 24 MFCs (48 in total)
Taken from Ieropoulos et al. (2010)

The EcoBot series (1-3) along with Slugbot and Gastrobot are excellent examples demonstrating that autonomous robotic systems need to collect energy from the environment and incorporate it into the robots' behavioral system.

1.5 MFC modelling and model classification

A number of biochemical coupled reactions and hysteresis characteristics are responsible for the MFC's significant nonlinear behavior. The intricacy of such a system makes it difficult to optimize and control the process of direct power generation. In addition, the inoculation of bacteria and performance assessment achieved through trials and experiments are both a tedious and economically inefficient process (Xia et al., 2018). Modeling is a helpful method

for acquiring a deeper knowledge of the MFCs due to its various cost- and time-saving benefits. A model's overarching purpose is to describe the MFC's performance with reference to a set of predetermined laws and equations. The level of complexity of any given model is contingent on a variety of elements, including the chosen dimension, the assumptions made, and the degree of specificity used when describing the processes involved (Ortiz-Martínez et al., 2015).

1.5.1 Comprehensive and specific models

Different classification can be made regarding the MFC models. Ortiz-Martínez et al. (2015) classified the MFC models in two main groups based on the authors' approaches: Comprehensive and Specific models. The overall behavior of the MFCs were comprehensively investigated in the first group of models while studies which focus on one or more key components or variables were categorized in the second group.

Under the Comprehensive models, the anode-based and anode/cathode-based models were studied. According to Ortiz-Martínez's model categorization, in the anode-based model, the anode is thought to be the system's limiting factor since all of the electrons and protons generated are used up in the cathode's oxygen reduction reaction. As a consequence, the anode activity is considered as the primary contributor in the MFC's energy generation. Martinez mentioned two important works in this category by Kato Marcus et al. (2007), and Picioreanu et al. (2007). Both studies contributed the functioning of the anode in the MFCs for achieving a high power output. Kato Marcus et al. (2007) developed a one-dimensional and dynamic conduction model that used a biofilm to transfer electrons directly from the substrate to the anode. In the proposed model, biofilm was introduced as a biological conductor which was represented by a K_{Bio} parameter-matrix for estimating its maximum value. The primary achievement in this study is that the conductivity of the biofilm is one of the system's most significant limiting variables which made this study an excellent reference for understanding the mechanics of electron transfer. Picioreanu et al. (2007) worked on a more complex approach with two and three-dimensional model simulations. He presented a computational model for the MFC based on redox mediators, several communities of floating and attached biofilm microorganisms, and different dissolved chemical species. The microbial activity of

the anode was subject to an exhaustive analysis in this study to get a deeper comprehension of the performance of the mediator-based MFC. The pH calculation was also considered in this study since the electrochemical mediator oxidation rate is influenced by it, which affects the PMS performance. However, in Kato Marcus et al. (2007) study, the pH calculation across the biofilm was not considered.

1.5.2 Mechanism-based and application-based models

In the anode/cathode-based model, the anode reaction was not considered as the limitation of the system. Ortiz-Martínez et al. (2015) mentioned that this model is scarce in the literature review. In one study, Zeng et al. (2010) proposed this model based on a two-chamber MFC including commercial Nafion-based membrane material, and platinum as the cathode catalyst. In one experiment, acetate and a buffer solution were employed for the anode, while in another, the suggested model was tested with a more complex substrate which involves artificial wastewater including glucose and glutamic acid. The Monod and Butler-Volmer equations were utilized in the modeling of the anode and cathode reactions and the chambers (anode and cathode) were modeled as continued stirred tank reactors (CSTR). Zeng et al. (2010) concluded that the kinetic constant of the anode reaction, change in fuel influent, and the charge transfer coefficient of the cathode reaction (β) all play important roles in the power generated by the MFC. In addition, sensitivity analysis identified the cathode reaction as a system limitation element, in contrast to the conclusion in the previous section, which identified the anode as the system limitation factor.

Under the specific models' key components, variables, or processes of the MFC were discussed from a comprehensive point of view. For instance, Garg et al. (2014) modeled the output voltage of the MFC based on three artificial intelligence (AI) methods. Multi-gene genetic programming (MGGP), artificial neural network (ANN) and support vector regression (SVM) methods were applied in order to study the effects of two variables (temperature and ferrous sulfate concentration) on the MFC's output voltage. Out of the three AI methods, the MGGP recorded an excellent performance to predict the MFC's performance.

In another study, Xia et al. (2018) discussed another MFC modeling classification in which two categories were identified: mechanism-based and application-based models (Figure 1.6). Mechanism-based models were grouped according to the various domains in which bioelectrochemical reactions in an MFC occur. This category included four different domains: bulk liquid, electrochemical, biofilm, and special models. The application-based models include the electrical model, which can be regarded as the most direct application of the MFC used for controlling and learning the model. In the learning model, by carrying out several experiments, the machine learning approach can be applied to obtain a mathematical model between the given input and the output variables. The electrical model is explored in the following section.

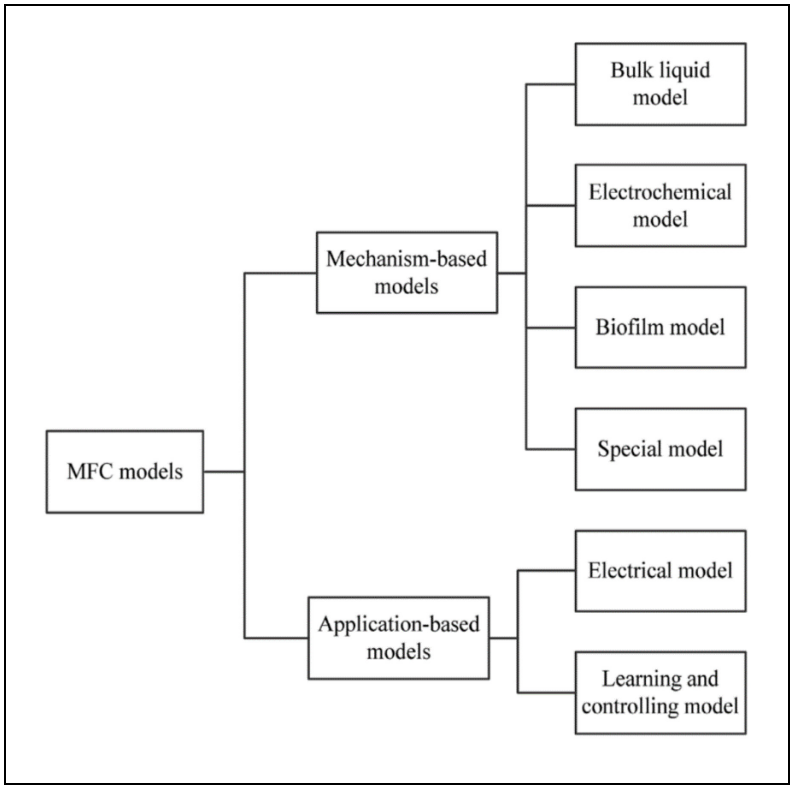

Figure 1.6 MFC modeling classification
Taken from Xia et al. (2018)

1.5.2.1 Electrical equivalent model

According to the equivalent electrical circuit modelling, Bioelectrorchemical system (BES) can be described as electrical circuits that represent MFC's fast electrical processes (on the order of milliseconds to seconds) (Recio-Garrido et al., 2016). The electrical model consists of components and parameters such as voltage, current, resistance and capacitance. In Figure 1.7, an equivalent electrical circuit model of the MFC is shown. V_{OC} is the open circuit voltage, R_1 represents the internal ohmic losses of the MFC which can be derived from a variety of sources, the most common of which are ion migration resistance, electron transport resistance, and contact resistance. In addition, R_1 is responsible for a considerable part of power losses in MFCs (ElMekawy et al., 2013). The activation and concentration losses are depicted as R_2 which are linked with the bacteria growth and carbon source consumption (Martin et al., 2013). C is the interfacial capacitance (Cooper & Smith, 2006), representing the system dynamics of the MFC. These modeled parameters of the MFC are connected to the external resistor R_{ext} through an electronic switch SW.

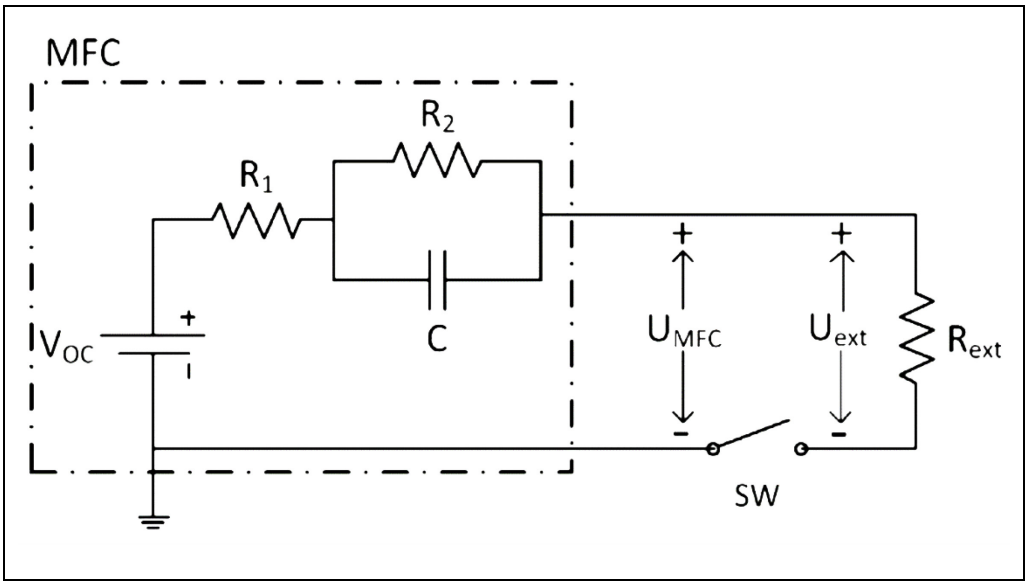

Figure 1.7 Equivalent electrical circuit model of MFC including R_1 and R_2 (internal MFC resistors), C (internal capacitor), V_{OC} (open circuit voltage), connected to an external load R_{ext} through a switch SW
Taken from Coronado et al. (2015)

1.6 Power management system

The PMS aligns the supply and demand in a power source. It is widely used for any sorts of power supplies on land or at sea including different types of renewable energy systems such as wind, tidal, solar, etc. PMSs automatically monitor and manage the system power, guaranteeing uninterrupted power and allowing the applicant to use it efficiently.

In MFC technology, the progress of the reactor's design, materials, and operation optimization of bioelectrochemical systems has resulted in several breakthroughs which reduced the reactor's chemical and physical restrictions (Logan, 2010). In spite of this, one of the most significant obstacles for MFCs or BESs to be used in actual applications is the low power output. In order to get around this hurdle, one of the main aspects is to consider how to harvest and realistically use MFC energy according to the system's true potential rather than just reporting the observed power density using external resistors. Therefore, a power management system is required to make the energy generated by the MFCs more practical for realistic applications (Mukherjee et al., 2022). The usage of MFC in wastewater treatment involves different applications, leading to a variety of potential PMS strategies for collecting and distributing energy. Therefore, choosing the right PMS method will benefit the system in several ways, including efficiency, affordability, reliability, and sustainability. The PMS is composed of electrical and electronic components working together as electrical circuits. This includes electronic switches (MOSFETs), capacitors, inductor, diode and a microprocessor. The fundamental notion of the PMS is to store the electrical energy generated by the MFCs in an electrical storage load (such as a supercapacitor) and then boost this energy to a practical level before releasing it to the load (Alipanahi et al., 2019).

1.6.1 Maximum power point tracking (MPPT) operation and methods

The typical reported voltage range for each MFC's output is 300-900 mV (Donovan et al., 2011). However, the input voltage required for biasing electronic devices or circuits is usually 3.3 V or higher. In this case, the MFC's output parameters (voltage, power) need to be optimized such that it can power the load (Donovan et al., 2011) carried out by the PMS.

In the PMS, different techniques such as maximum power point tracking (MPPT) (Molognoni et al., 2014) and pulse width modulation (PWM) (Coronado et al., 2013) can be employed in order to enhance the MFCs' performance. In DC sources, the maximum power will be transferred to the load when both the load and source resistance are equal. Also in the MFCs, when the internal resistor (R_{int}) equals to external resistor (R_{ext}), maximum power transfer will occur (Logan et al., 2006). The power can drop more than half if the external resistor cannot match itself with the internal resistor (Woodward et al., 2010). Methods using real-time MPPT can be applied to the system to avoid this power loss. Pinto et al. (2010) examined the impact of R_{ext} on the power and microbial population by periodically adjusting that parameter during the duration of the experiments. The maximum power and growth in anodophilic microorganisms were obtained when R_{int}=R_{ext} (defined as the optimal condition), while in the non-optimal condition where R_{ext} and R_{int} are not equal, an increase in the population of methanogenic microorganisms as well as power loss were observed. Woodward et al. (2010) studied and compared three methods which were used in MPPT. The first method was perturbation and observation (P/O), in which a potentiometer (as the MFC's R_{ext}) was initially set to 75 Ω and was updated at every minute by a perturbation of $\Delta R = 2.5$ Ω. Based on the sign of gradient which is determined according to the changes in the output power (ΔP) to ΔR, the direction of ΔR is adjusted for the next perturbation. These steps are repeated until the R_{ext} oscillates around an average point (R_{eq}). In this method, maximum power was obtained after 25 minutes. Next, in the gradient method, there are two steps in each iteration. First, the constant perturbation step at ΔR which is the same as the P/O, and second, the variable amplitude step based on the gradient value. Therefore, the amplitude of the move is proportional to the value of estimated gradient. From the two MFCs used in the experiments, one of them reached its maximum power value after 30 minutes while the other one experienced instability near the optimal range. Multiunit optimization (MU) was the last method which controlled the external resistance of two identical MFC units by a multiunit optimization algorithm. An offset of ΔR between the units was kept throughout the experiment, and the initial value of the external resistance was the same as the one used in previous experiments. The experiments demonstrate the fast convergence for reaching the optimal external resistance after only one minute for both MFC units (Figure 1.8). The author observed

that, although (theoretically) the multiunit method response was significantly faster than the P/O method, the setup was challenging. However, the P/O offered robust performance and was simple to tune.

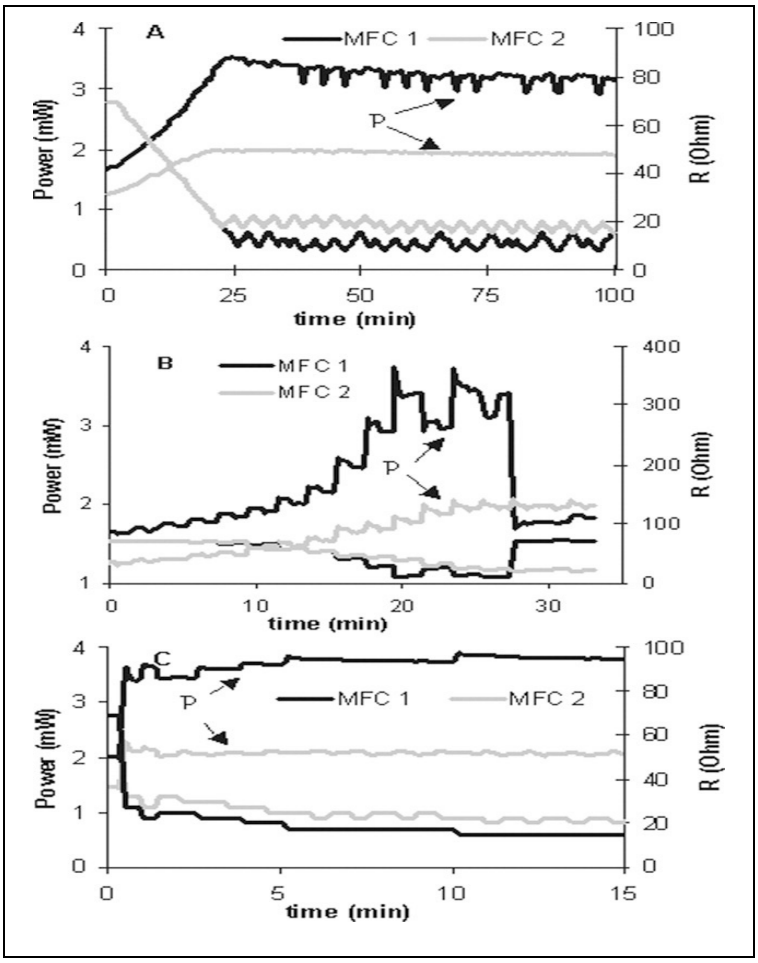

Figure 1.8 Comparison of (A) P/O, (B) gradient, and
(C) MU methods, with $\Delta R = 2.5\ \Omega$ and interval t = 1min
Taken from Woodward et al. (2010)

1.6.2 Pulse width modulation technique

In another study, Grondin et al. (2012) proposed a practical method to improve the power output of the MFC through intermittent connection and disconnection of R_{ext}. In this study, whenever the voltage of the MFC decreased below a predefined value (minimum voltage), the R_{ext} was disconnected. Once, the voltage of the MFC exceeded another predefined voltage

level (maximum voltage), R_{ext} was reconnected again. This technique contributed to maximising the MFC's power output. Inspired by Grondin's study, Coronado et al. (2013) used the PMW by intermittently connecting and disconnecting the R_{ext} (R-PWM). In this work, two MFCs were operated at different frequencies starting from 0.1 Hz up to 1000 Hz to observe the R-PWM effects on MFCs' operation. Several tests were carried out at a constant duty cycle of 50% while the frequency was varying. In another set of tests (D-test), the frequency was fixed at 500 Hz, and the duty cycle varied from 5% to 100%. Overall, an increase in the average output voltage and power were observed for frequencies exceeding 100 Hz. In the R-PWM mode, the performance of the MFC was significantly enhanced where the power output increased by at least 22% up to 43% as opposed to using a constant connection where R_{ext} is equal to R_{int}. The P/O algorithm was used to optimize the R_{ext} value and to compare with the R-PWM mode (Woodward et al., 2010). The power output's range under the R-PMW mode was between 3.6 and 3.8 mW while the range under the P/O algorithm was between 2.6 and 3.5 mW.

1.7 MFCs in the stack

A single MFC's power density is usually quite low (in range of 50–200 mW/m^2). According to one study (Ahn & Logan, 2012), although the maximum power density of 975 mW/m^2 was obtained, it is not enough to power even a typical semiconductor such as a temperature sensor. Consequently, one approach is to configure multiple MFCs connected in series, in parallel, or a combination of both to compensate for this lack of electrical power (Prasad & Tripathi, 2020).

1.7.1 Electrical configuration (series, parallel, series and parallel)

Prasad and Tripathi (2020) tested four different electrical configurations for sediment microbial fuel cells (SMFC). As demonstrated in Figure 1.9, all four configurations consist of three parts: the series-parallel connection of the SMFCs, PMS, and DC to AC inverter. All four systems used a 12 V battery charged by the supercapacitor connected in parallel with the SMFCs. The inverter was used to convert the DC voltage of the battery to an AC voltage which is required to power an LED bulb load. The voltage of all systems remained usually constant

(5.18 V, 5.21 V, 5.23 V and 5.26 V) since all modules used five SMFCS in series. Subsequently, the short circuit current of the modules increased in proportion to the number of parallel connections (1051 µA, 3081 µA, 5201 µA and 7160 µA for modules a, b, c and d respectively). Therefore, the fastest rate of charging the supercapacitor recorded for module d varied from 2.26 V to 4.5 V in 30 min.

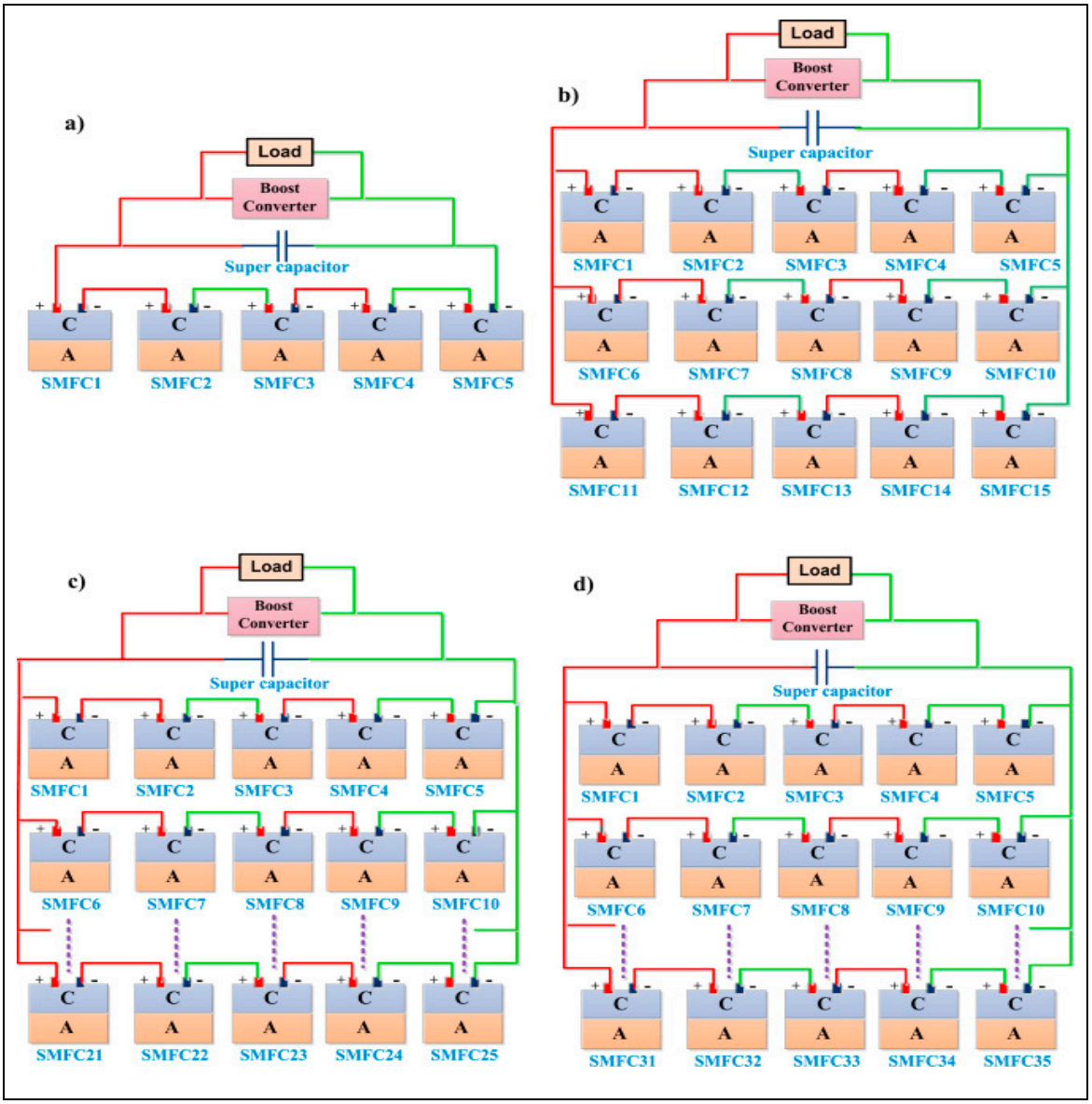

Figure 1.9 Schematic of modules: a) 5 series connected SMFCs b) 3 parallel connection of 5 series SMFCs c) 5 parallel connection of 5 series SMFCs d) 7 parallel connection of 5 series SMFCs
Taken from Prasad and Tripathi (2020)

In another study, Nguyen et al. (2019) proposed a energy harvesting system by stacking the MFCs with a high coulombic efficiency (up to 85%). The three continuously-fed air-cathode MFCs used in the stack were controlled by a PMS for bioelectrochemical systems with complex nonlinear dynamics. Each MFC was connected to a capacitor via a single pole single throw (SPST) switch. These capacitors were connected in series to increase the voltage level collected from the MFCs. An online MPPT algorithm ensured that the MFC's voltage remains around the half of its open circuit voltage (OCV) where MPP happens (Carreon-Bautista et al., 2015). This approach enabled estimation of the OCV without knowing of MFC internal parameters. Figure 1.10 shows the PMS utilized in Cong Long study, where the *n*th MFC (n=1,2,3), charges its corresponding capacitor C_n through a SPST switch S_n. This switch maintains the voltage of capacitor C_n around half of the *n*th MFC V_{OCN}. When S_n is closed, the C_n voltage is increased until it reaches an upper threshold, V_{UN} where the switch S_n will open (equations (1.1) and (1.2)). Meanwhile, the switch between the n capacitors and the supercapacitor, S_S, was open.

$$V_{CN}(t) \geq V_{UN}(t) \tag{1.1}$$

where,

$$V_{CN}(t) = (0.5 + \Delta_N)\, V_{OCN}(t) \tag{1.2}$$

Taken from Nguyen et al. (2019)

As soon as the voltage of one of the capacitors, C_n, reaches the upper voltage threshold (when equation (1.1) is validated), the corresponding switch, S_n, is open and the PMS keeps on monitoring the voltage of the rest of the capacitors. Once all the n switches (S_n) are open, the S_s is closed, and the supercapacitor is charged. The discharge of each C_n to the SC continues until they reach their exclusive lower limit, V_{LN} (equations (1.3) and (1.4)). Once the voltage of capacitors reached V_{LN}, PMS disconnects them from the supercapacitor and connect them to their corresponding MFC to be charged again.

$$V_{CN}(t) \leq V_{LN}(t) \tag{1.3}$$

where

$$V_{LN}(t) = (0.5 - \Delta_N)\, V_{OCN}(t) \tag{1.4}$$

Taken from Nguyen et al. (2019)

The summed voltage in the supercapacitor (around 0.6 V) was boosted by a DC-DC step-up converter to a load-applicable level. The schematic of the PMS is shown in Figure 1.10. While the MPPT could perform effectively without considering the internal bioelectrochemical parameters of the MFCs, this approach can still be improved as explained. If one MFC cannot supply its corresponding capacitor temporarily, the whole system will be shut down. Therefore, a maintenance feature enabling each MFC to disconnect from the system without interrupting overall energy harvesting is required. Next, there is a possibility that one or more MFCs charge their capacitors more slowly than the others. In this case the overall system would experience energy loss. The PMS also would become useless while waiting for the weak MFC until it charges its capacitor before allowing the rest of capacitors to discharge.

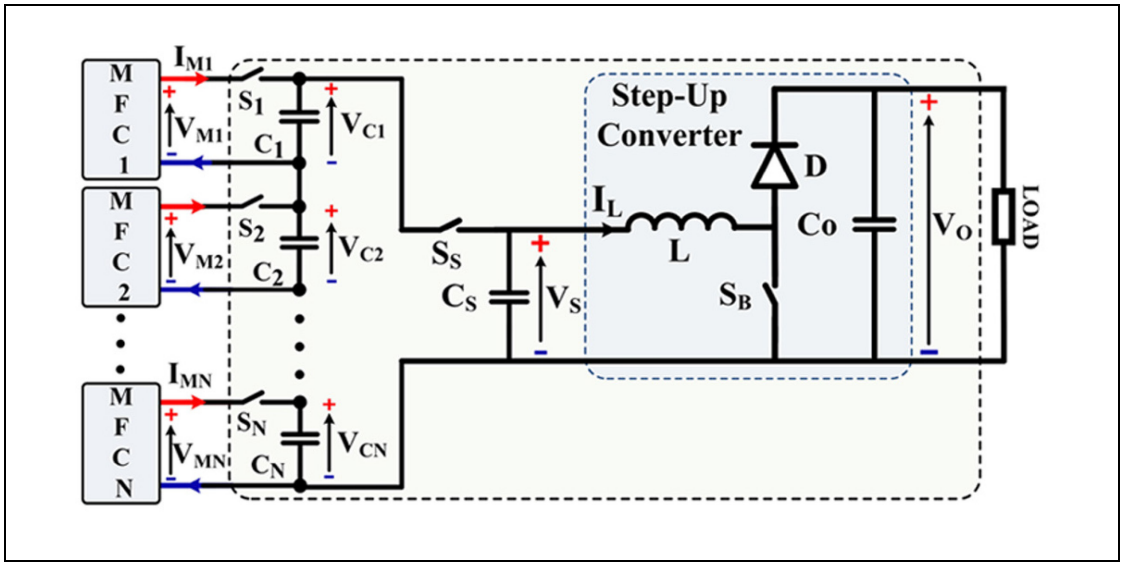

Figure 1.10 The proposed PMS by Nguyen for stack of MFC using MPPT algorithm
Taken from Nguyen et al. (2019)

Different methods of charge/discharge are possible in capacitor-based energy harvesting systems, mentioned as follows: direct charging, parallel charging/series discharging (Ren et al., 2013), intermittent energy harvesting (IEH) (Dewan et al., 2009), alternate charging and discharging of capacitor (ACD) (Liang et al., 2011).

Charge-pump converter are used to obtain higher voltage levels using capacitors. A voltage doubler is a good example for comprehending the basis of charge-pump operation (Figure 1.11). Two states of charge and discharge are displayed in Figure 1.11. In the charging state (A), C_1 is charged through V_{IN} and discharges to the C_2 in the second state (B). The voltage of C_2 gradually approaches $2V_{IN}$ as the charging and discharging operation continues (Harres, 2013).

Briefly, a charge-pump system is an inductor-less converter utilizing capacitors as the energy storage and energy transfer in order to increase or decrease the voltage level.

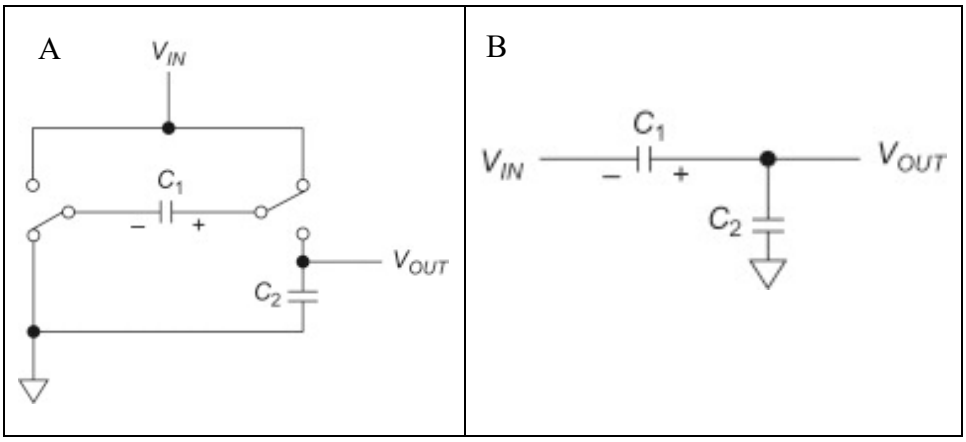

Figure 1.11 Two phases of charge transfer (A) C_1 charging state
(B) C_2 discharging state, in a voltage doubler pump-charge circuit
Taken from Harres (2013)

Zhang et al. (2012) compared a charge-pump-capacitor-converter and a capacitor-transformer-converter as the PMS of a single 316 mL air-cathode MFC. While the charge-pump-capacitor-converter efficiency was higher, the capacitor-transformer-converter could support lower input voltages. During the start-up phase, it took 22 h for the charge-pump-capacitor-converter to

reach the output voltage of 3.3 V while it took just 2.5 h for the capacitor-transformer-converter to reach the same output voltage. It can be concluded that the charge-pump based circuit was significantly slower than transformer-based circuit in terms of harvesting electrical energy. Wang et al. (2012) implies the same issue for the charge-pump based PMS compared to the MPPT PMS, in which the total energy harvested from the MPPT technique was 76 times higher than charge-pump technique during 18h due to the input current limitation of the charge-pump.

Park and Ren (2012) proposed a PMS based on parallel connection of two MFCs that could be extended to N-MFCs. The PMS consists of two layers of DC-DC converters. At the first layer, each MFC was connected to its own energy harvester (a DC-DC converter). Each energy harvester functioned independently due to the MPP of its corresponding MFC, and the harvested energy stored in a capacitor. The second layer converter boosted the voltage of the capacitor to a usable level for the load. Therefore, employing N MFCs requires N+1 DC-DC converters (N converters for the first layer and 1 converter for the second layer). The parallel connection of MFCs increases the output current and power. In parallel connection of MFCs, however, the current reversal can influence the overall performance and efficiency of the stack and causes power loss. In one study (Wu et al., 2016), the increase of the V_{OC} differences among the MFCs as well as the enlargement in value of external resistance is concluded as the reason of the current reversal phenomena.

1.8 DC-DC Boost Converter

The low output voltage of MFC necessitates the usage of voltage booster usable for the load application. The DC-DC boost converter is widely employed for energy harvesting from the MFCs because of its simplicity and high efficiency. It converts the low input voltage of the MFCs to higher levels according to the load voltage requirement. Degrenne et al. (2011) compared three different step-up DC-DC converter topologies in order to harvest energy from 10 1-liter MFCs connected in parallel. A conventional DC-DC boost converter previously proposed by Pollak et al. (2008) was studied as the first topology, while flyback and oscillator

voltage-lifted topologies were proposed and compared as the second and third topologies, respectively. The following parameters are considered as the criteria for comparing converters: robustness, step-up ratio, efficiency and cost.

In terms of robustness, flyback converter was very sensitive to the parasitic parameter of the circuit among the others. Therefore, the weakest robustness was reported for this topology. However, it benefitted high step-up ratio (similar for the oscillator voltage-lifted topology) and high efficiency equal to the conventional topology (80.6% for both topology, and 66.5% for the oscillator voltage-lifted topology). In terms of cost, the highest rate was reported for the flyback topology while the other topologies were also not cost-effective due to usage of large inductive components.

In Nguyen et al. (2019) study which was previously discussed, a conventional DC-DC boost converter with the efficiency above 90% was used to obtain the overall system power conversion efficiency of 86%. The converter consisted of an inductance, an SPST switch, a Schottky diode and an output capacitor (Figure 1.10). The converter voltage boost ratio and the efficiency curves are shown in Figure 1.12. The optimal output power obtained at efficiency of slightly above 90% where the duty cycle was about 80% and the boost ratio was 5.

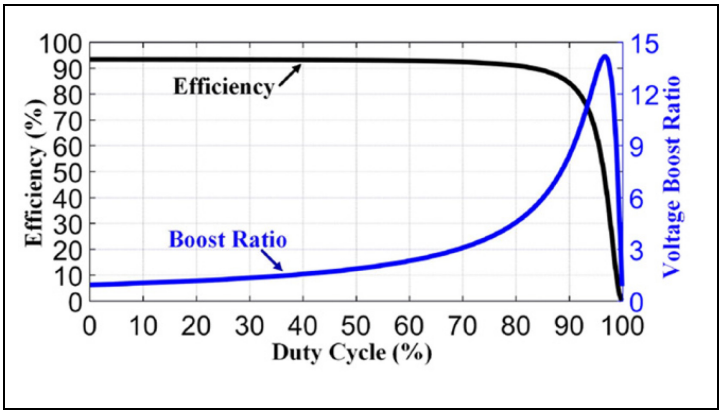

Figure 1.12 Converter efficiency and voltage boost ratio curves
Taken from Nguyen et al. (2019)

1.9 Voltage regulation techniques

Since the output voltage of a single MFC (or MFCs in a stack) is not a fixed value and can have disturbances, it is not suitable for the most of load applications which demand a regulated input voltage as their DC supply voltage. As a result, a voltage regulator (VReg) is required to offer a fixed output voltage irrespective of alterations caused by the input source (MFCS), the nonlinearity in the converter, and the load variations.

To date, different control topologies have been proposed to call the issues, from linear methods including conventional proportional-Integral controller (PI) (Alvarez-Ramirez et al., 2001) to nonlinear techniques (Hiti & Borojevic, 1995), and from fuzzy logic (Gupta et al., 1997) to sliding mode control (Mattavelli et al., 1997).

1.9.1 Proportional-Integral controller (PI)

Alvarez-Ramirez et al. (2001) discussed the stability and instability of buck/boost DC-DC power converters when a PI controller was utilized as the control technique. To accomplish this, the effect of the right-hand-side (RSH) zero on the proposed controller was studied. The results illustrated that the gain's constraints placed by the RSH were due to the fundamental nature rather than a specific design criterion. Weak control performance of integrating process and prolonged processing latency are the limits of PI controllers (Sung & Lee, 1996).

1.9.2 Fuzzy logic controller

The control action of a fuzzy logic controller is determined by assessing a set of basic linguistic rules. The construction of the rules needs a comprehensive knowledge of the process to be controlled. However, a mathematical model of the system is unnecessary. Consequently, the method is general, allowing the same control system to be used to other types of DC-DC converters. Gupta et al. (1997) represented a buck/boost DC-DC converter under a fuzzy controller technique and using an 8-b microcontroller (Philips Semiconductors 87C752 microcontroller). Since the microcontroller benefits having a five-channel multiplexed 8-b A/D converter and an 8-b PWM output, no more digital/analog electrical components were

needed. One of the features of this study was that the fuzzy algorithm was applied for both buck and boost converters without modification, still the output voltage was regulated in both converters. Moreover, the fuzzy logic is an affordable approach that can be implemented in the DC-DC converters without the need for costly specialized hardware. However, complexity in design, lack of simple rules and systematic approach to solve a problem, as well as limitations of DSP systems with non-linear arithmetic can be considered as the disadvantages of fuzzy controller technique.

1.9.3 Sliding mode control

Sliding mode control (SMC) is a nonlinear control method which can be a suitable option to maintain a regulated output voltage regardless of the wide input voltage range and the load variations in MFC systems. In addition, the SMC technique is capable of controlling the variable structure systems (VSS) such as switching converters (Ramos et al., 2009) that are also used in MFC systems. The robustness, accuracy, and simplicity of tuning and implementation, as well as the low cost, make this method of control particularly appealing. Utkin (1977), which is an important study in this area, described the basic principles of SMC. Guldemir (2005) studied the performance of SMC in the DC-DC boost converter with respect to the load and input step variations. Although large input disturbances and load variations applied to the system during the simulation, the proposed controller showed robustness, stability, and good dynamic behaviour. In our study, the SMC method was used, and its performance was assessed as the VReg of the DC-DC boost converter.

CHAPTER 2

METHODOLOGY

Figure 2.1a shows the block diagram of the proposed system where the energy is being harvested from the stack of MFCs through a control block called power management system (PMS). The harvested energy is then transmitted to the DC-DC boost converter block to step-up the low voltage of MFCs to higher levels required by the load. Finally, the voltage regulator block aids the system to become insensitive to the uncertainties caused by both the input of the converter and the load. The schematic of the proposed system is also depicted in Figure 2.1b.

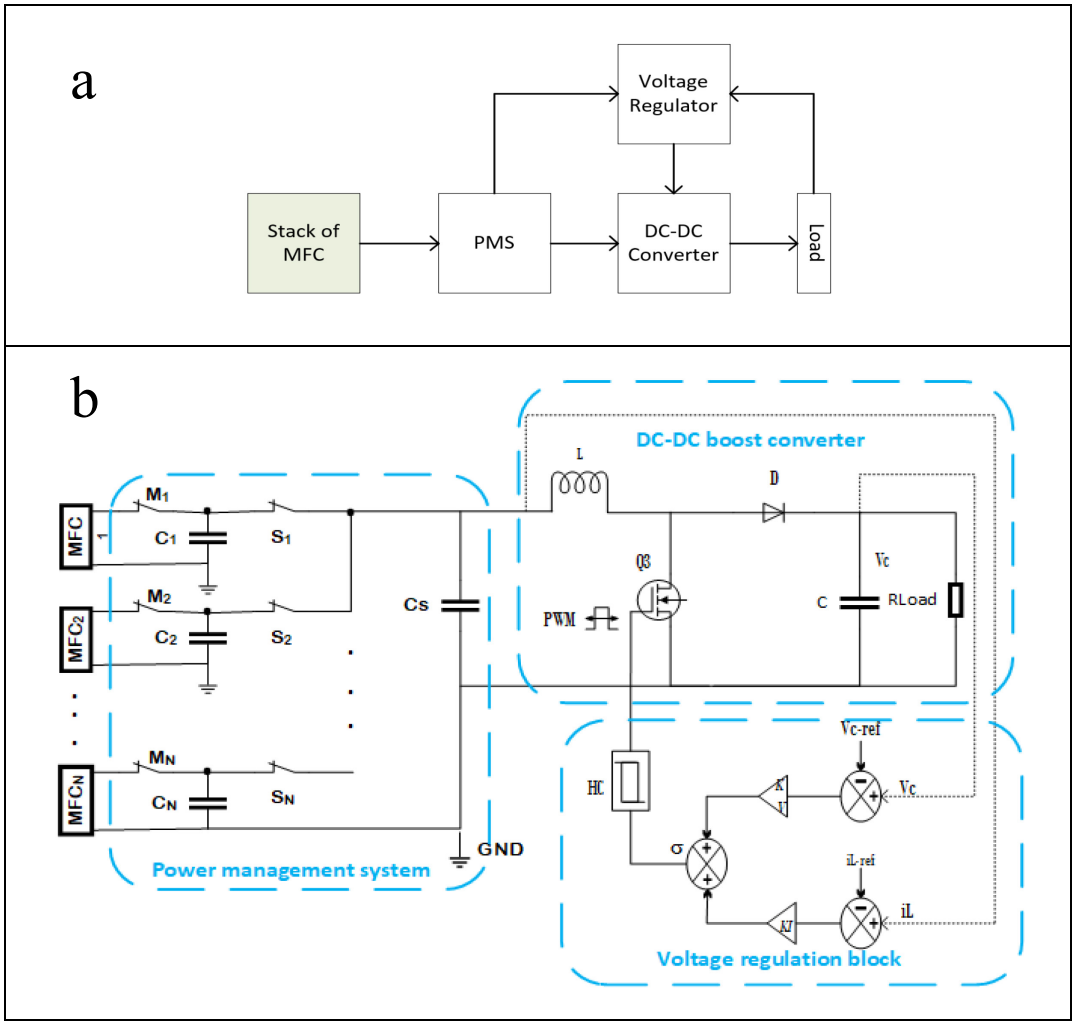

Figure 2.1 (a) The block diagram and (b) the schematic of the proposed system

2.1 Power Management System

Figure 2.2 illustrates the schematic of the proposed power management system, which can potentially harvest energy from N MFC units. However, for practical reasons four MFCs in the stack were used in this work. Each MFC is connected to its corresponding capacitor (C_i) via the switch M_i. When the capacitor C_i is charged up to a predefined high voltage limit (VcH_i), the switch S_i is closed while switch M_i is opened to allow the capacitor (C_i) to discharge down to a predefined low voltage limit (VcL_i) in the supercapacitor (C_S) while the other S_is remain open. The proposed topology leads the charge and discharge of each C_i independently from other units. This means that C_i start and stop charging decisions are made exclusively based on C_i and MFC_i conditions. This feature isolates MFCs from each other. However, the capacitors' discharge to the supercapacitor is managed sequentially.

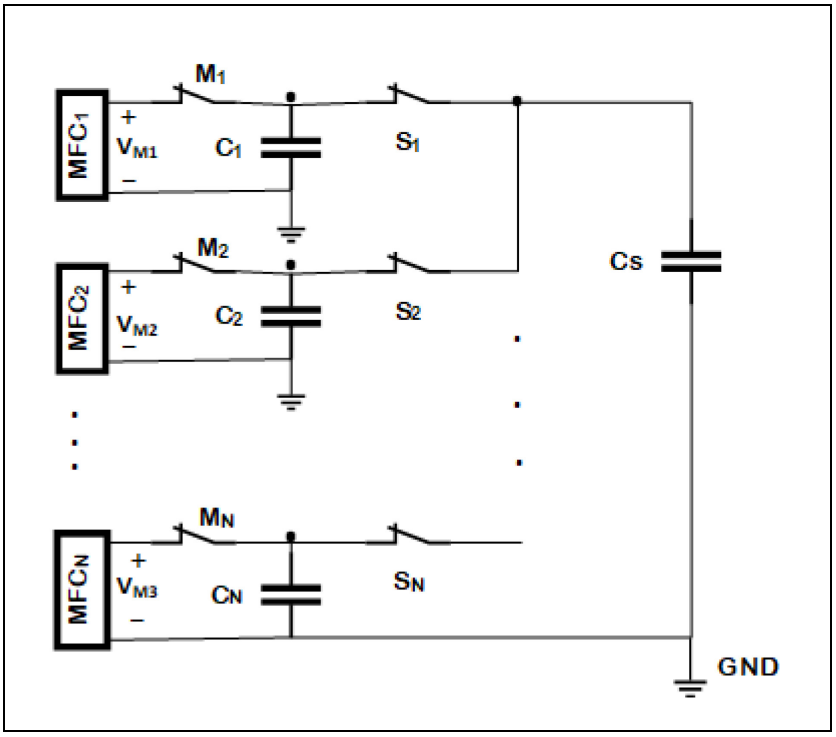

Figure 2.2 Schematic of the power management system (PMS)

During the discharge time of C_i to the supercapacitor, the other C_is are being charged or are waiting for their turns to be discharged. In this process, the C_is will be discharged in the

supercapacitor sequentially. The PMS determines the sequence order according to the first in, first out principle (FIFO), meaning that the Vc_i reaching its higher threshold (VcH_i) first, is allowed to discharge first.

In an exceptional circumstance, by the end of discharge of one C_i capacitor, if two capacitors (C_is) have passed their VcH_is, the PMS will choose the one according to their numerical order from smaller to larger (1→2→3→4), to be discharged first.

Given the fact that the C_i capacitors only discharge once they reach their V_cH_i, if one or multiple MFCs are malfunctioning or not charging their capacitor (C_i) for any reason, the PMS will discard the respective capacitor from the discharging process. This algorithm should be able to deliver uninterrupted power even with only one functioning MFC unit as long as the supercapacitor can be charged to the minimum voltage required at the input of the boost converter.

The example in Figure 2.3 demonstrates how C_is are discharged based on their charging order. At time zero, the C_is are starting to be charged from 0 V to their VcH_i. First, C_3 reaches its higher threshold, hence it begins discharging to the supercapacitor. Then C_2 reaches VcH_2 and starts being discharged until it attains VcL_2. Next, C_4 reaches its VcH_4 sooner than C_1 and is discharged after. Finally, C_1 discharges to the supercapacitor. Table 2.1 shows C_is' discharging order to the supercapacitor, ranked regarding their order of reaching their VcH_i.

Table 2.1 C_i's charge order in one example cycle

Device	Capacitor1	Capacitor2	Capacitor3	Capacitor4
Ranks	4th	2nd	1st	3rd

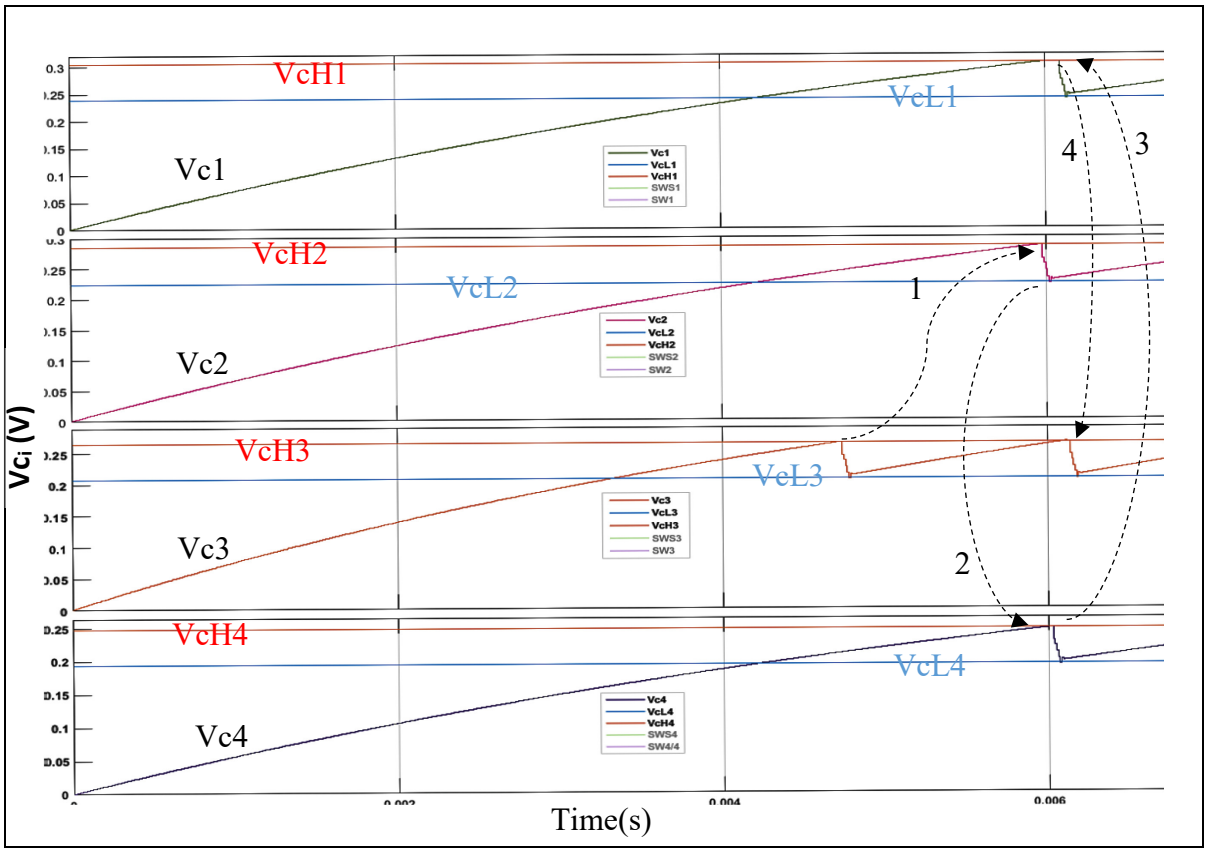

Figure 2.3 The Capacitors voltage (Vc_i), C_i discharging sequence based on ranking presented in Table 2.1 in one cycle of energy harvesting

2.1.1 Maximum power point tracking (MPPT)

The optimal point for the MFCs operation according to maximum power transfer theorem is around half of its open-circuit voltage (V_{OC}). This point is defined as the maximum power point (MPP). The proposed PMS integrates a maximum power point tracking algorithm (MPPT) for each MFC.

The values of V_CL_i and V_CH_i are predefined close to 50% of open-circuit-voltage of MFC_i, as shown in equations (2.1) and (2.2) (Nguyen et al., 2019).

$$V_CH_i = (0.5 + M)\, V_{OCi} \quad (2.1)$$

$$V_C L_i = (0.5 - M)\, V_{OCi} \quad (2.2)$$

Where M is chosen small (0.02<M<0.1) to keep the Vc_i close to the half of $V_{OC\text{-}MFCi}$.

Figure 2.4 shows an example of how the voltage of capacitor C_3 (in blue), which is connected to MFC_3, varies between its upper (VcH_3) and lower (VcL_3) thresholds shown by the red lines, respectively.

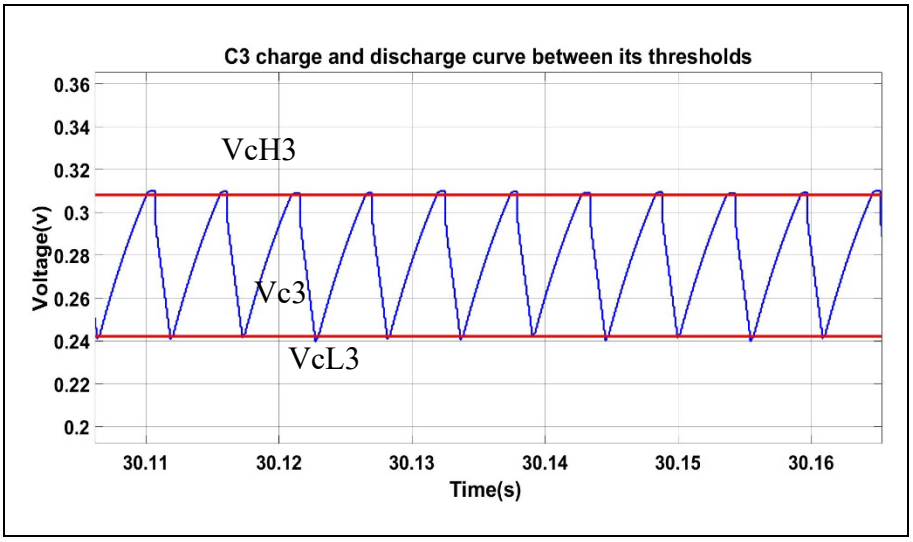

Figure 2.4 An example of Vc_3 variations between its upper and lower thresholds

2.1.2 Online estimation of MFC open-circuit voltage

One main challenge in utilizing MPPT method is online estimation of V_{OC}. We used the method to estimate the V_{OC} of MFC online despite its variation and without disconnecting the circuit introduced by Nguyen et al. (2019). Considering the *i*th MFC of MFCs when the switch M_i is open (Figure 2.2), the output voltage of the MFC (V_{Mi}) is calculated as follows:

$$V_{Mi}(t) = VOC_i - V_{Ii} e^{\frac{-t}{\tau}} \quad (2.3)$$

where $\tau = R_{2i}C_i$ and V_{Ii} is the voltage across the internal capacitor C_i in the electrical equivalent circuit of the MFC in Figure 1.7. By selecting three moments during the discharge of C_{1i}, starting at the time the switch M_i is turned off, $t_1 = 0$, and $t_2 = \lambda$, and $t_3 = 2\lambda$, the OCV can be determined. It should be noted that the interval between t_1 and t_3 should be lower than the τ value. The following equations (2.4) to (2.7) yield to the V_{OCi} equation. With this approach, the real time identification of V_{OC} values is feasible without needing to identify the MFC's internal capacitor and resistors.

$$V_{Mi}(0) = VOC_i - V_{Ii} \tag{2.4}$$

$$V_{Mi}(\lambda) = VOC_i - V_{Ii}e^{\frac{-\lambda}{\tau}} \tag{2.5}$$

$$V_{Mi}(2\lambda) = VOC_i - V_{Ii}e^{\frac{-2\lambda}{\tau}} \tag{2.6}$$

$$VOC_i = \frac{V_{Mi}(0)V_{Mi}(2\lambda) - V_{Mi}^2(\lambda)}{V_{Mi}(0) - 2V_{Mi}(\lambda) + V_{Mi}(2\lambda)} \tag{2.7}$$

2.1.3 Health protection of the MFCs using hysteresis control

The MFCs operate in different ambient or internal conditions. thus, they can have a wide range for their V_{OC} during their operation. In certain conditions, where the concentration of the organic matter or water levels in the reactor are low, the V_{OC} levels drop significantly. If the MFC stays connected to the circuit charging a capacitor, in such condition this can have a detrimental effect on microorganism's health (Costilla Reyes et al., 2018). Hence, PMS disconnects MFCs with low V_{OC}s from the system by opening their M_i between the ith MFC and the corresponding capacitor C_i. The disconnected MFC unit recovers and increases its voltage gradually while being disconnected.

The health protection algorithm consists of two constant values, V_{High} and V_{Low}, defined as the lower and upper limits for the lower threshold of Vc_i (VcL_i). These limits are applied on VcL_i

since it is the lowest point that MFC_i voltage reaches at each charge-discharge cycle and helps to catch the voltage dropping faster before the V_{MFC} reaches the critical point. According to equations (2.1) and (2.2), the lower threshold of VcL_i is in direct relation to the V_{OCi}.

When VcL_i reaches the lower limit V_{Low}, MFC_i is disconnected from the system, and it will recover until its VcL_i reaches V_{High} which is the hysteresis band for VcL_i in order to avoid repetitive disconnections and reconnections. Meanwhile, the algorithm continues to harvest energy from the rest of the MFCs in the stack. At V_{High}, the PMS allows the MFC to start charging its capacitor again.

The MFCs had been connected continuously to a resistive load and operated for a couple of years, starting Sep. 2017. The voltage of the MFC (V_{MFCi}) values were collected while the MFCs operated in a variety of ambient and internal conditions. According to the long-term observation of the V_{MFCi} variations, the lowest V_{MFCi} was obtained in the low chemical oxygen demand (COD) and low water level condition where the MFC_i was still functional. Functional MFC_i is defined as an MFC_i that is responsive to the changes in COD and water levels and shows an increase in the power and voltage. The "malfunction'' MFC_i is defined for a low power and voltage MFC_i, lower than in low COD, low water conditions, which does not show any reaction to an increase in inlet substrate concentration. The value of V_{Low} was a reasonable estimate based on the patterns observed in the historic data from functional and malfunctioning MFCs. Hence, to determine the value of V_{Low}, the lowest V_{MFCi} in the low COD, low water conditions is chosen as the reference for critical voltage level.

2.1.4 Mitigating C_i waiting time in case of long discharge time

While one C_i is discharging to the supercapacitor, the other capacitors might also be ready to discharge. However, since the PMS is programmed in a way to discharge one C_i at a time, the other units would wait for their turn to be discharged. This operation is not optimal since the interval where the MFCs are waiting to be discharged to the supercapacitor is potential energy loss. To reduce the potential loss, the PMS incrementally (α) increases the VcH_i threshold of the waiting unit temporarily according to equation (2.8) to continue charging the C_i so its

waiting time can be utilized for power extraction. The V_{CH_i} is increased in increments of few percent ($1<\alpha<1.02$) at each sampling time of the simulation until it passes a predefined maximum (α_{max}), at which point the VcH_i stops increasing and waits for its turn to be discharged. This process is depicted in the following equations.

$$V_{cH_i}{}^{k+1} = \alpha . V_{cH_i}{}^{k} \tag{2.8}$$

$$V_{cHi}^{k} < \alpha_{max} V_{cHi}^{0} \tag{2.9}$$

where, VcH^0 is the original VcH_i calculated based on V_{OC} and the rest of the VcH^k values are the incremental increases. The maximum α multiplied to the $V_{cH}{}^0$ in equation (2.1) is small enough ($\alpha_{max}<1.05$) to keep the Vc_i reasonably close to MPP, this condition is shown in equation (2.9). The increased value of VcH_i will go back to the original value based on V_{OC} as soon as the C_i is discharged to the supercapacitor. Therefore, for the next cycle of charge/discharge, VcH_i will be calculated via equation (2.1) again. In Figure 2.5, while the capacitor 4 is discharging, Vc_2 in point A reaches its upper limit (VcH_2). Since it cannot discharge, its upper limit increased by two increments ($VcH_2{}^2$) and then the PMS allows it to discharge. The $VcH_2{}^2$ goes back to the $VcH_2{}^0$ as soon as it starts to discharge to the supercapacitor. In point B, the same happens to the C_3 and after two increments its VcH_i reaches its maximum $VcH_3{}^{max}$. Therefore, it waits for C_2 to discharge, since C_2 reached its upper limit first, and after that it discharges to the super capacitor. In point C, VcH_1 is mitigating since C_3 is still discharging and as soon as its discharged PMS allows C_1 to discharge.

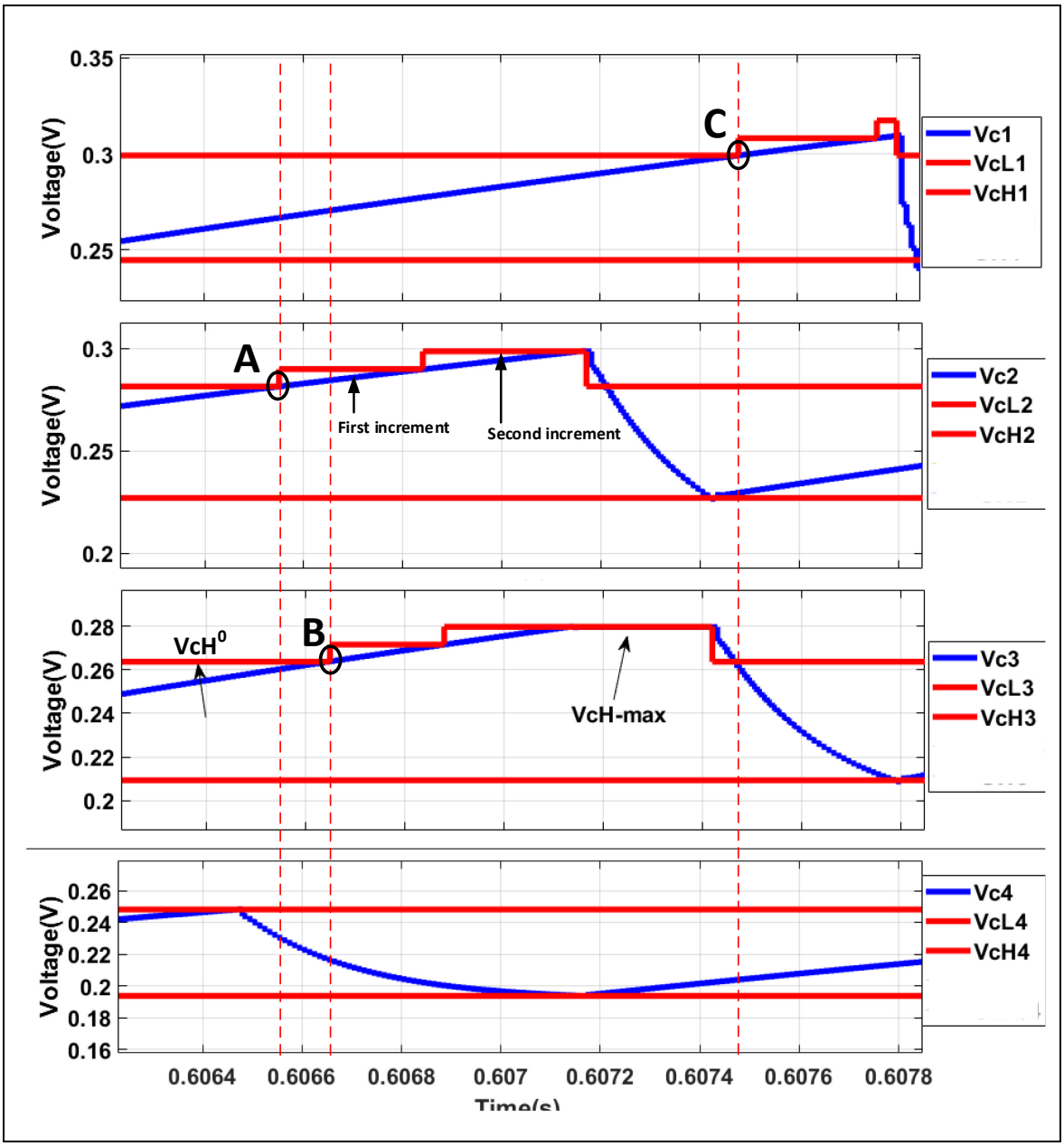

Figure 2.5 An example of mitigating $C_{(2,3)}$ (point A and B) while C_4 is discharging, and mitigating C_1 (Point C) waiting time while C_3 is discharging

2.1.5 Maximum discharge time of C_i (T_{d_max})

Sometimes in the operation of the PMS, when the load is drawing lower power than produced by the input source (MFCs), the supercapacitor does not discharge as fast as it is charged. In

such cases, the supercapacitor remains in the higher voltage level and hence the discharge of the capacitor C_is charged at a low voltage to the supercapacitor takes a considerably long time. When C_i cannot discharge to the supercapacitor as fast as the other capacitors since its voltage is closer to the supercapacitor voltage, the waiting time of other C_is becomes significant, increasing the energy loss of the entire system. Hence, to avoid this problem, the PMS terminates the discharging process of C_i to the supercapacitor if it takes longer than a predefined value (T_{d_max}) even if $VcL_i < Vc_i < VcH_i$ and moves on to discharge the next capacitor. Figure 2.6 depicts the control flowchart of the PMS characteristics, as mentioned in subsections of the PMS, where N MFCs and their corresponding capacitors are controlled by the two sets of switches M_i and S_i at each sampling time t.

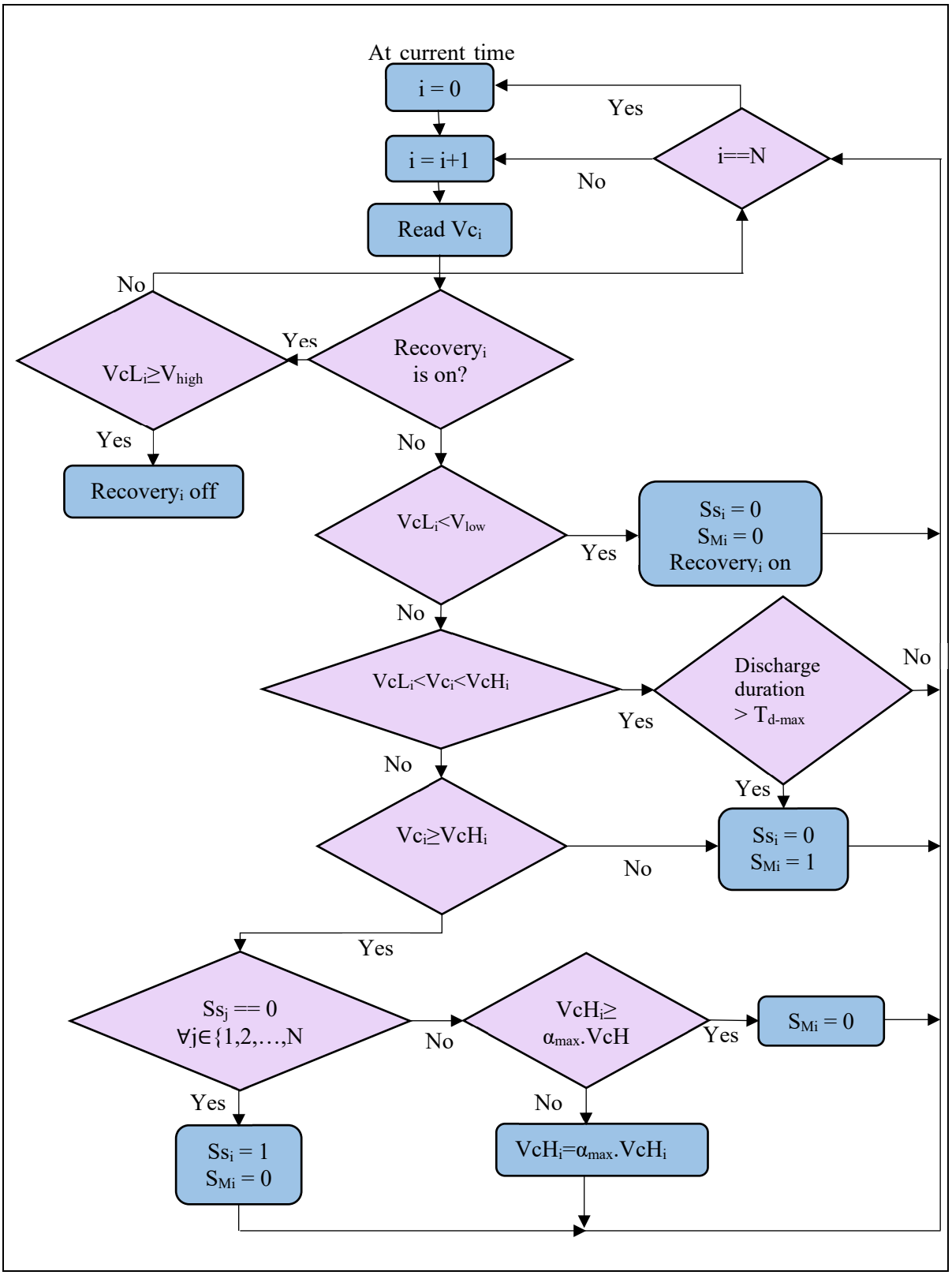

Figure 2.6 Flowchart of the control logic used at each sampling time by the proposed PMS

2.2 DC-DC boost converter

MFC's ultra-low power applications including temperature sensor or IoT (Chong & Kumar, 2003), and typical electrical circuits often need input voltages ranging from 2.5 V to 5 V. Because of the uncertainty and low voltage level of MFCs, they cannot be directly connected to and power these applications. In one example, Figure 2.7 displays the output power and voltage of MFC_1, for the first 800 days after start-up which was continuously connected to the resistive loads with different values to obtain the maximum power. The MFC_1's low and fluctuating output voltage implies that a direct MFC_1 connection to the load is not feasible.

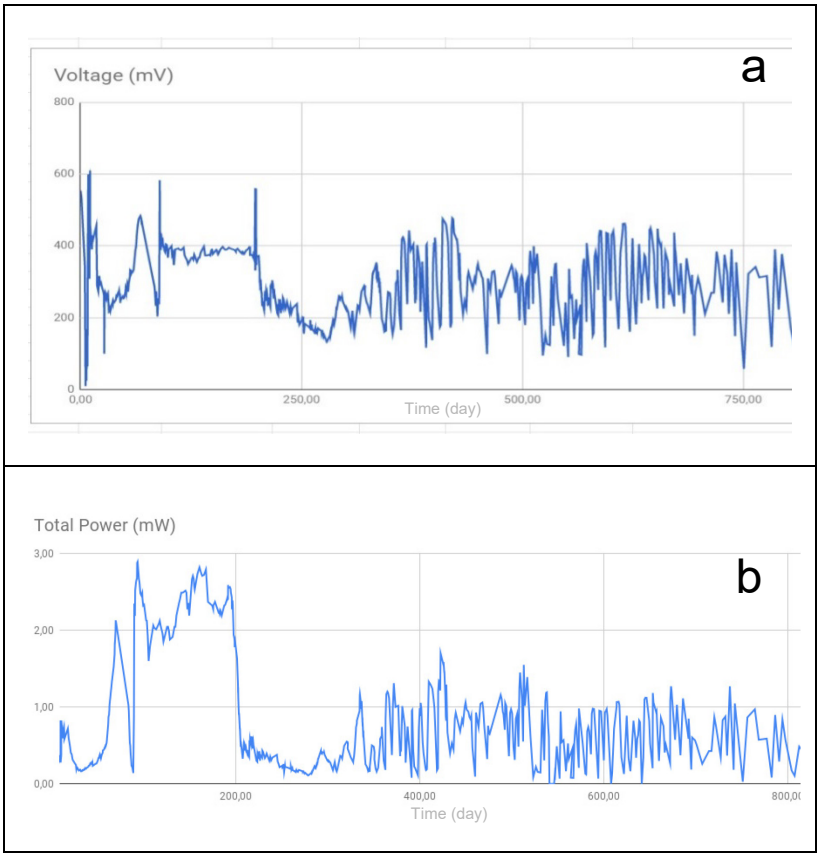

Figure 2.7 (a) Voltage and (b) Power output of MFC_1 for the first 800 days after start-up

As a consequence, a DC-DC boost converter is required to increase the load voltage to the desired level for the applications. Given the fact that the power and voltage of MFC are low, the efficiency demand will be high. Figure 2.8 depicts the fundamental schematic of the high-

efficiency boost converter employed in the proposed energy harvesting system. V_S is the supercapacitor voltage at the input of the converter. The converter consisted of an inductor (L), a switch (SW_B), a diode (D), and an output capacitor (C). The converter contains a few electrical elements which contribute to its simplicity and cost-effectiveness. The efficiency and the voltage boost ratio of the converter are influenced by the parasitic resistance that are responsible for the power losses. The equivalent electrical circuit with parasitic resistances is demonstrated in Figure 2.9.

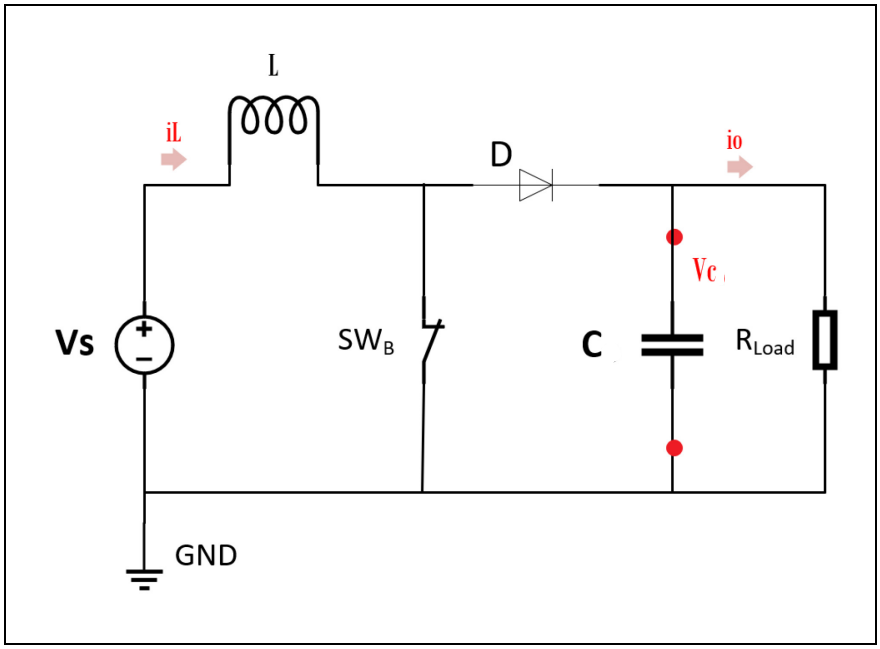

Figure 2.8 Boost converter fundamental circuit

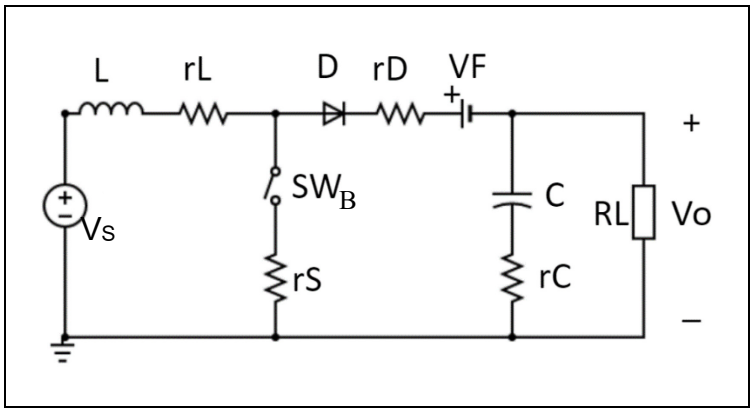

Figure 2.9 The electrical equivalent circuit of the converter with parasitic resistances

The total power loss in the converter is equal to the sum of parasitic losses which can be expressed as follows (Nguyen et al., 2019):

$$P_{TL} = P_L + P_S + P_D + P_C = \left[\frac{r_L + Dr_S}{(1-D)^2 R} + \frac{r_D + Dr_C}{(1-D) R} + \frac{V_F}{V_O}\right] P_O \quad (2.10)$$

Therefore, the converter efficiency is

$$\eta = \frac{P_O}{P_O + P_{LOSS}} \quad (2.11)$$

and the boost ratio of the converter can be calculated by the following equation

$$B = \frac{V_O}{V_I} = \frac{\eta}{1-D} = \frac{1}{(1-D)\left[1 + \frac{r_L + Dr_S}{(1-D)^2 R} + \frac{r_D + Dr_C}{(1-D) R} + \frac{V_F}{V_O}\right]} \quad (2.12)$$

where η and D are the converter efficiency and duty cycle of switch SW_B, respectively, V_O and V_I are the output and input voltage of the converter. r_L, r_C r_S, and r_D are the equivalent series

resistance (ESR) of the inductance L, ESR of output capacitor C, switch resistance (on-state) of SW_B, and forward bias resistance of the diode D, respectively.

2.2.1 Sliding mode control as the voltage regulation technique

SMC is designed to map the system states to a desired surface which is known as sliding surface in the state space. Once the sliding surface is reached, sliding mode control maintains the conditions in the vicinity of sliding surfaces. Sliding mode control's robustness is its key asset. Since the control can be basic as a switch between two states 'ON' and 'OFF' or 'forward' and 'reverse'. The sliding-mode control technique includes selection of a sliding surface so that the system trajectory shows acceptable behaviour when reaches this surface. In addition, it includes feedback gains to keep the system trajectory on the surface and sliding near it. The system's dynamic behavior can be modified in the SMC by selecting the appropriate sliding surface.

The DC-DC boost converter's input voltage varies due to the voltage volatility of the MFC voltage. Therefore, it is essential to develop a controller that can respond quickly to the variations in the input and the load parameters of the DC-DC boost converter. The control technique for the proposed DC-DC boost converter needs to cope with input variations, and warranty stability in any operating condition while providing a fast transient response (Spiazzi et al., 1997). In this study, the sliding mode technique is chosen for controlling the output voltage of the proposed DC-DC converters. Figure 2.10 demonstrates the schematic of the SMC for the proposed converter.

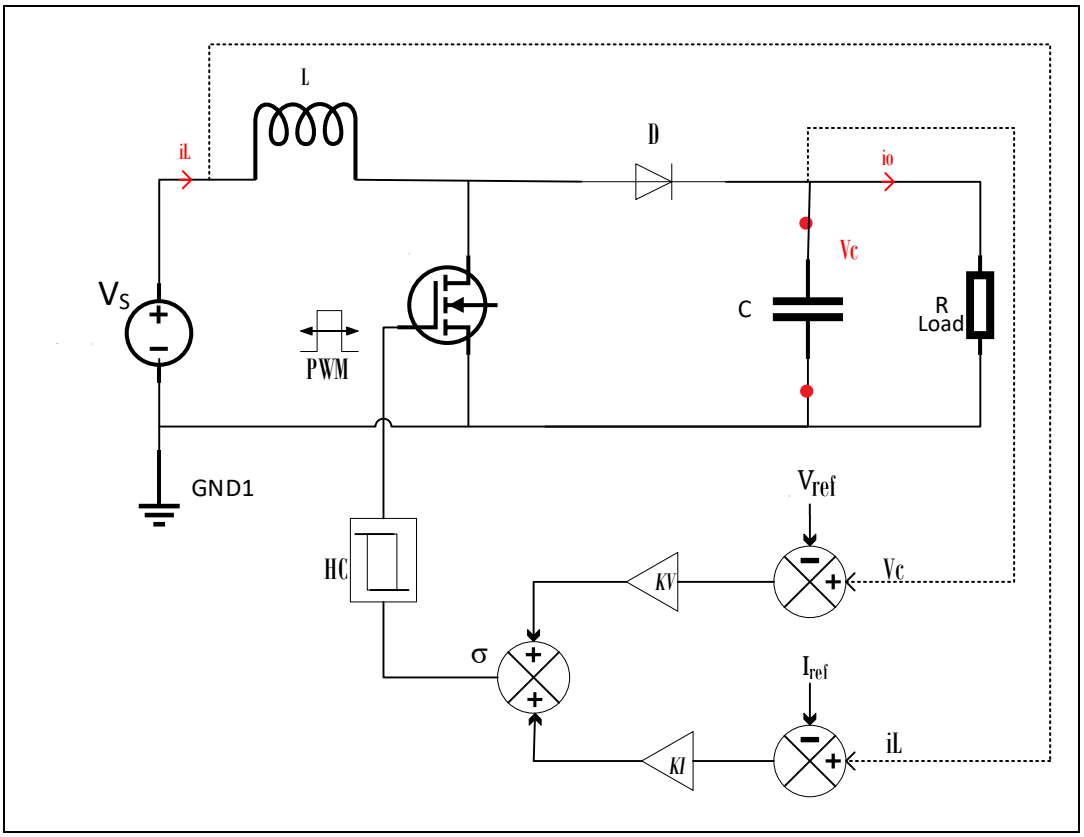

Figure 2.10 Schematic of the Sliding Mode controller
for the DC-DC boost converter

2.2.1.1 State-space modeling of the DC-DC boost converter

In control systems, a state-space representation is a mathematical model of a physical system composed of input, output, and state variables linked by first-order differential equations or difference equations. State variables are variables whose values alter based on the values they have at any given time as well as the values of input variables imposed externally. The values of output variables depend on the values of state variables (Vora, 2020). The state-space modeling fundamental is introduced in equations (2.13) and (2.14),

$$\dot{X} = AX + BU \tag{2.13}$$

$$Y = CX + DU \tag{2.14}$$

- Where X and $\dot{X}$ are the state variable and the differential state variable, respectively;

- U and Y are input and output, respectively;
- A is the system matrix. B and C are the input and the output matrices;
- D is the feed-forward matrix.

DC-DC boost converters including Buck, Boost, and Buck-Boost topologies can be mathematically modeled using state-space modeling approach. Figure 2.11 shows the ON (a) and OFF (b) state equivalent circuits of the DC-DC boost converter.

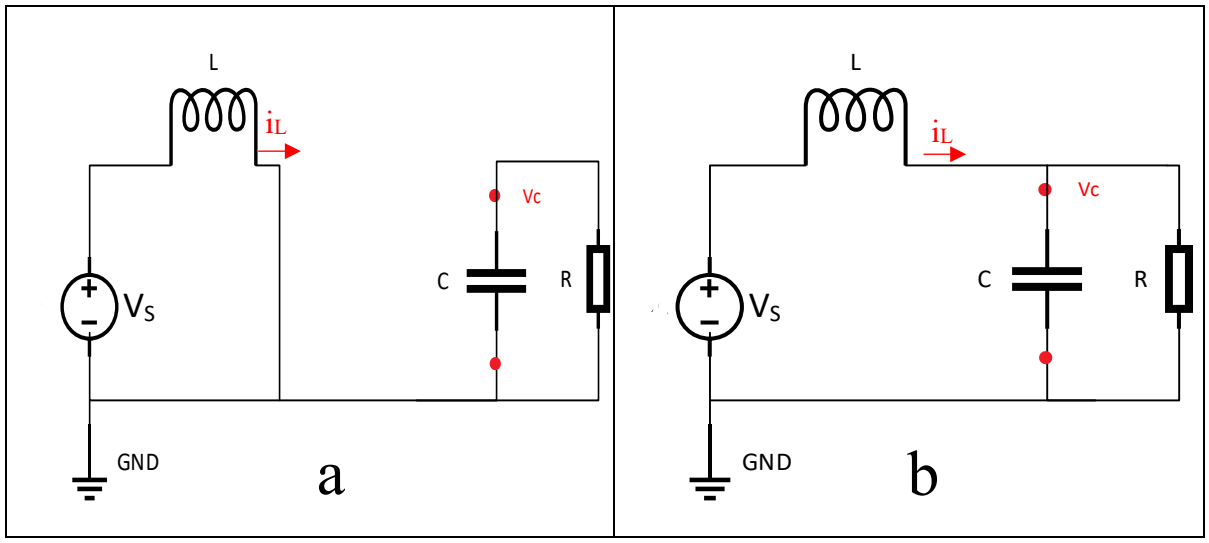

Figure 2.11 a) ON and b) OFF equivalent circuits

In Figure 2.11, the inductor and the capacitor are two storage elements in the proposed boost converter. Hence, the number of state variables is equal to the number of storage elements. The state variables are the current flowing through the inductor (L), and the voltage across the capacitor (C) which is defined by V_C. During the 'ON' state, the inductor is charged via input voltage which is the voltage of the supercapacitor as per Figure 2.11. Consequently, no current flows through the capacitor C and the load R. The equations (2.15) and (2.16) represent the circuit "ON" state.

$$V_S = L\,\frac{di_L}{dt} \tag{2.15}$$

$$0 = C\frac{dVc}{dt} + \frac{Vc}{R} \tag{2.16}$$

The matrix form of equations (2.15) and (2.16) is:

$$\begin{bmatrix} \dot{i_L} \\ \dot{V_C} \end{bmatrix} = \begin{bmatrix} 0 & 0 \\ 0 & -\frac{1}{RC} \end{bmatrix} \begin{bmatrix} i_L \\ V_C \end{bmatrix} + \begin{bmatrix} \frac{1}{L} \\ 0 \end{bmatrix} [V_S]. \tag{2.17}$$

Where $\dot{i}_L$ and $\dot{V}_C$ are the time derivative of i_L and V_C, respectively.

Equations (2.18) and (2.19) represent the boost converter entering the "OFF" state where the current flows through the capacitor C and resistor R (Figure 2.11).

$$V_c = V_S - L\frac{d_i}{d_t} \tag{2.18}$$

$$i_L = C\frac{dVc}{dt} + \frac{Vc}{R} \tag{2.19}$$

the matrix for "OFF" state is:

$$\begin{bmatrix} \dot{i_L} \\ \dot{V_C} \end{bmatrix} = \begin{bmatrix} 0 & \frac{-1}{L} \\ \frac{1}{C} & -\frac{1}{RC} \end{bmatrix} \begin{bmatrix} i_L \\ V_C \end{bmatrix} + \begin{bmatrix} \frac{1}{L} \\ 0 \end{bmatrix} [V_S] \tag{2.20}$$

considering the control input u which is the status of the switch SW_B (u=0 'OFF' state, u=1 'ON' state), the compact form of state equations can be written as follows:

$$\dot{i_L} = -\frac{v_C}{L}(1-u) + \frac{v_S}{L} \tag{2.21}$$

$$\dot{V_C} = \frac{i_L}{C}(1-u) - \frac{v_C}{RC} \tag{2.22}$$

2.2.1.2 The SM Controller parameters

The inductor current error and the capacitor voltage error (Martinez-Treviño et al., 2019) are the state variables for the proposed SM controller shown in Figure 2.10 and equation (2.23).

$$x := \begin{cases} x_1 = i_L - i_{ref} \\ x_2 = V_c - V_{ref} \end{cases} \tag{2.23}$$

Where V_{ref} and i_{ref} are the reference values for the inductor current and the capacitor voltage, respectively. V_{ref} is a constant value which is the desired output voltage of the converter. Instead of having a constant reference current which cannot ensure the output voltage regulation based on the input voltage variation, the adaptive law in POPI converter ($P_{IN} = P_{OUT}$) is used to instantly update i_{ref} according to the input voltage variation (Martinez-Treviño et al., 2019). Therefore, i_{Lref} can be formulated as follows:

$$i_{ref} = \frac{{V_{ref}}^2}{V_S R} \tag{2.24}$$

(σ) is a linear combination of the state variables called sliding function which is expressed in the equation (2.25).

$$\sigma = KIx_1 + KVx_2 \tag{2.25}$$

where KV and KI are positive values referred to as the sliding coefficients that adjusts the controller's response speed. Thus, the control law is stated as follows:

$$u = \begin{cases} 0 & \text{for } \sigma > 0 \\ 1 & \text{for } \sigma < 0, \end{cases} \tag{2.26}$$

A hysteresis controller (HC) implements the control law (2.26), which maintains the sliding function (state trajectory) near zero, leading to the following sliding trajectory:

$$\sigma = KIx_1 + KVx_2 = 0 \tag{2.27}$$

The voltage reference across the capacitor C, V_{ref} is the reference value of the load voltage which can be tuned regarding the input voltage value (V_{SC}) and the gain of the DC-DC boost converter.

2.2.1.3 Condition for the existence of sliding mode control

The following limits expressed in inequality (2.28) direct the state trajectory toward the sliding trajectory and ensure it will not leave the sliding trajectory region which is near the equilibrium point (Spiazzi & Mattavelli, 2018).

$$\begin{cases} \lim_{\sigma \to 0^+} \dot{\sigma} < 0 \\ \lim_{\sigma \to 0^-} \dot{\sigma} > 0 \end{cases} \Rightarrow \begin{cases} \dot{\sigma} < 0 \\ \dot{\sigma} > 0 \end{cases} \text{ when } \begin{matrix} \sigma > 0 \\ \sigma < 0 \end{matrix} \Rightarrow \dot{\sigma}.\sigma < 0, \tag{2.28}$$

where $\dot{\sigma}$ is the time derivative of sliding function σ presented in equation (2.25).

The dynamic of the DC-DC boost converter for both 'ON' and 'OFF' state of converter switch SW_B is required to enforce the limits (2.28) to the equilibrium point. The converter dynamic is presented in the (2.21) and (2.22) equations.

According to equation (2.25) and with respect to the inductor current and capacitor voltage steady state values, $\dot{\sigma}$ will be:

$$\dot{\sigma} = KI\ (\dot{i_L} - \dot{i_{ref}}) + KV\ (\dot{V_C} - \dot{V_{ref}}) \tag{2.29}$$

by substituting equations (2.21) and (2.22) in (2.29), the following equation is originated

$$\dot{\sigma} = \ (KV\frac{i_L}{C} - KI\frac{v_C}{L})(1-u) - KV\frac{v_C}{RC} + KI\frac{v_S}{L} \tag{2.30}$$

Considering the control law in (2.26), and merging it with (2.30) results in

$$(KV\frac{i_L}{C} - KI\frac{v_C}{L})(1-u) - KV\frac{v_C}{RC} + KI\frac{v_S}{L} < 0 \tag{2.31}$$

$$KV\frac{i_L}{C} - KI\frac{v_C}{L} < KV\frac{v_C}{RC} - KI\frac{v_S}{L}, \qquad for\ \mathrm{u} = 0$$

$$-KV\frac{v_C}{RC} + KI\frac{v_S}{L} > 0, \qquad for\ u = 1$$

Therefore, one inequality can be derived as follows:

$$KV\frac{i_L}{C} - KI\frac{v_C}{L} < KV\frac{v_C}{RC} - KI\frac{v_S}{L} < 0 \tag{2.32}$$

The optimal values of KV and KI were obtained through the trial-and-error method. The hysteresis band amplitude and the rate of trajectory change determine the SM controller's switching frequency (Spiazzi & Mattavelli, 2018).

CHAPTER 3

DATA ACQUISITION AND SIMULATION

3.1 Data Acquisition process and parameter estimation

This section explains the process of data acquisition as well as the MFCs' construction principles. The MFC's output power is not steady, and it is changed by the internal parameters of the reactor and the external ambient that MFC is surrounded by. The volatility in the output power of the MFC challenges the PMS performance. Therefore, to evaluate the PMS functionality, realistic MFC data is needed as an input of the PMS.

3.1.1 Laboratory setup

Four membrane-less air-cathode MFCs were fabricated and used in the process of experimental data acquisitions. The anode, which is a 5 mm-thick graphite felt measuring 18 cm × 8 cm four sides, was placed in the MFC reactor (Speer Canada, Kitchener, ON, Canada). The air-breathing cathode for each MFC was 21 cm × 8.9 cm, four sides, included manganese oxide in the act of the oxygen-reducing catalyst (Electric Fuel Ltd., Bet Shemesh, Israel). The advantages of using manganese oxide over a Pt-based cathode include improved MFC long-term performance and cost savings (Li et al., 2010).

The 3D model of the MFC rectangular reactor, is shown in Figure 3.1a (Chassé, 2018). The cathode was attached directly to the outer walls of the MFC in order to be exposed to the air, and the anode to the inner walls, so that the anodic compartment was anaerobic. A polyester piece of cloth was inserted between the two electrodes as an electrical isolation between them. The solid substrate consists of two types of organic matter, humus and peat moss, in equal volume proportion. The two substrates were mixed with approximately 600ml of water until desired consistency. Then the mixture was poured into the cell, filling the entire volume and checking that the material did not leak from the sides. Finally, the MFC was closed with its upper cover by fixing it with screws. The Silicone was then applied to the joints of the stack to

seal them, and a water container with an opening was placed on the lid, so as to ensure the supply of water to the stack at any time. The final assembly of the MFC is shown in Figure 3.1b. Since the MFCs have been harvested from June 2017, as time went by, they generated lower level of power relying only on a primary substrate. To increase the power density of the MFC, 800 mg of sugar as the inlet substrate is added every couple of days (fed-batch mode); and to balance the pH, a 20 mL buffer solution consisting of 21.7g of K_2HPO_4 and 33g of $Na_2HPO_4H_2O$ were also diluted in 100mL of water along with the sugar for each fed-batch cycle.

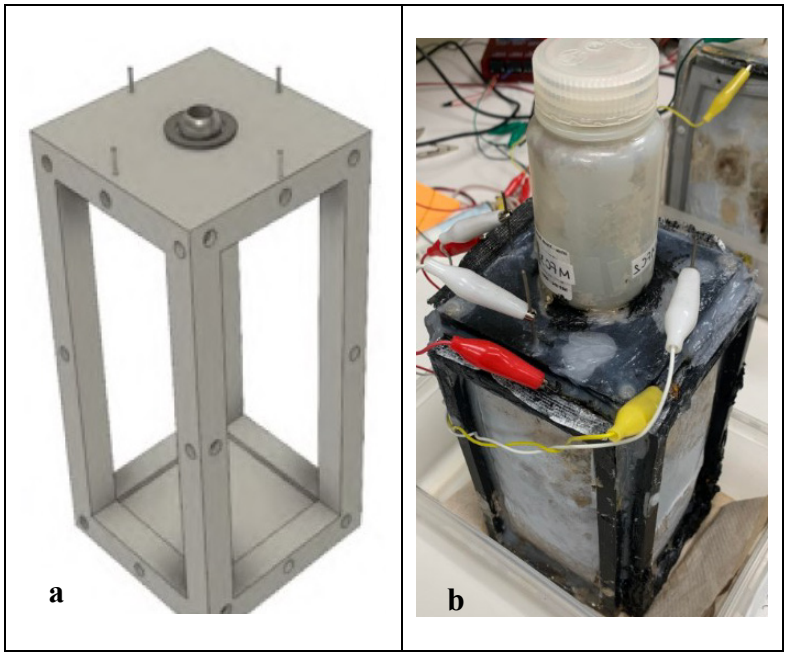

Figure 3.1 (a) 3D model of one MFC (Chassé, 2018)
(b) the final assembly of the MFC

3.1.2 MFC equivalent electrical model

The MFC equivalent electrical model is required to configure the circuit components parameters of MFC. The voltage response of the cell is analyzed to optimize the coulombic efficiency and output power of the MFC. The equivalent electrical model of the MFC used in this work (Coronado et al., 2015), previously discussed in section 1.5.2.1, is shown in Figure 3.2a. The model shown for the i^{th} MFC contains an electromotive force the V_{OC}-i (open-circuit

voltage), solution resistance and activation losses are modeled by R_1-i and R_2-i, respectively. The dynamic behavior of the system is represented by the capacitor C_1-i. In Figure 3.2b, the MFC's output, V_{MFC}, is connected to the resistive load via a single pole, single throw (SPST) toggle switch$_L$.

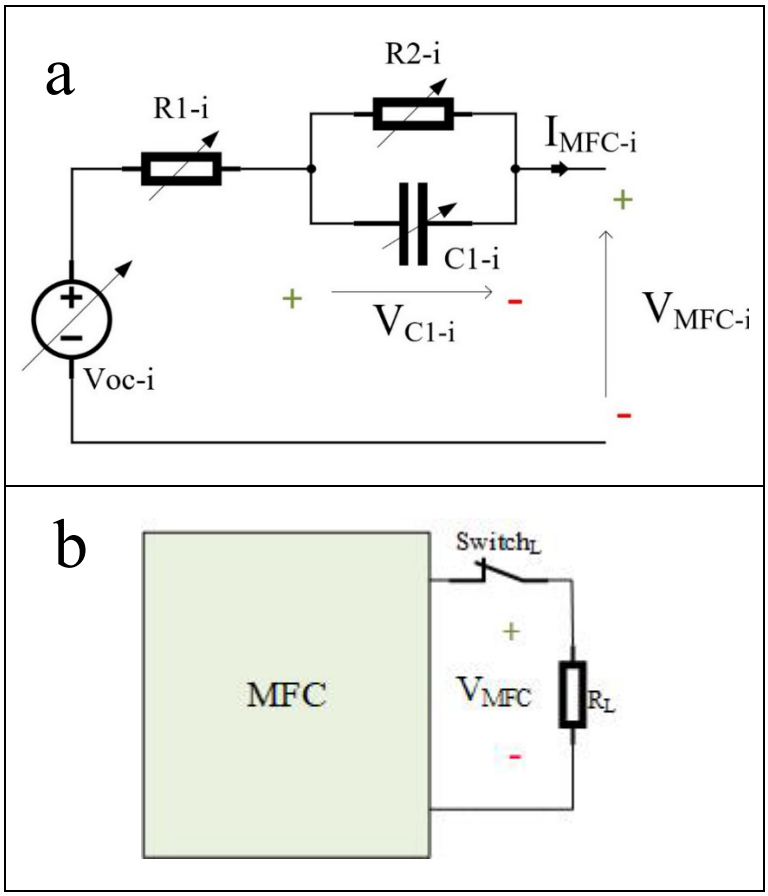

Figure 3.2 (a) Electrical model of MFC$_i$ (b) The MFC$_i$ was connected to R_{load_i} through switch L_i

3.1.3 Offline internal parameter estimation

The equivalent electrical model of the MFC is made up of four parameters (V_{OC}, R_1, R_2, and C) represented in Figure 3.2a. However, it is impossible to directly measure these parameters. The only real data we can collect from the MFC is V_{MFC} represented in Figure 3.3. Therefore, an offline optimization algorithm was developed to estimate the internal parameters of each MFC's electrical equivalent circuit (EEC) model based on the recorded V_{MFC} values from

several experiments. This algorithm was developed using the MATLAB (MathWorks, Natick, MA, USA) optimization Toolbox.

The estimation of MFC's EEC model internal parameters was performed by solving an optimisation problem which aims to minimize the MMSE observed between the MFCs voltage measurements and the voltage output of the EEC model.

The bound constraints and the initial values were defined according to the values presented in Table 3.1. The boundaries were selected by trial-and-error method. The operation was done in MATLAB and by using fmincon function provided by the MATLAB optimization toolbox.

Table 3.1 Lower and upper boundaries of MFC internal parameters used in the optimisation routine

	Voc (V)	R1 (Ω))	R2 (Ω)	C (F)
Initial Values	0.45	7	10	0.7
Lower boundary	0.1	0.2	1	0.001
Upper boundary	0.8	50	200	20

3.1.4 Experimental data processing

The experimental MFC data collected was required for generating a realistic context for the simulation including the PMS, DC-DC boost converter, and the voltage regulation method (SMC). During a period of one month, MFCs' behavior was observed under different ambient conditions including variation in the chemical oxygen demand (COD) (Zhang et al., 2015), water level, and temperature. These conditions were defined in 5 distinct categories represented in Table 3.2. Two full cycles of categories I to IV were recorded during the measurements.

Table 3.2 Different ambient conditions applied to collect the measurements

Order	Starting time of the measurments collected	Duration	Ambient condition
I	Right after feeding	24h	MFCs digesting the freshly added sugary solution (transient condition)
II	One day after feeding	10 days	High COD (Normal operation of MFCs)
III	11 days after feeding	2 days	Low COD, Low water level
IV	14 days after feeding, and 1 day after filling the MFCs with only water	2 days	Low COD, High water level
V	24h after feeding, and 30 minutes after the environmental chamber has settled on the new and increased temperature	1hour	High COD, variable temperature

3.1.5 Experiment conditions

All data was collected from four available MFCs in the lab and then used in the simulation. Before each measurement, each MFC was disconnected from the resistive laod for 45 minutes to estimate the V_{OC}. Then each MFC was connected to a resistive load (Rload=150 Ω) via a SPST (single pole, single throw) toggle switch, shown in Figure 3.2b. According to previous experiences performed in the lab, R_{load} of 150 Ω was observed to be in the range of optimal resistive load for the MFCs. V_{MFC} measurement started when the MFCs were open circuit, then immediately (in a few seconds) the 150Ω load was connected to the MFCs through the mechanical switch and it stayed connected through the entire 15 minutes measurement interval.

The rationale for selecting 15 minutes as the MFCs' measurement period was to ensure the MFCs reached their steady-state. As it is demonstrated in Figure 3.3, after about 550 seconds, the slope of the V_{MFC} curves approaches 0 (Barua & Deka, 2010), indicating that the transient

state of the MFCs was completed and the linear variations in V_{MFC} was due to the slow changes in V_{OC}.

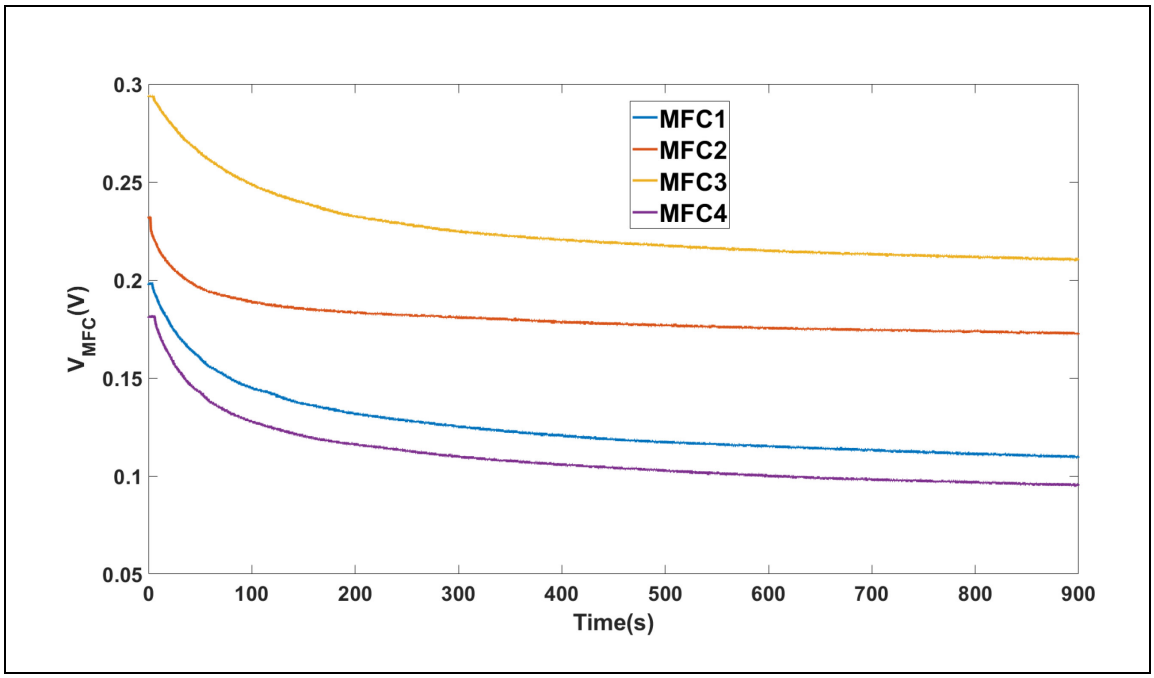

Figure 3.3 V_{MFC} curves in one measurement before and after connecting to their R_{loads} through switches L

More than 400 V_{MFC} measurements for the four MFCS (100 each) were collected. We aimed to run the simulation over the longest possible period in order to evaluate the long-term performance and reliability of the proposed PMS. The order in which the experiments were carried out and duration of each measurement are represented in a block diagram in Figure 3.4.

The low-voltage data acquisition board (Labjack model U3-LV) shown in Figure 3.5 was used to measure the voltage level of each MFC, $V_{MFC,}$ in both on and off states of switch_L. Each set of experimental data points collected from MFC_i was saved to a MATLAB file for further processing and for estimating the internal parameters of MFC_i.

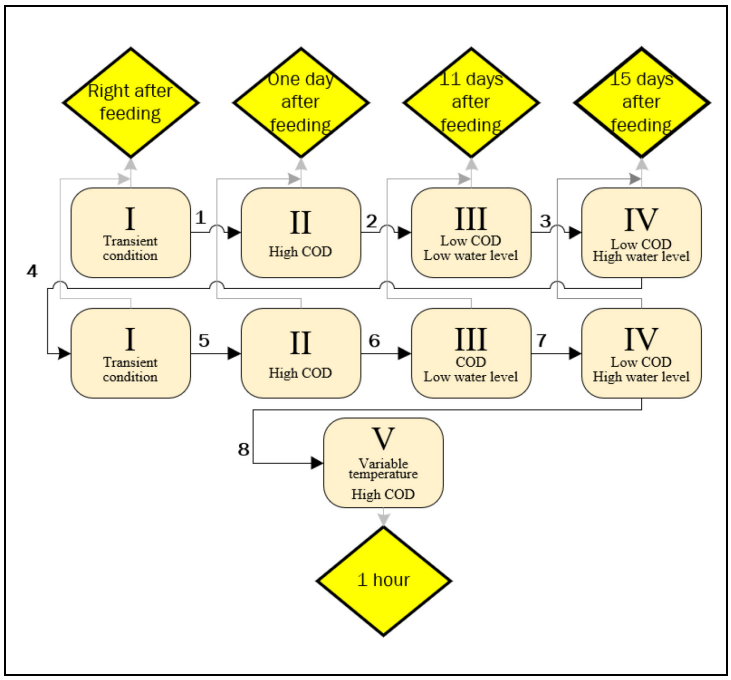

Figure 3.4 Block diagram of data points order (internal parameters) used in the simulation for each MFC according to the measurements in Table 3.2

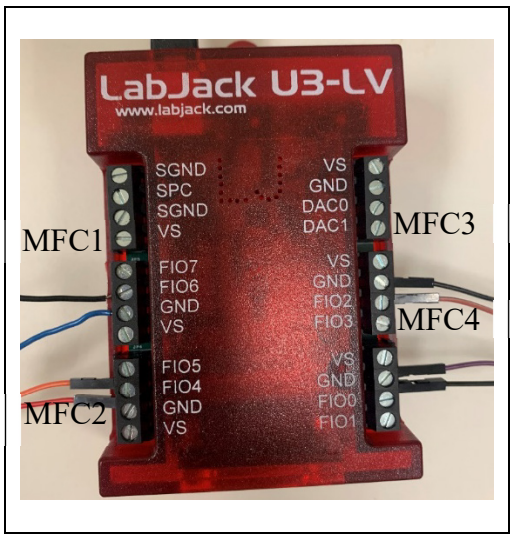

Figure 3.5 Data acquisition board Labjack model U3-LV

3.1.6 Experimental errors and uncertainty

A few experiments were not accurate; therefore, we did not consider and use them in the simulation. In three measurements, due to the unstable electrical connection of the wires, the MFCs were disconnected and reconnected unintentionally. Another inaccurate data was because of the noise and electrical connection/disconnection of the cables attached to the reactor (12 experiments). Hence, the V_{MFC} could not be logged properly. Figure 3.6 shows an example of experimental error that occurred during the measurements. At t_4=6.5 s, MFC_4 was disconnected due to the unstable and weak electrical connection of the wires between the MFCs and its resistive load. However, at t_4=8.19 s, MFC_4 reconnected again until t_4=35.91 s, and then, it was disconnected again for the rest of measurement. The same electrical instability of wire happened to the MFC_3, and it was first disconnected at t_3=3.6 s for about 3 seconds and then was connected to its resistive load at 6.4 s.

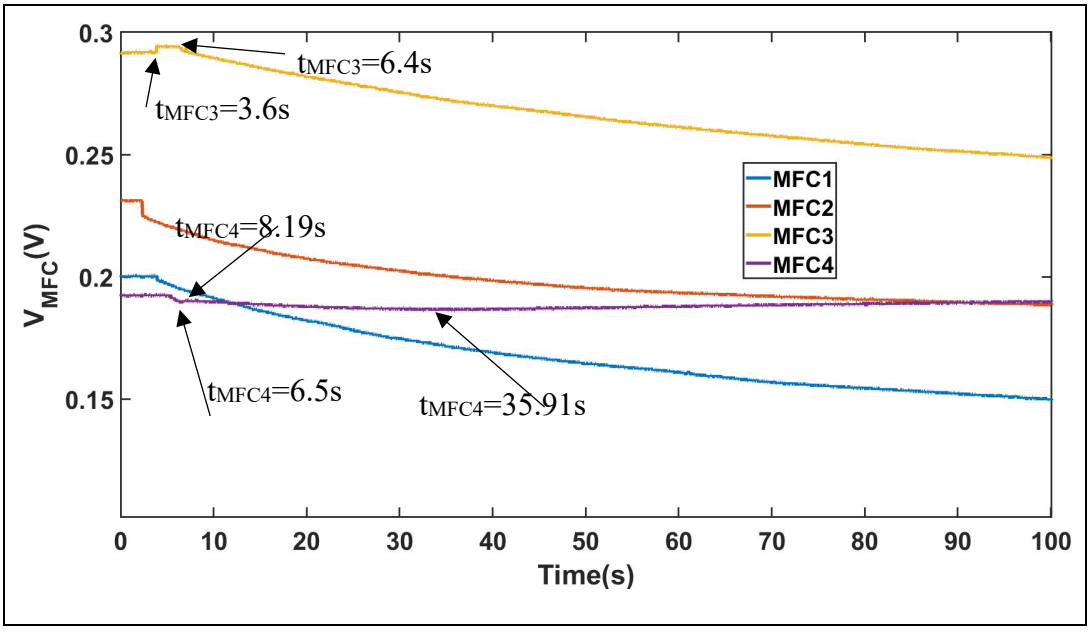

Figure 3.6 An example of experimental error which was eliminated from MFC's sorting data points process

3.1.7 Data point selection

In this section, we aimed to stich the estimated internal parameter values therefore, we can feed them to the simulations and assess the PMS performance based on real-world data collected from the MFCs in different conditions. The selected data were in the same chronological order as the measurements according to the Table 3.2. Only the data with the coefficient of determination (R-squared) R^2>95% were selected and we made sure to include at least two set of data from each category of measurements. The selected estimated parameters (V_{OC}, R_1, R_2, and C) are shown in Figure 3.7. Then, the eligible estimated parameters were selected as data points, however we can only use a handful of these data points (22 data points) as input to our simulation due to computational limits. These data points are going to determine the behavior of the MFCs in the simulation, which will be a good test of PMS performance since the data points are obtained through real-world experiments.

Based on observation from earlier simulations, after each alteration of internal parameters of MFC, about 60 s is enough for the V_{MFC} to be settled. Given this fact and since the longest possible simulation time with the current simulation and system parameters is 1400 s, we chose to have a maximum of 22 data points in each set of data points. From now on these sets of 22 discrete data points 64 s apart that span the whole 1400 s of the simulation are going to be referred to as “Benchmarks”. During the runtime of the simulation, Simulink needs MFC data in between these data points as well, which is why we have decided to interpolate the data for the interval in between these data points. As an example, if R_1 value in t_1=0 s is 7.9 Ω and in t_2=64 s is 7.6 Ω, the value of R_1 at any point between t_1 and t_2 would lie on the straight line connecting these two points. This interpolation serves two purposes, first, it provides a value in a valid range for every increment of the simulation and second, the change in the values of internal elements happen in a more natural and smooth way rather than an abrupt shock.

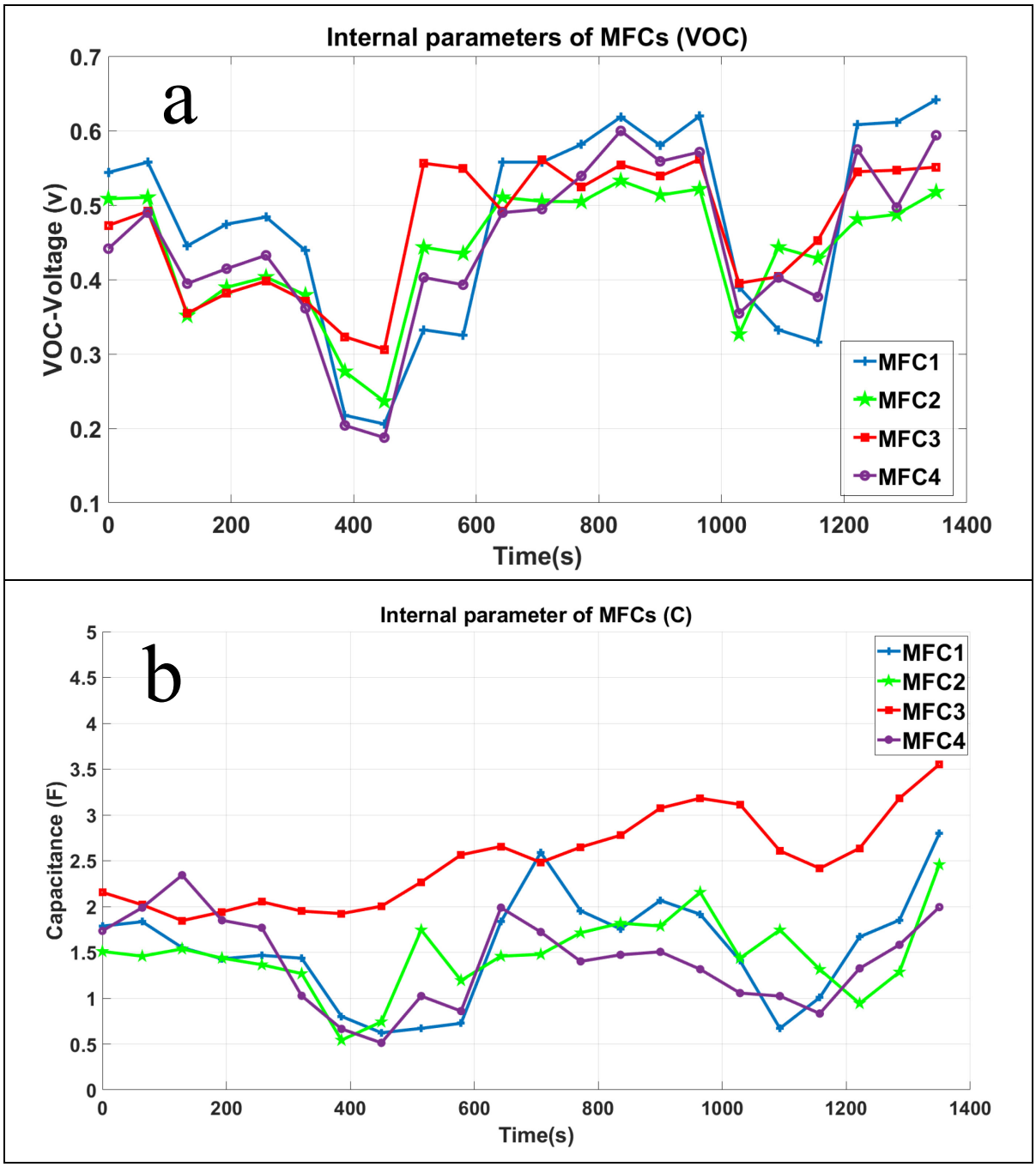
Internal parameters of MFCs (VOC)
a
VOC-Voltage (v)
Time(s)
MFC1
MFC2
MFC3
MFC4
Internal parameter of MFCs (C)
b
Capacitance (F)
Time(s)
MFC1
MFC2
MFC3
MFC4

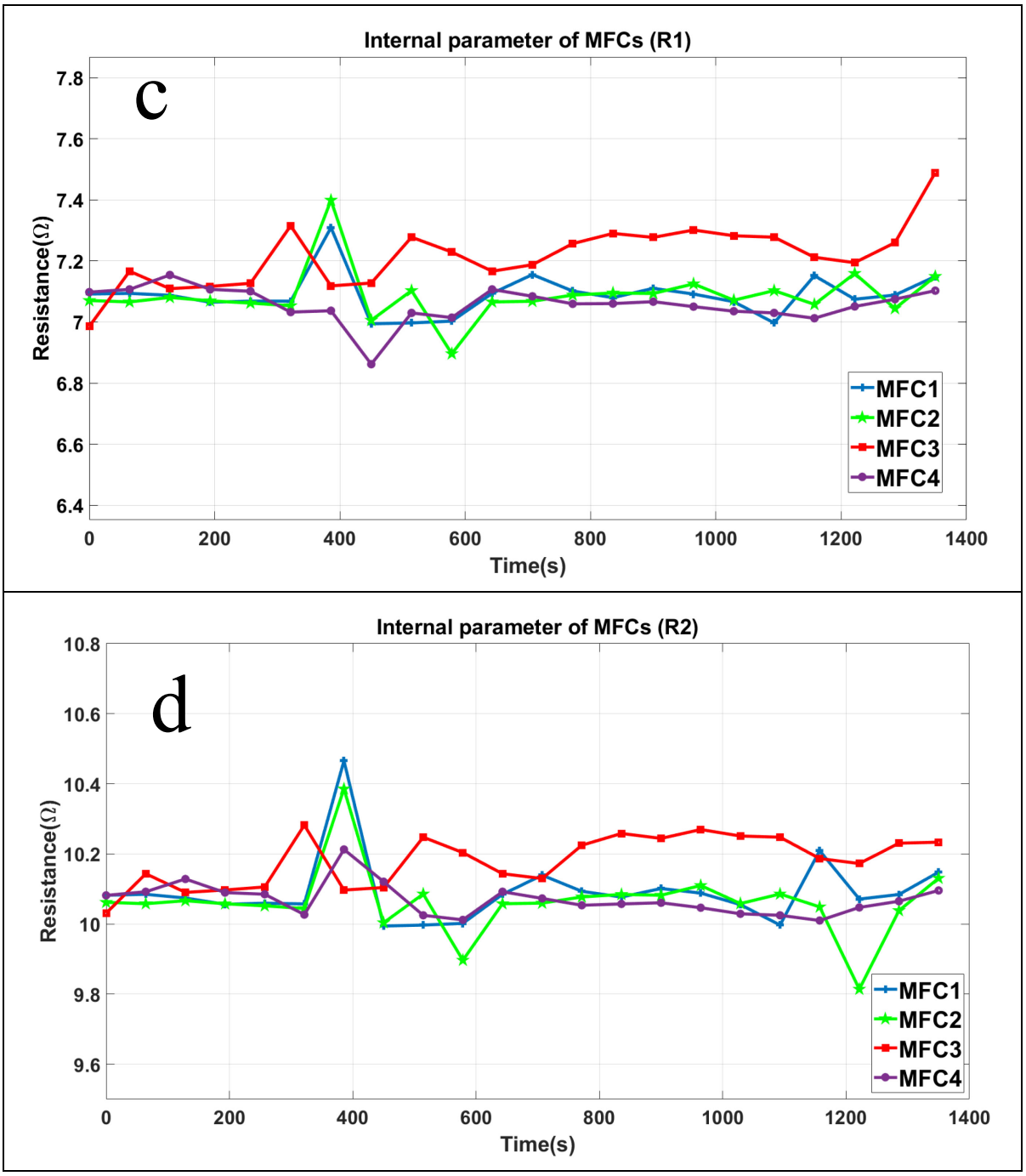

Figure 3.7 Estimated values for the internal parameters of MFCs$_{1\text{-}4}$ (a) V$_{OC1\text{-}4}$ (b) Capacitor$_{1\text{-}4}$ (c) R1$_{1\text{-}4}$ (d) R2$_{1\text{-}4}$ with $R^2 \geq 95$ for each parameter

3.1.8 Benchmark construction

To evaluate the capabilities of the proposed PMS, we need to examine its behavior under different scenarios corresponding to various MFC operational conditions. In order to accomplish a successful testing and comparison system, three benchmarks were devised using the experimental data obtained and processed in 3.1.4.

"Benchmark1" represents a healthy condition for all MFCs and the electrical circuit, where all MFCs are in a healthy voltage range and there are no faults in electrical or electronic elements. Benchmark1 comprises of 22 distinct data point, where each data point consists of the value for the internal elements of all the MFC electrical equivalent circuits. In this study, a stack of four MFCs is used in the simulation, and each one has four internal elements: R_1, R_2, C_{int}, and V_{OC}. The selection process of these data points is explained in detail in 3.1.7. Benchmark 1 serves as the basis of other benchmarks and in other benchmarks only some data points are manipulated to recreate certain MFC behaviors that were not reflected in benchmark 1. In Figure 3.7a, the V_{OC} curves for MFC1-MFC4 is illustrated.

"Benchmark 2" exemplifies a scenario where the V_{OC} of one or more MFCs are lower than the operational point of it, even lower than MFC's voltage in low COD, low water ambient condition described in Table 3.2. To accomplish this scenario, we modified benchmark 1 by lowering down the V_{OC} of MFC 3 to the 0.05 V from data points 6 to 8 for 128s and we named it a critical V_{OC} level, the curve in red in Figure 3.8. The remaining MFCs' data points (1 to 4) maintained the same as of in benchmark 1. The benchmark 2 was set up to assess the functionality of the PMS health-protection algorithm explained in section 2.1.3.

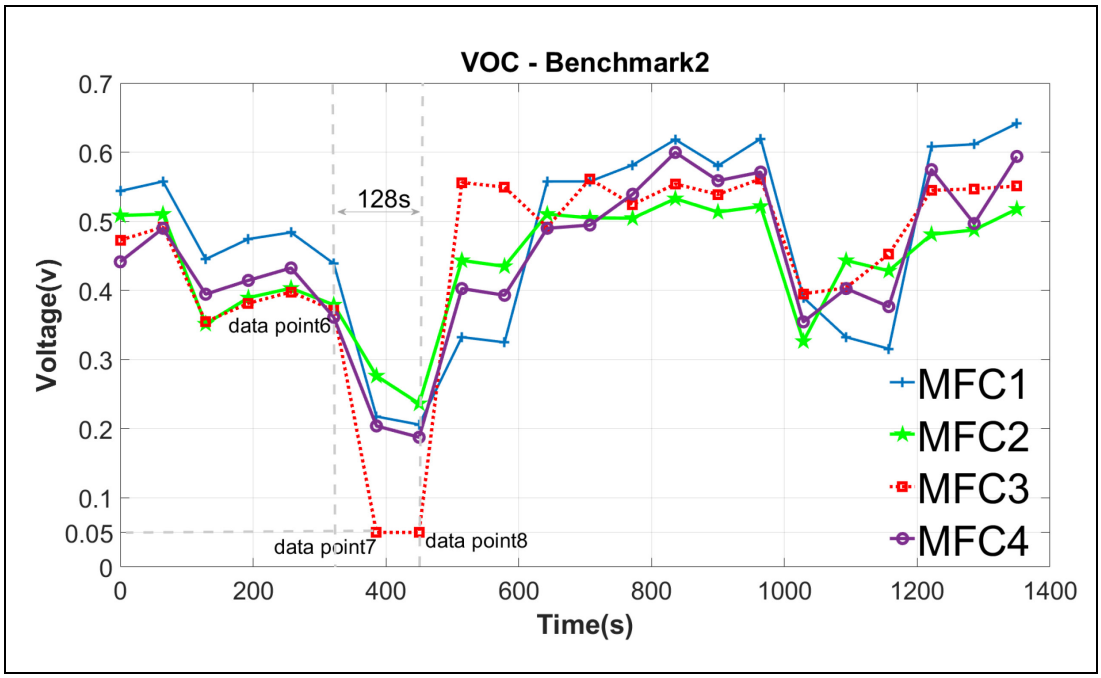

Figure 3.8 V_{OC} of MFCs 1 to 4 where the V_{OCMFC3} was modified and decreased to 0.05V for about 128s from data point 6 to data point 8

"Benchmark 3" resembles an unpredictable and unstable situation in the system input where MFCs are connected and disconnected multiple times from the PMS during the energy harvesting process. The goal to represent this scenario is to examine the PMS performance in the event of unexpected disconnections of multiple MFCs. As it is shown in Figure 3.9, we modified the V_{OC}s to zero between data points 10 and 11 for MFC3, data points 16 and 17 for MFC1, data points 20 and 21 for MFC4, and data point 22 for MFC2. The other data points retained the same according to MFCs' internal parameters in benchmark 1.

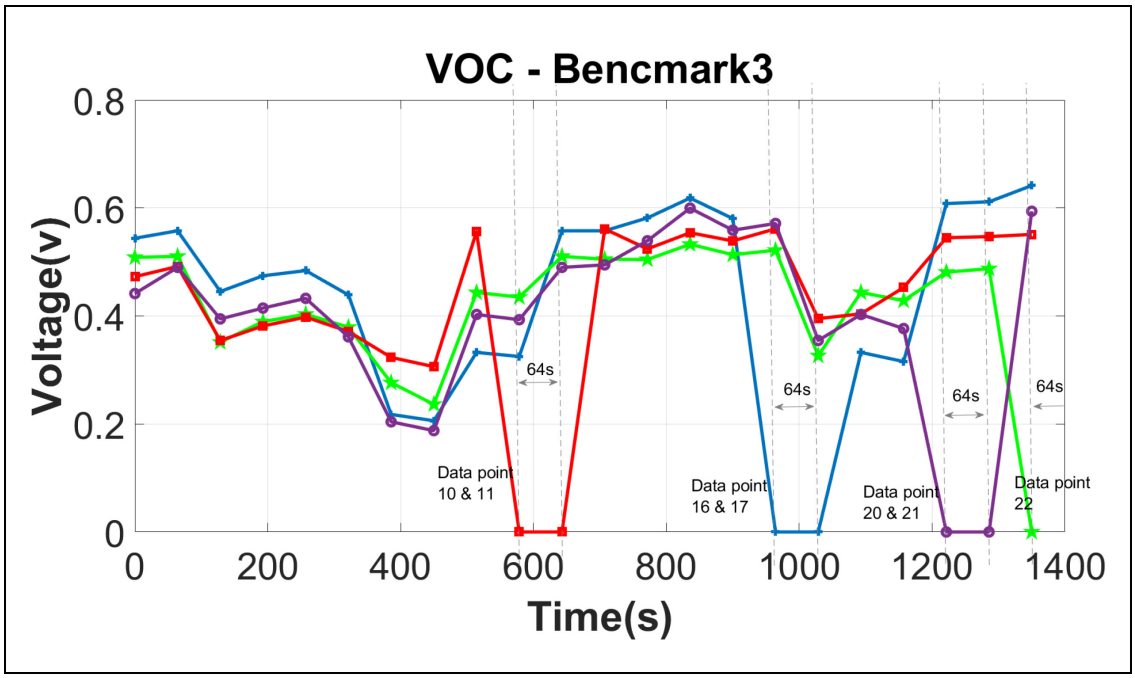

Figure 3.9 V_{OC} of MFCs 1 to 4 are modified to asses the performance of PMS, facing multiple connection and disconnection at the input

3.2 Simulation

Simscape library from MATLAB was used for designing the schematic of the system. Figure 3.10 illustrates the system schematic including electrical model of four MFCs in the lab, PMS, DC-DC boost converter, voltage regulation and R_{load}. Our computers let us select maximum of 1400s as the duration of the simulation and 0.0001s for the sampling time. Longer simulation time helped us comprehensively observe the PMS performance against the MFCs' behavior under different conditions. The PMS consists of capacitors C_i connected in parallel with their MFC_i, two sets of switches M_is and S_is controlled by the PMS algorithm block designed to perform multiple control tasks.

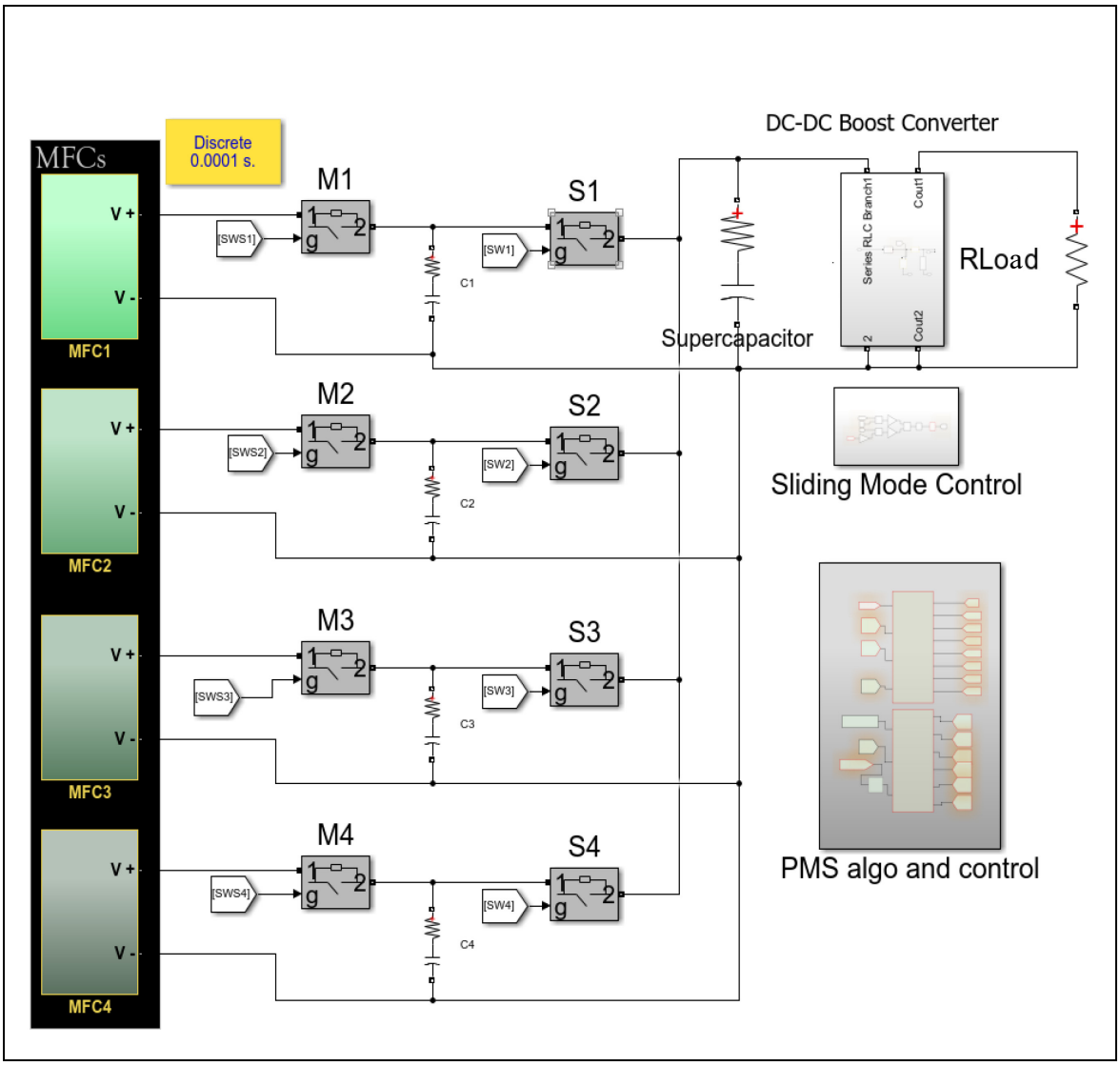

Figure 3.10 Schematic of the system in MATLAB Simulink including MFCs, PMS, DC-DC boost converter, voltage regulation, and Rload

Inside the green blocks, named MFC1 to MFC4, are the equivalent electrical models of the MFCs. The equivalent electrical circuit schematic of MFC_1 block is shown in Figure 3.11. The estimated values were given to the electrical components using MATLAB time-series format by receiving the data from the MATLAB workspace.

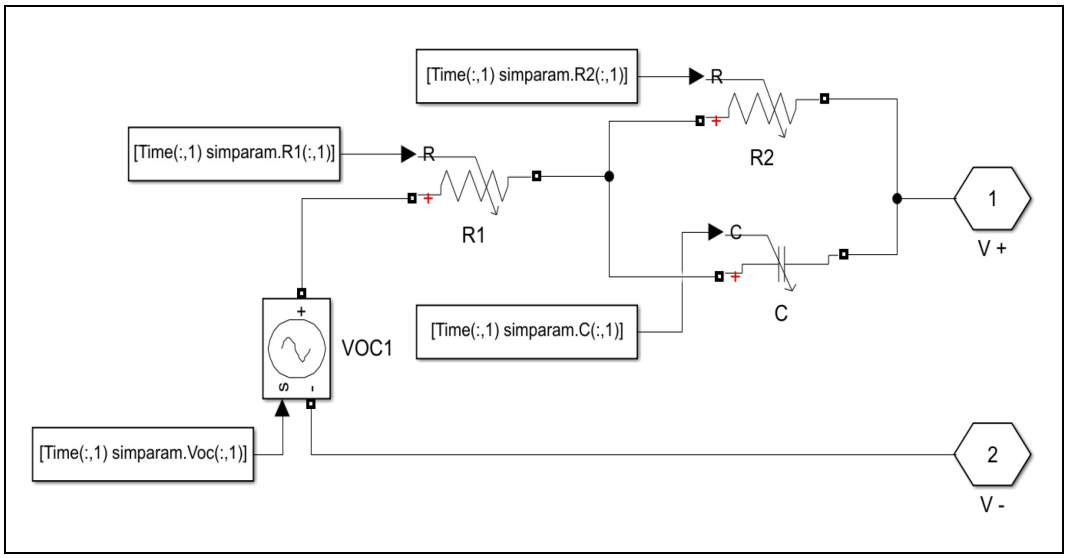

Figure 3.11 The MFC1 schematic of electrical equivalent circuit

3.2.1 Simulation parameter values

The PMS parameters used in the simulation are listed in Table 3.3.

Table 3.3 The proposed power management system parameters used in the simulation

	Switches M1 to M4 S1 to S4 converter	C1-4	SC	L	V_F Diode	C_{out}	R_{Load}
		uF	F	mH	V	uF	Ω
		1000	0.2	50	0.22 v	100	5000
Parasitic resistance (Ω)	300m	400m	1	600m	240m	15m	

Another important parameter for the operation of the PMS is the maximum time a C_i can discharge (T_{d_max}) to the supercapacitor which is discussed in section 2.1.5. For determining this time threshold, different values in the range of [0.0001 s-0.2 s] were tested while other parameters of the PMS were kept constant as presented in Table 3.3. The values within the range of [0.001 s-0.028 s] resulted in optimal power output, however inside this range, no

significant correlation (22%) between the value of the parameter and the output power was noticed. The standard deviation of mean output power while selecting T_{d_max} in the range of [0.001 s-0.028 s], was small as well (σ=6.6%). Having a range to choose T_{d_max} rather than a value can be helpful since it will make the tuning process for future systems easier. It was observed that by using maximum discharge time of 14 ms, the output voltage was the most stable, hence this value was chosen to be used in the rest of the study.

3.2.2 Modelling the MFC's recovered voltage

While MFC units were disconnected from the energy harvesting process, their voltage increases gradually. This phenomenon can be partly understood on explained by the electrical equivalent circuit of MFC, where after disconnection of the external capacitor, internal capacitor starts to dissipate its voltage on the R_2 resistor and therefore the V_{MFC} voltage gets closer to the V_{OC} value. The other justification of this increase in V_{MFC} voltage is originated in the biological aspect of the MFC where the microorganisms recover and produce a higher potential difference between anode and cathode. While the electrical justification affects the voltage immediately in a matter of a second, the biological recovery has a much slower dynamic and takes minutes to hours to show its effect.

To incorporate the recovery phenomenon in the simulation, it needed to be modeled based on real data. Multiple measurements were conducted to retrieve and duplicate the behavior of the MFC after it has been disconnected from the load (Figure 3.2). Once the $switch_L$ opens, measurement starts and tracks the voltage of the MFC for a long period (16 h-21 h) to show the short electrical response and longer biological response of the MFC. The same measurement was then repeated in different ambient and internal conditions. The gathered voltage curves were linearly fitted, and the slope was averaged between different measurements to form a single line. This linear growth of the voltage was used in the simulation to imitate the voltage recovery. The intervals where the recovery can be observed in the course of simulation are pretty short (seconds or a few minutes), which is why a linear growth adequately represents the recovery phenomenon. The slopes of these lines were then

averaged to obtain the final VOC recovery trendline for each MFC, formulated in equations (3.1) and (3.2).

$$\mathrm{m}_i = \frac{\Delta V_{OC_i}}{\Delta \mathrm{t}_i} \tag{3.1}$$

$$m_{average} = \frac{\sum_1^k m_i}{k} \tag{3.2}$$

where $\Delta \mathrm{t}_i$ is the time period where V_{OCi} is being recovered, ΔV_{OC_i} is the total increase of V_{OCi} during the recovery period, m_i is the slope, and k is the number of set of measurements for each MFC.

3.3 Results

3.3.1 Benchmark 1 tests, results, and discussions

According to the equations (2.10) to (2.12), the efficiency and the boost ratio of the DC-DC boost converter used in this study are affected by the duty cycle, the switching frequency of the boost converter (f) as well as the inductor value. Different values of inductor were given to the converter in order to obtain its optimal operational point, as listed in Table 3.4. In this table, L is the inductor value, $P\text{-}MFC_{ave}$ is the average output power of the MFCs, $P\text{-}IN_{ave}$ is the average input power of the DC-DC boost converter, η_1 and η_2 are respectively the efficiency values for the converter and the overall system. $P\text{-}load_{ave}$ is the average power of the load during the course of simulation, which is the total energy dissipated at the load divided by time. The same parameters are used to show the performance of PMS in different conditions in all tests and tables in the following sections (3.3.2 to 3.3.4).

Table 3.4 Simulation results of the proposed system for benchmark 1, using two-level voltage reference (6.3 V, 2.5 V) for different values of L

L	Parasitic Resistance	P-MFCs (ave)	P-IN (ave)	P-load (ave)	$\eta_1 = \frac{P_{load}}{P_{IN}}$	$\eta_2 = \frac{P_{Load}}{P_{MFCs}}$
(H)	(Ω)	(mW)			(%)	
0.001	0.3	12	3.92	0.155	3.95%	1.29%
0.005	0.4	9.7	7.38	2.86	38.75%	29.48%
0.0075	0.45	9	7	3.46	49.43%	38.44%
0.01	0.4	8.29	6.54	3.77	57.65%	45.48%
0.03	0.55	8.49	6.69	4.96	74.14%	58.42%
0.04	0.6	8.65	6.8	5.07	74.56%	58.61%
0.05	0.6	8.71	6.83	5.16	75.55%	59.24%
0.06	0.61	8.74	6.81	5.21	76.51%	59.61%
0.07	0.63	8.79	6.85	5.245	76.57%	59.67%
0.1	0.65	5.77	4.66	3.84	82.40%	66.55%
0.3	0.7	5.1	4.32	3.5	81.02%	68.63%
0.8	1	3.37	2.47	2.1	85.02%	62.31%

The maximum $P_{load_{ave}}$ was 5.245 mW for L=0.07 H. However, the smoothest regulated voltage observed across the R_{load} was obtained for L=0.05, with $P_{load_{ave}}$ of 5.16 mW and the efficiency of 76% for the converter and 60% overall (Figure 3.12). Due to the high volatility in the converter's input voltage (V_{SC}), if the load voltage reference is set to a relatively high value in the SMC configuration, the converter may fail to regulate voltage when the input is low. This failure to regulate the voltage, can cause instability and divergence in voltage regulating process (SMC) and eventually stop the energy delivery to the load. On the other hand, choosing a relatively low load voltage reference in the SMC can limit the output power

in case of a resistive load. Hence, to avoid limiting power efficiency, a two-level load voltage reference was applied to the voltage regulator (SMC) which are switched according to the variations in the converter input voltage. For instance, if the voltage reference is adjusted to 5 V, when the V_{SC} value drops below the maximum boost ratio of the DC-DC boost converter, the converter would not be able to boost the voltage to the reference voltage of the SMC. As a result, a power interruption will occur at the output. To address this issue, a two-level voltage reference was defined for the voltage regulation in this series of tests (6.3 V and 2.5 V). This strategy aids the PMS in delivering more power to the load without experiencing disruption. In addition, a single-level voltage reference was also defined and used for the voltage regulation in order to observe and compare the system parameters such as input and output power for both single and two voltage reference levels. As an example, in Figure 3.12, the V_{SC} was not high enough, and the converter could not keep boosting the voltage around the upper level of voltage reference during the "t_1" interval. As a result, the SMC selected the lower voltage reference level at 2.5 V for "t_1" interval, and the load voltage dropped to this level. In this study, we aim to harvest the maximum power with regard to the load regulated voltage quality (less disturbance) and called this condition 'optimal'. The optimal point of the system was obtained for L=0.05 H.

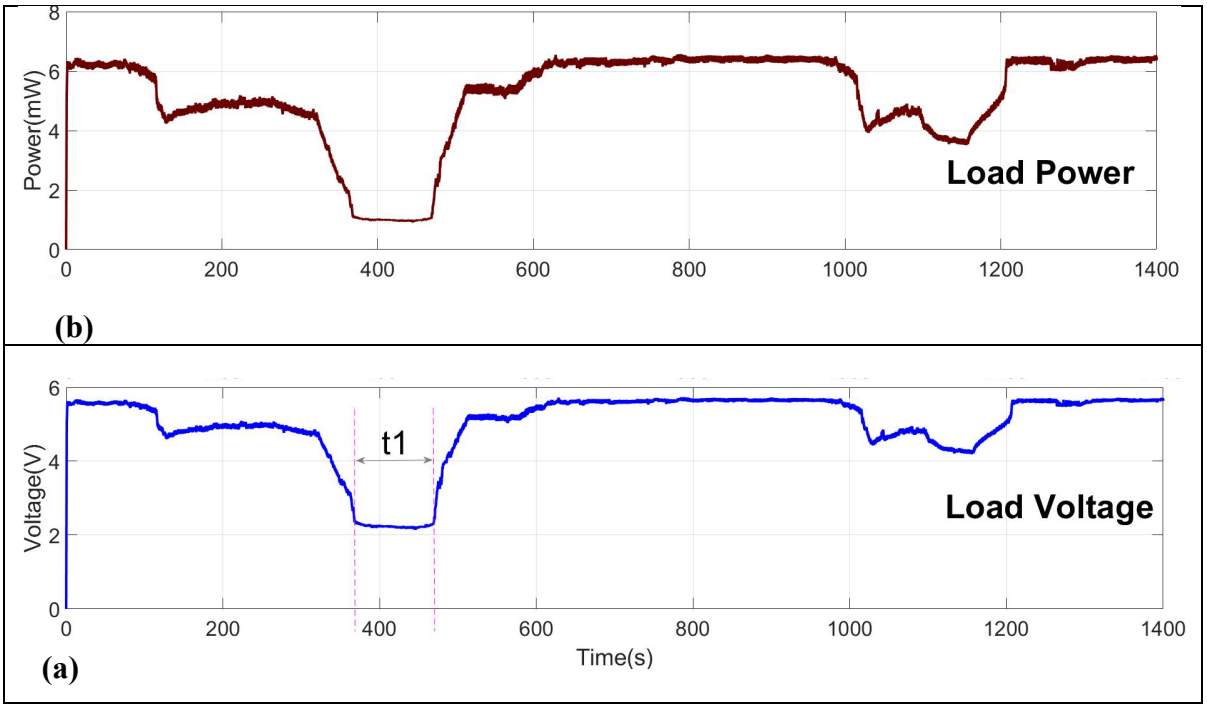

Figure 3.12 Benchmark 1 results, The load optimal parameters after identifying L=0.05$_H$, using two-level voltage reference (a) Voltage of electrical load (R_{load}) (b) $Pload_{ave}$

In another set of tests, only single-level voltage reference was applied to the SMC. Different values were inputted as the load voltage reference to compare its effect on the $Pload_{ave}$. The average output power the PMS delivered to the load was evaluated at 1.5 mW (Figure 3.13a) where the voltage reference was adjusted to 3 V and the load voltage did not show any significant distortion (Figure 3.13b). According to Table 3.5, in the optimal operation of the converter, the voltage reference of 3 V had the highest converter efficiency of 81.12% among all tests and an overall system efficiency of 63.61%. Therefore, both the converter and overall system efficiencies improved by 7.4% under a single-level voltage reference when compared to a two-level voltage reference. In addition, the $Pload_{ave}$ in two-level voltage reference was 3.44 times higher than its value in single level. This test demonstrates that by using two levels of voltage regulation, the PMS is able to harvest significantly more energy from the MFCs. Additionally, the system does not experience load interruptions when the input voltage is low.

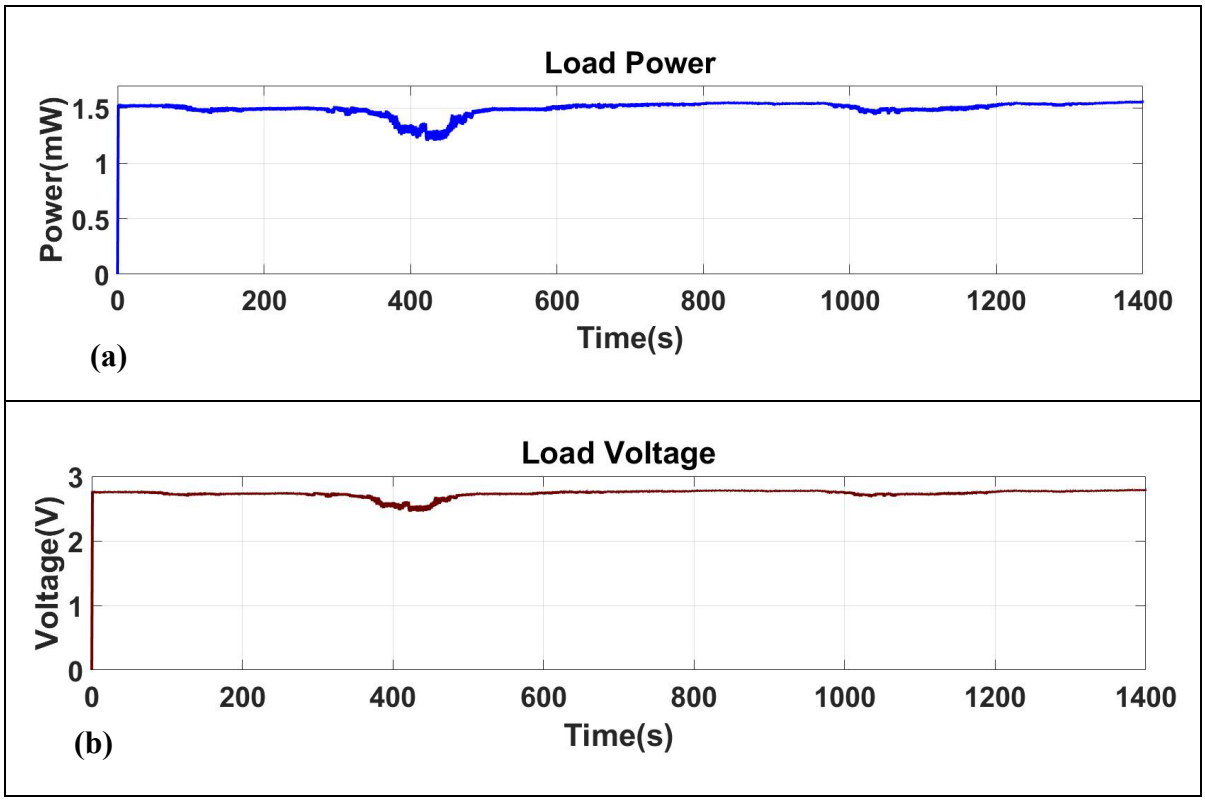

Figure 3.13 Benchmark 1 results, The load parameters after identifying L=0.05H, and considering single-voltage reference for the SMC (a) Load power (b) load voltage

Table 3.5 Simulation results of the proposed system for benchmark 1, using single-voltage references

L	Parasitic Resistance	Voltage Reference	Vload	P-MFCs (ave)	P-IN (ave)	P-load (ave)	$\eta_1 = \frac{P_{load}}{P_{IN}}$	$\eta_2 = \frac{P_{Load}}{P_{MFCs}}$
(H)	(Ω)	(V)		(mW)			(%)	
0.05	0.6 ohm	2.8	2.51	2.15	1.56	1.23	78.85%	57.21%
		2.9	2.65	2.21	1.73	1.405	81.21%	63.57%
		3	2.74	2.358	1.84	1.5	81.12%	63.61%
		3.2	2.58	3.27	1.97	1.46	74.11%	44.65%

3.3.2 Benchmark 2 tests, results, and discussions

Figure 3.14 presents the curves of V_{OC3} (in blue), VcL_3 (in red), and Vc_3 (in yellow). In this test, the PMS disconnected C_3 and MFC_3 at point A (V_{Low} = 0.08 V) until the VcL_3 reached point B (V_{High} = 0.15 V). As demonstrated in Figure 3.14 during this time interval (from point A to B), the MFC_3 was recovering. After the VcL_3 reached V_{High}, the PMS let the MFC_3 be connected to the energy harvesting process again. This test demonstrates the viability of the PMS health protection mechanism by preventing the weak MFC from participating in the energy harvesting process. The PMS then monitor the real-time V_{OC} of the weak MFC to be notified when the V_{MFC} is recovered and then connects it to the system again. This method uses hysteresis control to make reconnection decisions. The simulation results are listed in Table 3.6.

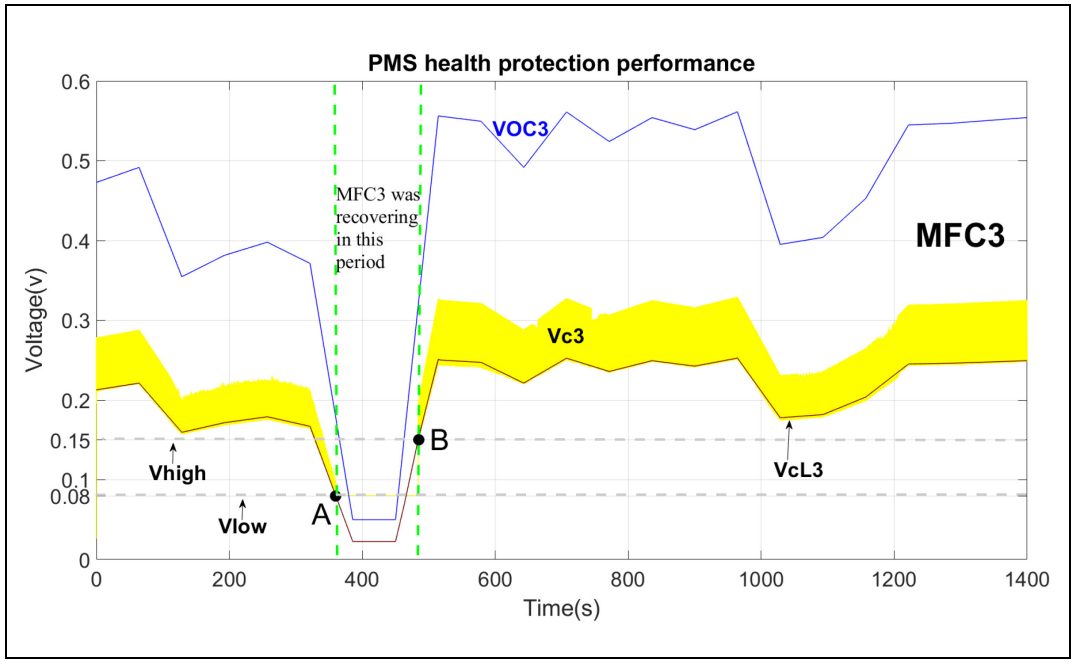

Figure 3.14 Vc_3 in yellow and its charge and discharge curve. C_3 is disconnected when VcL_3, became lower than the PMS's V_{Low} (point A), and reconnected when its VcL_3 reached V_{High} (point B)

The load average powers and voltages curves are shown in Figure 3.15 in both modes of single and two-level voltage reference. Since the voltage of MFC1, MFC2, and MFC4 were low

between point A and B, and also the V_{OC} of MFC3 converges to zero in this time interval (Figure 3.8), the converter could not boost the input voltage and transfer the power to the load. This can simply be avoided by selecting a lower voltage reference, explained in the following section. For the rest of the simulation, the PMS managed to harvest the power from the MFCs and delivered it to the load in both single and two voltage reference modes.

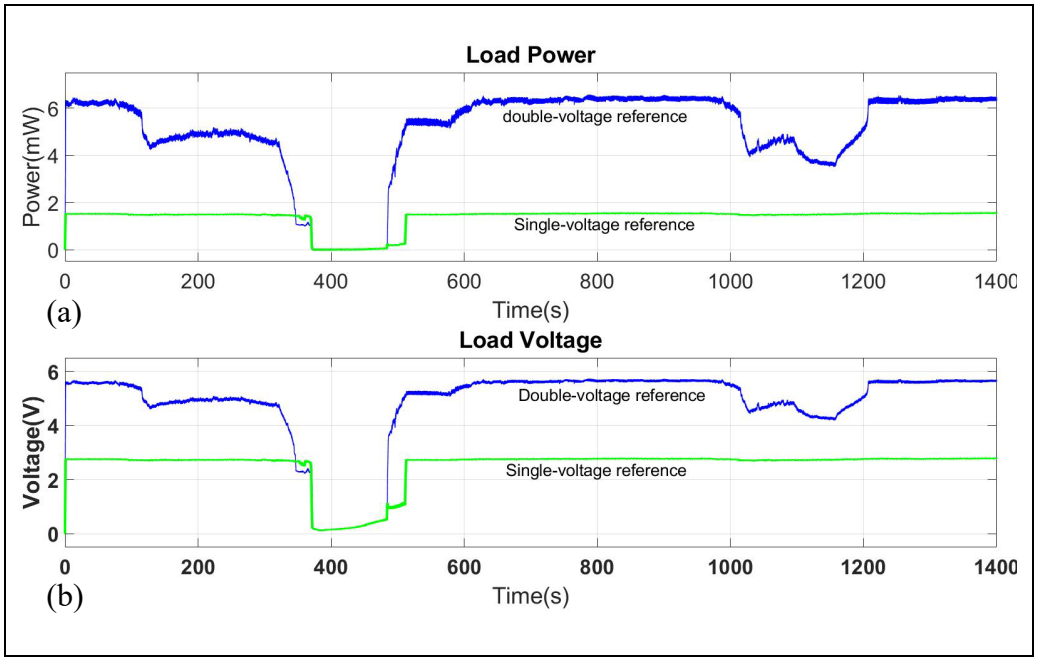

Figure 3.15 Benchmark 2 results, $Pload_{ave}$ (a), and Vload curves (b) using single (curves in green), and two (curves in blue) level of voltage reference

Table 3.6 Simulation results according to benchmark 2

voltage reference	P-MFCs (ave)	P-IN (ave)	P-load (ave)	$\eta_1 = \frac{P_{load}}{P_{IN}}$	$\eta_2 = \frac{P_{Load}}{P_{MFCs}}$
(V)	(mW)			(%)	
Two-level 6.3, 2.5	8.6	6.6	5	75.76%	58.14%
Single 3	2.43	1.73	1.37	79.19%	56.38%

3.3.3 Benchmark 3 tests, results, and discussions

The simulation results for this benchmark demonstrate that the PMS could harvest energy without interruption despite the occasional disconnection of the MFCs. Figure 3.16 shows the voltage of C_i for the four MFCs in the stack. When one C_i was unable to charge the supercapacitor because the MFC_i was disconnected from the system, the other capacitors continued to be charged by their corresponding MFCs and discharged to the supercapacitor in chronological order.

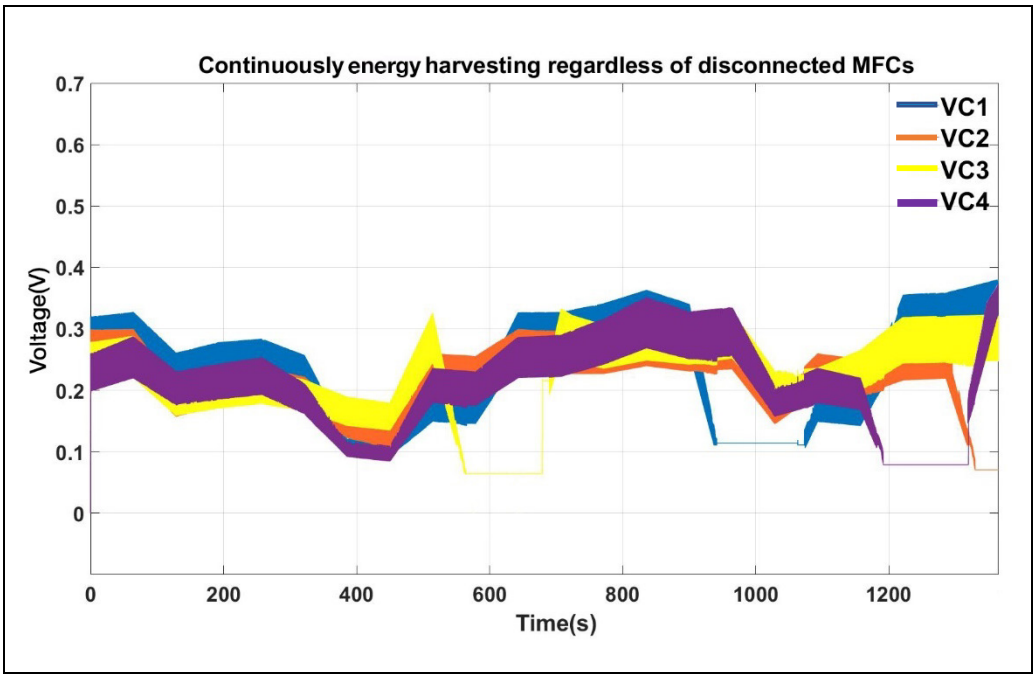

Figure 3.16 C_is voltage and their charge and discharge curves when the MFCs were disconnected from the PMS at different time intervals

Having the MFCs' V_{OC} set to zero for 256 s of the simulation period prevented the converter to continue boosting the supercapacitor voltage efficiently to the upper voltage reference value (6.3V) in the two-level voltage reference mode. As a consequence, a load voltage disturbance was noticed (Figure 3.17 Benchmark 3 results, curves in red). Although the SMC maintained the duty cycle around 96%, resulting in the converter voltage boost ratio around 10, the very low input voltage of the converter hinders it from boosting the voltage to the predefined voltage reference's upper level (6.3 V). While decreasing this voltage reference results in reduction in

the output power, there will be minor disturbances in the load voltage, and also the efficiency will improve. There is a trade-off between the required load power, the voltage boost ratio, the quality of the load voltage, and the system efficiency.

Therefore, in the second simulation, the upper voltage reference was lowered to 5 V while the lower voltage reference was maintained at a constant 2.5 V in both simulations. The converter effectively boosted the input voltage without any load voltage disturbance noticed. (Figure 3.17 Benchmark 3 results, curves in blue). According to the Table 3.7, the $Pload_{ave}$ dropped by 18% from 5 mW to 4.1 mW while the overall efficiency of the system improved by 7% from 58% to 62%.

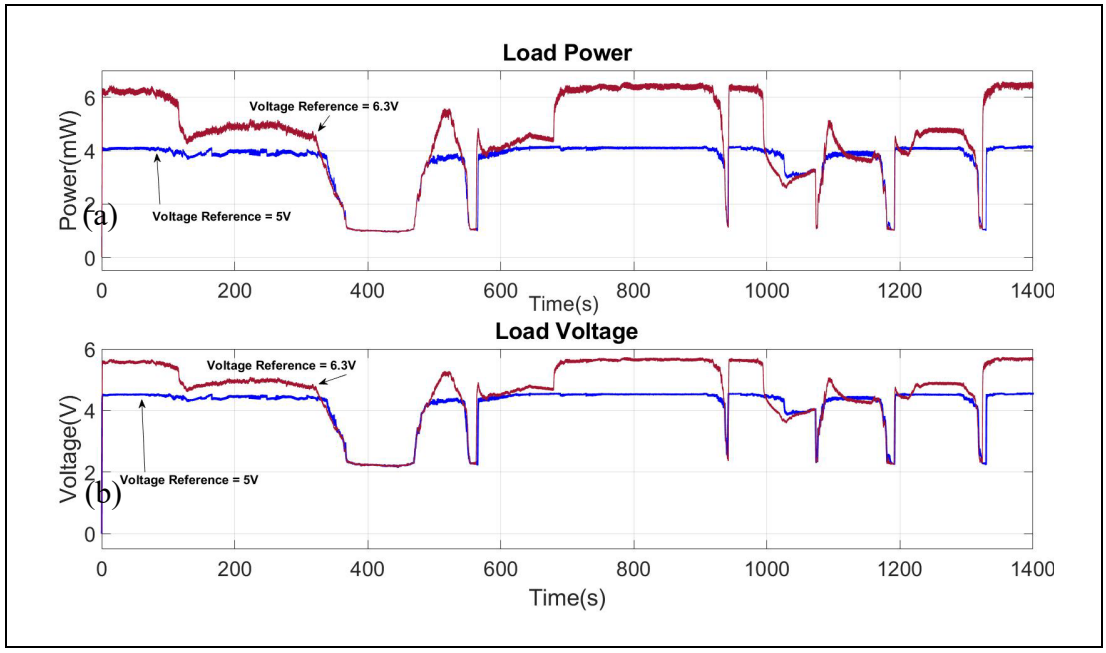

Figure 3.17 Benchmark 3 results, (a) $Pload_{ave}$ (b) V_{load} curves using 6.3 V (the red curves) and 5 V (the blue curves) for the upper level of voltage reference while the lower level of voltage reference kept constant at 2.5 V

The subsequent test was carried out for the single-level voltage reference mode (3 V). Figure 3.18 demonstrates that the quality of voltage regulation was decent, despite having multiple MFCs connection and disconnection. The proposed PMS could successfully transfer uninterrupted power to the load while there were significant irruptions in the system input. In

certain periods of the simulation, the voltage difference among V_{OC} of MFCs was observed as high as 0.6 V. In one example, starting from 1200 s, $V_{OC\text{-}MFC1}$ reached 0.6 V while $V_{OC\text{-}MFC4}$ was 0 V. However, the load voltage was regulated near 3 V at this moment, making the proposed PMS a reliable choice for the applications demanding uninterrupted power source. In this test, the $Pload_{ave}$ was obtained 1.5 mW with the highest converter efficiency of 81%. The simulation results for this test are demonstrated in Table 3.7.

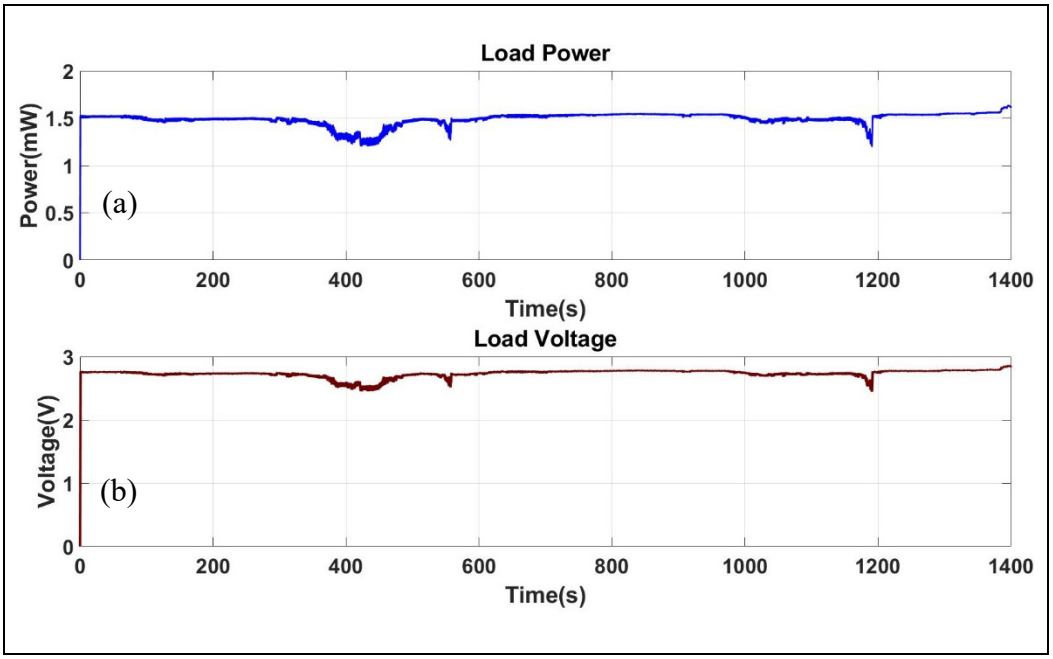

Figure 3.18 Benchmark 3 results, (a) $Pload_{ave}$, and (b) Voltage curve utilizing single-level voltage reference, 3V

Table 3.7 Simulation results according to benchmark 3

Voltage Reference	P-MFCs (ave)	P-IN (ave)	P-load (ave)	$\eta 1=\frac{P_{load}}{P_{IN}}$	$\eta 1=\frac{P_{Load}}{P_{MFCs}}$
(V)	(mW)			(%)	
6.3v, 2.5v	8.6	6.6	5	75.76%	58.14%
5v, 2.5v	6.74	5.25	4.1	78.1%	60.83%
3v	2.38	1.85	1.5	81%	63.03%

3.3.4 Comparison of proposed and a previous PMS

In this section, we applied benchmarks (1 to 3) to the PMS proposed by Nguyen et al. (2019), which was previously designed in our lab, and explained in section 1.7.1 of the literature review. A comparison of the proposed and Nguyen et al. (2019) studies was conducted after. From here on, Nguyen et al. (2019) study will be abbreviated as "CL". In order to have a reliable comparison, this time, we changed and adjusted our proposed PMS parameters values equal to the CL's PMS parameter values, listed in Table 3.8. In the converter block, the duty cycle and frequency of the DC-DC boost converter switch remained leveled at 0.7 and 100_{Hz}, respectively and without implementing the voltage regulator for both PMSs. Different values of L were given to the converter in benchmark 1, in order to obtain the maximum and optimal power input and output, listed in Table 3.9 L = 0.25 H in the CL converter block and L = 0.016 H in ours yielded the optimal operating point for both PMSs, which was also used for the benchmarks 2 and 3.

Utilizing benchmark 1, the $Pload_{ave}$ (highlighted in green) was quite similar for both PMS (4.75mW for the proposed PMS and 4.78 mW for CL PMS). The average power produced by the MFCs for the proposed PMS was 14% more than the CL PMS, 8.15 mW and 7.15 mW, respectively. The system's overall efficiency for CL PMS obtained 14.7% more compared to the proposed PMS (66.89% and 58.33%, respectively), considering the comparison was conducted using CL PMS parameters values.

The maximum power generated by the MFCs for the proposed and CL PMS were 12.23 mW and 10.15 mW, respectively. As a result, the proposed PMS could obtain 20.5% more power from the MFCs than CL PMS (highlighted in purple). The maximum $Pload_{ave}$ obtained for the proposed and CL PMS were respectively 5.65 mW and 4.78 mW, 18.2% greater than CL for the proposed PMS. The system's maximum efficiency was comparable to that of the proposed (83.17%) and CL PMS (81.84%), a few percent more for the proposed PMS. The $Pload_{ave}$

values were also similar in the maximum efficiency (1.46 mW for the proposed, and 1.55 mW for CL PMS).

In benchmark 2, the CL PMS could deliver 14.2% more power to the load than the proposed PMS, 4.75 mW and 4.16 mW, respectively. In this benchmark, the MFC health protection feature of the proposed PMS was activated approximately for 200s for MFC3 and prevented it from being connected to the energy harvesting process during this period.

Table 3.8 CL PMS parameter values were used in the proposed PMS to have a reliable comparison

	Switches M1 to M4 S1 to S4 $S_{converter}$	C1-4	SC	$V_{F\text{-}Diode}$	C_{out}	R_{Load}
		(uF)	(uF)	(V)	(uF)	(Ω)
		3000	1000	0.21	2000	5000
Parasitic resistance(mΩ)	300	100	300	240	150	

Table 3.9 Identifying the optimal L value for both CL and proposed PMS, and comparison of the proposed and CL PMS using benchmark 1 to 3

Maximum / Optimal		This study					CL study				
Benchmark 1											
L	Parasitic resistance	P-MFC$_{ave}$	P-IN$_{ave}$	P-Load$_{ave}$	η_1	η_2	P-MFC$_{ave}$	P-IN$_{ave}$	P-Load$_{ave}$	η_1	η_2
(H)	(Ω)	(mW)			(%)		(mW)			(%)	
0.001	0.3	12.23	4.95	0.0065	0.13	0.05	10.15	0.291	0.0051	1.75	0.05
0.007	0.3	12.17	8.773	4.85	55.28	39.85	10.15	0.298	0.103	34.56	1.01
0.009	0.3	12	9.35	5.65	60.43	47.08	10.15	0.348	0.147	42.24	1.45
0.01	0.4	11.11	8.88	5.375	60.53	48.38	10.15	0.395	0.173	43.80	1.70
0.016	0.4	8.15	6.77	4.754	70.22	58.33	10.14	0.619	0.373	60.26	3.68
0.017	0.4	7.71	6.44	4.628	71.86	60.03	10.14	0.658	0.409	62.15	4.03
0.018	0.45	7.137	5.999	4.372	72.88	61.26	10.14	0.721	0.461	63.94	4.55
0.02	0.5	6.55	5.54	3.99	72.02	60.92	10.14	0.784	0.513	65.43	5.06
0.05	0.6	3.072	2.718	2.267	83.41	73.80	10.12	1.927	1.577	81.84	15.58
0.2	1	1.765	1.63	1.468	90.06	83.17	7.775	4.3	3.95	91.86	50.80
0.25	1	1.789	1.66	1.488	89.64	83.17	7.149	5.15	4.78	92.82	66.86
0.3	1.2	1.4	1.31	1.165	88.93	83.21	6.705	5.01	4.66	93.01	69.50
0.4	2	0.99	0.92	0.803	87.28	81.11	5.55	4.407	4.088	92.76	73.66
1	2.5	0.526	0.447	0.385	86.13	73.19	2.71	2.3	2.14	93	78.97
1.5	2.5	0.437	0.363	0.31	85.40	70.94	1.9	1.68	1.555	92.56	81.84
Benchmark 2											
0.016	0.4	7.46	5.89	4.16	70.63%	55.76%					
0.25	1						7.32	5.11	4.75	92.95%	64.89%
Benchmark 3											
0.016	0.4	7.23	5.52	3.88	70.29%	53.67%					
0.25	1						4.51	2.95	2.75	93.22%	60.98%

In benchmark 3, multiple interruptions were observed in the Pload for CL PMS, shown in Figure 3.19a. In Figure 3.19b, the voltage curves of MFCs corresponding capacitors 1 to 4 are presented for the CL PMS, which indicates the charge and discharge of the capacitors. Areas A (voltages of capacitor 3), B (voltage of capacitor 1), C (voltage of capacitor 4), and D (voltage of capacitor 2) have voltage equal to zero volt since their corresponding MFCs were disconnected from the system. Due to the configuration of C_is (series connection), the PMS stopped energy harvesting process each time there was a disconnected MFC in the system

which causes multiple load power interruptions. Unlike the proposed PMS that could proceed in harvesting power from the other MFCs, charging and discharging their corresponding capacitors (C_i) when there was a disconnected MFC in the system for the same areas A to D. Therefore, no interruption was observed at the load (Figure 3.20a). The Vc_is curve (charge and discharge of C_is) are illustrated in Figure 3.20b. Consequently, the $Pload_{ave}$ in the proposed PMS was obtained significantly higher than CL's (41% more) at 3.88 mW vs 2.75 mW.

In another comparison, the $Pload_{ave}$ of the CL PMS decreased by 42.5% in benchmark 3 compared to its $Pload_{ave}$ in benchmark 1. The average power produced by the MFCs was obtained 37% less in benchmark 3. However, for the proposed PMS, $Pload_{ave}$ was decreased only by 18.4% in benchmark 3 compared to benchmark 1. The average power produced by the MFCs was only 11.3% less for benchmark 3 compared to benchmark 1.

In overall, the results indicate that the proposed PMS is more reliable when confronting MFC failure and it can harvest more power from the stack of MFCs. In addition, the health of MFCs is considered by implementing the voltage protection algorithm which can expand the MFC’s lifetime and overall energy generation. The PMS is developed to do more complex tasks than basic ones, such as delivering uninterrupted power to the load while simultaneously increasing or maintaining the load's power.

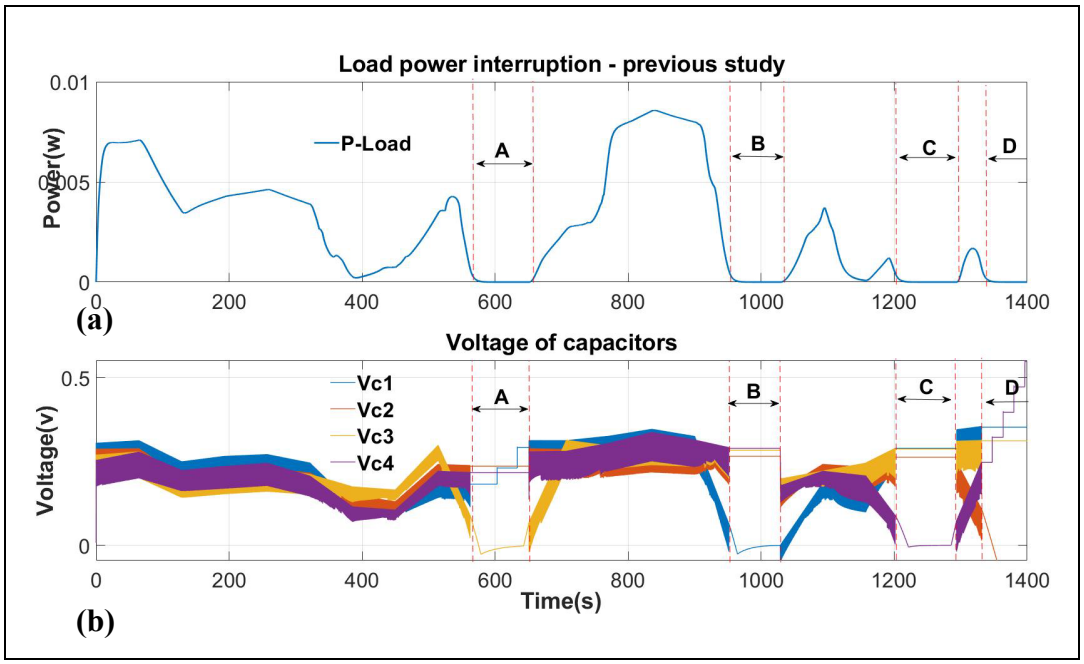

Figure 3.19 (a) Multiple load power interruptions occurred in CL PMS
(b) C_is voltage curves for benchmark 3 (connection/disconnection of MFCs)

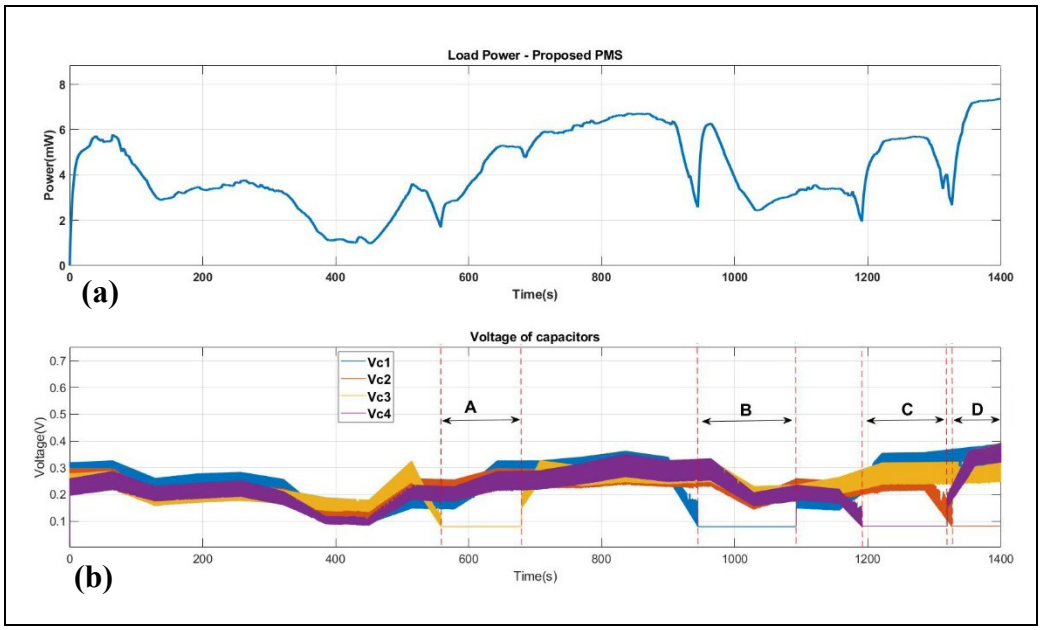

Figure 3.20 The proposed PMS (a) load power uninterrupted curve
(b) C_is voltage curves for benchmark 3 (connection/disconnection of MFCs)

CONCLUSION

Power management systems (PMS) are necessary parts of energy harvesting from the MFCs, due to their low power density which can be damaged if connected directly to the load. The ideal PMS would maximize the output power and minimize the health hazards that can damage the MFCs permanently. However, most PMSs are far from ideal and it's important to realize the limitations and downsides of the PMS and improve on them. The output parameters of multiple MFCs, including voltage and power, are not necessarily similar when they are connected in parallel or series in a stack. Voltage reversal phenomenon is one downside of the stack configurations of the MFCs which can potentially result in power loss. The previous study in the laboratory (Nguyen et al., 2019) designed a PMS connecting the corresponding capacitor of each MFC in series instead of connecting the MFCs directly together. However, in this strategy, the PMS would lose a considerable amount of time and become useless while waiting for the weak MFC in the stack to charge its capacitor before allowing the remaining capacitors to discharge. Another issue is the harvesting of power from the MFC regardless of its operating condition. Continuous energy harvesting from an MFC over time with a critical V_{OC} level might cause the MFC to degrade due to excessive energy-depletion. Next, to investigate and compare different PMSs performance including the proposed one, and to decide which PMS would have superior performance on the laboratory's MFCs, it is preferable to test them through simulation first. This may reduce the time required to conduct experimental testing and the expense of MFC maintenance. To do this, a PMS testing framework based on real-world MFC circumstances is required. Finally, due to the low input voltage of the MFC and its wide range of volatility, a practical fixed output voltage for the DC-DC boost converter becomes more challenging since it needs to withstand the load behaviors too.

As a result, the following is an outline of the thesis's primary contributions:

1. Building a new PMS that can be adapted to the isolated configuration of four laboratory scaled MFCs in the stack and harvest maximum energy from them while preserving their viability by preventing the weak MFC(s) from being power over-depleted;

2. Applying a robust voltage regulation technique (SMC) to the DC-DC boost converter that regulates the output voltage regardless of the MFCs voltage volatilities, as well as the load voltage disturbances;
3. Construction of a PMS testing framework to analyze the efficacy of the proposed and previous PMS in the literature according to the experimental data obtained from the four solid MFCs in the lab based on wide range of possible ambient and internal MFC conditions. Hence, the collected data (i.e., mean output power, output voltage, efficiency, etc.) can be a reliable measure of the evaluated PMS. This testing framework can be applied to compare other PMSs from an objective perspective.

The proposed PMS can be utilized in real-world small electronic applications like small waste gathering robots running with MFCs. Therefore, the robots can do energy intensive tasks given the higher power at its disposal. In addition, the health protection algorithm allows the MFCs to power the robots for a longer period, and the isolated configuration of the MFCs in this PMS aid the robots to perform with minimal interruptions.

In this thesis, chapter 1 represents the literature review about the MFC technology. In the first part, the MFC's principle is described, and next, three approaches for adding the mediums to the MFC to feed the microorganisms are introduced. Some important applications, and numerical models of the MFC are later discussed in distinct sections. Furthermore, the importance of utilizing PMS in MFC technology as well as its various implementation techniques including MPPT and PWM are discussed. The last two sections of this chapter are devoted to presenting the DC-DC boost converter topologies according to the MFC equivalent electrical model low output power and voltage. The second part describes the voltage regulation approaches and discusses their pros and cons.

Chapter 2 focuses on the methodology. In an overview, the proposed PMS and its features, the DC-DC boost converter topology, and the voltage regulation technique are discussed in this chapter. The PMS section includes the electrical circuit schematic, the MPPT technique to harvest the maximum power from the MFCs, the voltage protection algorithm that considers the health of the MFCs, and. Some subsections are provided which represent potential

strategies for overcoming the limitations of maximum energy harvesting in the proposed configuration of MFCs. Next, the DC-DC boost converter, the regulation technique principles, and the mathematical model of the converter to be applied in the voltage regulation configuration are considered.

Chapter 3 is divided into two parts. The first part is about the experimental data acquisition process and the second part is about the results and discussions obtained from the simulation. In the first part, several lab experiments on the solid MFCs' stacks were carried out. All the MFCS in the stack were tested under various ambient conditions simultaneously. Therefore, the experiment conditions were similar for all of the MFCs. The acquired data was then processed through an optimization algorithm in order to estimate the electrical-based-model internal parameters of the MFCs. The experiments were conducted through several days according to the MFCs' various internal and ambient conditions. However, to be able to observe all of the MFCs' characteristics resulting from the said setup in the simulation, a concatenation of data was sorted in a defined time-frame that covered all of the internal and ambient conditions of the MFCs. This procedure is defined as "benchmark 1". In addition to this, two other benchmarks (2 and 3) were also derived with some data modifications. Each of them represents a state of the MFCs that does not occur under the MFCs' normal operational conditions (benchmark 1). This criterion allows for thorough analyses and comparison between various PMSs in a simulated environment with real-world data acquired from the MFCs prior to any expensive PMS implementation.

The schematic of the system in the simulation, along with its parameter values are targeted in the second half of Chapter 3. Following that, the simulation results for each benchmark are presented and analyzed. The last part of this chapter compares the proposed and previous PMS using the comparison procedure described in the first part. The results are briefly discussed as follows:

For benchmark 1 to 3, all the tests were carried out using a single-level and two-level voltage reference for the voltage regulation technique (SMC). The two-level voltage reference was applied to the SMC therefore the load can receive additional power and a higher output voltage

level when the MFCs' power and voltage are high. In benchmark 1, the load optimal average power ($P_{load_{ave}}$) in the two-level voltage reference was obtained by 5.16 mW, which is 3.44 times more than 1.5 mW $P_{load_{ave}}$ in the single-level voltage regulation. The “optimal” condition was defined as the maximum load power considering the quality of load regulated voltage. Therefore, all the value of power (including P-MFCs and Pload) were measured for the optimal condition. However, the converter efficiency decreased by 6%, from 81% for the single-level to 76% for two-level voltage reference. The total system efficiency was also reduced by 6%, from 64% for single-level to 60% for two-level voltage reference. As a result, by applying a two-level voltage reference, the power output was increased almost 3 times and a half more while the efficiency was reduced by 6%. In benchmark 2, to test the PMS health-protection algorithm, a critical low V_{OC} scenario was conducted. The V_{OC} of MFC3 was modified for 120 s and decreased to 0.05 V while the remaining MFCs’ data points (1 to 4) maintained the same values as in benchmark 1. This test demonstrated the viability of the PMS health protection mechanism by preventing the low voltage MFC (considering as an unhealthy situation for the MFC) from being connected to the energy harvesting process. Using a two-level and single-level voltage regulation for which, respectively, the values were 5 mW and 1.37 mW for $P_{load_{ave}}$, the converter efficiency values were 76% and 79%, and the overall system efficiency were 58% and 56%. The obtained power values for two-level voltage reference indicate while the PMS disconnected MFC3 for about 200 s out of total simulation period, 1400 s, it could manage to reach the $P_{load_{ave}}$ of 5 mW, only 3% less than the $P_{load_{ave}}$ = 5.16 mW, obtained in benchmark 1. Therefore, while the unhealthy MFC was protected, no significant decrease was observed for the $P_{load_{ave.}}$ The last test was conducted for benchmark 3 where the MFCs were connected and disconnected from the PMS during the simulation for multiple times. The aim for this scenario was to examine the PMS performance in continuedly powering the load in the event of unexpected disconnection and connection of the MFCs. The simulation results for this benchmark indicate that the PMS was able to harvest energy and deliver it to the load without interruption. The $P_{load_{ave}}$ of 4.1 mW and 1.5 mW were obtained for a two-level and single-level voltage reference respectively, with their corresponding converter efficiencies of 78% and 81% and total system efficiencies of 57% and 63%. While each MFC were disconnected for 64s (256s in total) during different time intervals, the $P_{load_{ave}}$

for the two-level voltage reference decreased by 20% compared to benchmark 1. The $Pload_{ave}$ ratio for benchmark 3 and 1 is even better for the single-level voltage regulation, which is close to one.

Next, a comparison between the proposed and the work previously done in the literature review by Cong-long (CL) (Nguyen et al., 2019) was conducted since some of the contributions in this study covered the limitations of CL PMS. The comparison was done through benchmark 1 to 3 using CL PMS parameters for both PMSs (not including the inductor value) and without using voltage regulation. The $Pload_{ave}$ in benchmark1 was 4.7 mW for both PMSs. The proposed PMS could harvest 14% more power ($P\text{-}MFCs_{ave}$) from the MFCs. However, the system's overall efficiency was 12.8% less. In benchmark 2, the CL PMS was able to transfer 14.2% more power to the load while the proposed PMS still managed to obtain 1.9% more power from the MFCs ($P\text{-}MFCs_{ave}$). In benchmark 3, the proposed system's $Pload_{ave}$ was 41% higher than CL's. Multiple interruptions were observed in CL's Pload during the simulation, unlike in the proposed system.

Altogether, the results imply that the proposed PMS is reliable in the case of MFC failure and is capable of extracting more energy from a stack of MFCs. In addition, the health of MFCs is considered by integrating the voltage protection algorithm, which can expand the MFCs' lifespan and long-term energy production. The PMS is designed to do more complicated tasks than simple ones, such as providing continuous power to the load while increasing or maintaining the load power simultaneously. The fast response of the nonlinear SMC in directing the trajectory state toward the equilibrium point ensures the output voltage robust from the wide input disturbance, making it an expedient voltage regulator for the MFC systems.

RECOMMENDATIONS

One important aspect in the MFC technology is self-sustainability. Due to the MFC's applications in remote areas where the electrical power may not be accessible, the PMS needs to control the MFCs without requiring additional power source. One potential approach is to add a self-oscillating start-up circuit to the converter for autonomous operation. To reach this aim, different circuit topologies can be implemented, described as follows:

The start-up circuit can be separated from the main converter. The classic boost converter with high efficiency can be used in this topology (Chen et al., 2010; Ramadass & Chandrakasan, 2010). The second approach is to merge the start-up with the main converter in order to reduce the electrical component numbers. The flyback converter can be used as the main converter in this circuit topology (Ben-Yaakov & Fridman, 2004). The next potential approach which is used for micro energy harvesting is implementing a transformer-based oscillating circuit with a voltage doubler circuit (Grgić et al., 2009).

It is important to consider where in their useful life the MFCs are. If they have served for a long time, it is preferable to replace them by new MFCs with fresh mediums capable of producing a higher level of power.

SM controllers are variable-frequency controllers in theory. However, to simplify the design of the circuit in the real-world, it is suggested to limit (ideally fixed) the switching frequency. This can be achieved by using a ramp signal applied to the system trajectory.

BIBLIOGRAPHY

Ahn, Y., & Logan, B. E. (2012). A multi-electrode continuous flow microbial fuel cell with separator electrode assembly design. *Applied microbiology and biotechnology*, *93*(5), 2241-2248.

Alipanahi, R., Rahimnejad, M., & Najafpour, G. (2019). Improvement of sediment microbial fuel cell performances by design and application of power management systems. *International journal of hydrogen energy*, *44*(31), 16965-16975.

Alvarez-Ramirez, J., Cervantes, I., Espinosa-Perez, G., Maya, P., & Morales, A. (2001). A stable design of PI control for DC-DC converters with an RHS zero. *IEEE Transactions on Circuits and Systems I: Fundamental Theory and Applications*, *48*(1), 103-106.

An, J., Gao, Y., & Lee, H.-S. (2019). Induction of cathodic voltage reversal and hydrogen peroxide synthesis in a serially stacked microbial fuel cell. *Journal of environmental management*, *241*, 84-90.

Barua, P. K., & Deka, D. (2010). Electricity generation from biowaste based microbial fuel cells. *International Journal of energy, information and communications*, *1*(1), 77-92.

Ben-Yaakov, S., & Fridman, I. (2004). SPICE compatible model of self-oscillating converter. 2004 23rd IEEE Convention of Electrical and Electronics Engineers in Israel,

Bond, D. R., Holmes, D. E., Tender, L. M., & Lovley, D. R. (2002). Electrode-reducing microorganisms that harvest energy from marine sediments. *Science*, *295*(5554), 483-485.

Booth, B. (2005). Hydrogen from a microbial fuel cell. *Environmental science & technology*, *39*(11), 235A.

Borjas, Z., Esteve-Núñez, A., & Ortiz, J. M. (2017). Strategies for merging microbial fuel cell technologies in water desalination processes: start-up protocol and desalination efficiency assessment. *Journal of Power Sources*, *356*, 519-528.

Brastad, K. S., & He, Z. (2013). Water softening using microbial desalination cell technology. *Desalination*, *309*, 32-37.

Breheny, M., Bowman, K., Farahmand, N., Gomaa, O., Keshavarz, T., & Kyazze, G. (2019). Biocatalytic electrode improvement strategies in microbial fuel cell systems. *Journal of Chemical Technology & Biotechnology*, *94*(7), 2081-2091.

Cao, Y., Hu, Y., Sun, J., & Hou, B. (2010). Explore various co-substrates for simultaneous electricity generation and Congo red degradation in air-cathode single-chamber microbial fuel cell. *Bioelectrochemistry*, *79*(1), 71-76.

Carreon-Bautista, S., Erbay, C., Han, A., & Sanchez-Sinencio, E. (2015). An inductorless DC–DC converter for an energy aware power management unit aimed at microbial fuel cell arrays. *IEEE Journal of Emerging and Selected Topics in Power Electronics*, *3*(4), 1109-1121.

Chassé, F. (2018). *Maximisation en temps réel de la puissance de sortie de piles à combustible microbiennes en utilisant l'optimisation par essaims particulaires* ÉCOLE DE TECHNOLOGIE SUPÉRIEURE].

Chen, P.-H., Ishida, K., Zhang, X., Okuma, Y., Ryu, Y., Takamiya, M., & Sakurai, T. (2010). 0.18-V input charge pump with forward body biasing in startup circuit using 65nm CMOS. IEEE Custom Integrated Circuits Conference 2010,

Cheng, S., Liu, H., & Logan, B. E. (2006). Increased performance of single-chamber microbial fuel cells using an improved cathode structure. *Electrochemistry communications*, *8*(3), 489-494.

Coronado, J., Perrier, M., & Tartakovsky, B. (2013). Pulse-width modulated external resistance increases the microbial fuel cell power output. *Bioresource technology*, *147*, 65-70.

Coronado, J., Tartakovsky, B., & Perrier, M. (2015). On-line monitoring of microbial fuel cells operated with pulse-width modulated electrical load. *Journal of Process Control*, *35*, 59-64.

Costilla Reyes, A., Erbay, C., Carreon-Bautista, S., Han, A., & Sánchez-Sinencio, E. (2018). A time-interleave-based power management system with maximum power extraction and health protection algorithm for multiple microbial fuel cells for internet of things smart nodes. *Applied Sciences*, *8*(12), 2404.

Degrenne, N., Allard, B., Buret, F., Morel, F., Adami, S.-E., & Labrousse, D. (2011). Comparison of 3 self-starting step-up DC: DC converter topologies for harvesting energy from low-voltage and low-power microbial fuel cells. Proceedings of the 2011 14th European Conference on Power Electronics and Applications,

Dewan, A., Beyenal, H., & Lewandowski, Z. (2009). Intermittent energy harvesting improves the performance of microbial fuel cells. *Environmental science & technology*, *43*(12), 4600-4605.

Donovan, C., Dewan, A., Heo, D., & Beyenal, H. (2008). Batteryless, wireless sensor powered by a sediment microbial fuel cell. *Environmental science & technology*, *42*(22), 8591-8596.

Donovan, C., Dewan, A., Peng, H., Heo, D., & Beyenal, H. (2011). Power management system for a 2.5 W remote sensor powered by a sediment microbial fuel cell. *Journal of Power Sources*, *196*(3), 1171-1177.

ElMekawy, A., Hegab, H. M., Dominguez-Benetton, X., & Pant, D. (2013). Internal resistance of microfluidic microbial fuel cell: challenges and potential opportunities. *Bioresource technology*, *142*, 672-682.

Flimban, S. G., Ismail, I. M., Kim, T., & Oh, S.-E. (2019). Overview of recent advancements in the microbial fuel cell from fundamentals to applications: Design, major elements, and scalability. *Energies*, *12*(17), 3390.

Franks, A. E., & Nevin, K. P. (2010). Microbial fuel cells, a current review. *Energies*, *3*(5), 899-919.

Fu, F., & Wang, Q. (2011). Removal of heavy metal ions from wastewaters: a review. *Journal of environmental management*, *92*(3), 407-418.

Gajda, I., Greenman, J., & Ieropoulos, I. A. (2018). Recent advancements in real-world microbial fuel cell applications. *Current opinion in electrochemistry*, *11*, 78-83.

Garg, A., Vijayaraghavan, V., Mahapatra, S., Tai, K., & Wong, C. (2014). Performance evaluation of microbial fuel cell by artificial intelligence methods. *Expert systems with applications*, *41*(4), 1389-1399.

Grgić, D., Ungan, T., Kostić, M., & Reindl, L. M. (2009). Ultra-low input voltage DC-DC converter for micro energy harvesting. Proc. Power MEMS,

Grondin, F., Perrier, M., & Tartakovsky, B. (2012). Microbial fuel cell operation with intermittent connection of the electrical load. *Journal of Power Sources*, *208*, 18-23.

Gude, V. G. (2016). Wastewater treatment in microbial fuel cells–an overview. *Journal of Cleaner Production*, *122*, 287-307.

Guldemir, H. (2005). Sliding mode control of DC-DC boost converter. *Journal of Applied Sciences*, *5*(3), 588-592.

Gupta, T., Boudreaux, R., Nelms, R. M., & Hung, J. Y. (1997). Implementation of a fuzzy controller for DC-DC converters using an inexpensive 8-b microcontroller. *IEEE transactions on Industrial Electronics*, *44*(5), 661-669.

Harres, D. (2013). *MSP430-based robot applications: a guide to developing embedded systems*. Newnes.

Hiti, S., & Borojevic, D. (1995). Robust nonlinear control for boost converter. *IEEE transactions on power electronics*, *10*(6), 651-658.

Hong, S. W., Kim, H. S., & Chung, T. H. (2010). Alteration of sediment organic matter in sediment microbial fuel cells. *Environmental Pollution*, *158*(1), 185-191.

Ieropoulos, I., Greenman, J., Melhuish, C., & Horsfield, I. (2010). EcoBot-III-A Robot with Guts. ALIFE,

Ieropoulos, I. A., Greenman, J., Melhuish, C., & Horsfield, I. (2012). Microbial fuel cells for robotics: energy autonomy through artificial symbiosis. *ChemSusChem*, *5*(6), 1020-1026.

Jacobson, K. S., Drew, D. M., & He, Z. (2011). Efficient salt removal in a continuously operated upflow microbial desalination cell with an air cathode. *Bioresource technology*, *102*(1), 376-380.

Kato Marcus, A., Torres, C. I., & Rittmann, B. E. (2007). Conduction-based modeling of the biofilm anode of a microbial fuel cell. *Biotechnology and bioengineering*, *98*(6), 1171-1182.

Kelly, I., Holland, O., & Melhuish, C. (2000). Slugbot: A robotic predator in the natural world. Proceedings of the Fifth International Symposium on Artificial Life and Robotics for Human Welfare and Artificial Liferobotics,

Khaled, F., Ondel, O., & Allard, B. (2014). Optimal energy harvesting from serially connected microbial fuel cells. *IEEE Transactions on Industrial Electronics*, *62*(6), 3508-3515.

Khaled, F., Ondel, O., & Allard, B. (2016). Microbial fuel cells as power supply of a low-power temperature sensor. *Journal of Power Sources*, *306*, 354-360.

Kim, B. H., Chang, I. S., & Gadd, G. M. (2007). Challenges in microbial fuel cell development and operation. *Applied microbiology and biotechnology*, *76*(3), 485-494.

Kim, H. J., Park, H. S., Hyun, M. S., Chang, I. S., Kim, M., & Kim, B. H. (2002). A mediator-less microbial fuel cell using a metal reducing bacterium, Shewanella putrefaciens. *Enzyme and Microbial technology*, *30*(2), 145-152.

Kim, M., Hyun, M. S., Gadd, G. M., Kim, G. T., Lee, S. J., & Kim, H. J. (2009). Membrane-electrode assembly enhances performance of a microbial fuel cell type biological oxygen demand sensor. *Environmental technology*, *30*(4), 329-336.

Kumar, R., Singh, L., Wahid, Z. A., & Din, M. F. M. (2015). Exoelectrogens in microbial fuel cells toward bioelectricity generation: a review. *International Journal of Energy Research*, *39*(8), 1048-1067.

Kumar, R., Singh, L., Zularisam, A., & Hai, F. I. (2016). Potential of porous Co3O4 nanorods as cathode catalyst for oxygen reduction reaction in microbial fuel cells. *Bioresource technology*, *220*, 537-542.

Li, J., Li, H., Fu, Q., Liao, Q., Zhu, X., Kobayashi, H., & Ye, D. (2017). Voltage reversal causes bioanode corrosion in microbial fuel cell stacks. *International Journal of Hydrogen Energy*, *42*(45), 27649-27656.

Li, W.-W., Yu, H.-Q., & He, Z. (2014). Towards sustainable wastewater treatment by using microbial fuel cells-centered technologies. *Energy & Environmental Science*, *7*(3), 911-924.

Li, X., Hu, B., Suib, S., Lei, Y., & Li, B. (2010). Manganese dioxide as a new cathode catalyst in microbial fuel cells. *Journal of Power Sources*, *195*(9), 2586-2591.

Liang, P., Wu, W., Wei, J., Yuan, L., Xia, X., & Huang, X. (2011). Alternate charging and discharging of capacitor to enhance the electron production of bioelectrochemical systems. *Environmental science & technology*, *45*(15), 6647-6653.

Lim, H. C., & Shin, H. S. (2013). *Fed-batch cultures: principles and applications of semi-batch bioreactors*. Cambridge University Press.

Liu, H., & Logan, B. E. (2004). Electricity generation using an air-cathode single chamber microbial fuel cell in the presence and absence of a proton exchange membrane. *Environmental science & technology*, *38*(14), 4040-4046.

Liu, Z., Liu, J., Zhang, S., & Su, Z. (2008). A novel configuration of microbial fuel cell stack bridged internally through an extra cation exchange membrane. *Biotechnology letters*, *30*(6), 1017-1023.

Logan, B. E. (2008). *Microbial fuel cells*. John Wiley & Sons.

Logan, B. E. (2010). Scaling up microbial fuel cells and other bioelectrochemical systems. *Applied microbiology and biotechnology*, *85*(6), 1665-1671.

Logan, B. E., Hamelers, B., Rozendal, R., Schröder, U., Keller, J., Freguia, S., Aelterman, P., Verstraete, W., & Rabaey, K. (2006). Microbial fuel cells: methodology and technology. *Environmental science & technology*, *40*(17), 5181-5192.

Logan, B. E., & Regan, J. M. (2006). Microbial fuel cells—challenges and applications. *Environmental science & technology*, *40*(17), 5172-5180.

Martin, E., Savadogo, O., Guiot, S. R., & Tartakovsky, B. (2013). Electrochemical characterization of anodic biofilm development in a microbial fuel cell. *Journal of Applied Electrochemistry*, *43*(5), 533-540.

Martinez-Treviño, B. A., El Aroudi, A., Vidal-Idiarte, E., Cid-Pastor, A., & Martinez-Salamero, L. (2019). Sliding-mode control of a boost converter under constant power loading conditions. *IET Power Electronics*, *12*(3), 521-529.

Mathuriya, A. S., & Yakhmi, J. V. (2016). Microbial fuel cells – Applications for generation of electrical power and beyond. *Critical Reviews in Microbiology*, *42*(1), 127-143. https://doi.org/10.3109/1040841X.2014.905513

Mattavelli, P., Rossetto, L., & Spiazzi, G. (1997). Small-signal analysis of DC-DC converters with sliding mode control. *IEEE transactions on Power Electronics*, *12*(1), 96-102.

Min, B., Cheng, S., & Logan, B. E. (2005). Electricity generation using membrane and salt bridge microbial fuel cells. *Water research*, *39*(9), 1675-1686.

Mologni, D., Puig, S., Balaguer, M. D., Liberale, A., Capodaglio, A. G., Callegari, A., & Colprim, J. (2014). Reducing start-up time and minimizing energy losses of microbial fuel cells using maximum power point tracking strategy. *Journal of Power Sources*, *269*, 403-411.

Moradian, J. M., Fang, Z., & Yong, Y.-C. (2021). Recent advances on biomass-fueled microbial fuel cell. *Bioresources and Bioprocessing*, *8*(1), 14. https://doi.org/10.1186/s40643-021-00365-7

Mukherjee, A., Patel, V., Shah, M. T., Jadhav, D. A., Munshi, N. S., Chendake, A. D., & Pant, D. (2022). Effective power management system in stacked microbial fuel cells for onsite applications. *Journal of Power Sources*, *517*, 230684.

NASA. (2013). *Graphic: Carbon dioxide hits new high*. https://climate.nasa.gov/climate_resources/7/graphic-carbon-dioxide-hits-new-high/

Nguyen, C.-L., Tartakovsky, B., & Woodward, L. (2019). Harvesting energy from multiple microbial fuel cells with a high-conversion efficiency power management system. *ACS omega*, *4*(21), 18978-18986.

Niessen, J., Schröder, U., Rosenbaum, M., & Scholz, F. (2004). Fluorinated polyanilines as superior materials for electrocatalytic anodes in bacterial fuel cells. *Electrochemistry Communications*, *6*(6), 571-575.

Oh, S., Min, B., & Logan, B. E. (2004). Cathode performance as a factor in electricity generation in microbial fuel cells. *Environmental science & technology*, *38*(18), 4900-4904.

Ortiz-Martínez, V., Salar-García, M., De Los Ríos, A., Hernández-Fernández, F., Egea, J., & Lozano, L. (2015). Developments in microbial fuel cell modeling. *Chemical Engineering Journal*, *271*, 50-60.

Pant, D., Van Bogaert, G., Diels, L., & Vanbroekhoven, K. (2010). A review of the substrates used in microbial fuel cells (MFCs) for sustainable energy production. *Bioresource technology*, *101*(6), 1533-1543.

Park, D. H., & Zeikus, J. G. (2003). Improved fuel cell and electrode designs for producing electricity from microbial degradation. *Biotechnology and bioengineering*, *81*(3), 348-355.

Park, J.-D., & Ren, Z. (2012). Hysteresis-controller-based energy harvesting scheme for microbial fuel cells with parallel operation capability. *IEEE Transactions on Energy Conversion*, *27*(3), 715-724.

Picioreanu, C., Head, I. M., Katuri, K. P., van Loosdrecht, M. C., & Scott, K. (2007). A computational model for biofilm-based microbial fuel cells. *Water research*, *41*(13), 2921-2940.

Pinto, R., Srinivasan, B., Manuel, M.-F., & Tartakovsky, B. (2010). A two-population bio-electrochemical model of a microbial fuel cell. *Bioresource technology*, *101*(14), 5256-5265.

Pollak, M., Mateu, L., & Spies, P. (2008). Step-up DC-DC-Converter with coupled inductors for low input voltages. *Fraunhofer IIS*, *86*, 625-632.

Potter, M. C. (1911). Electrical effects accompanying the decomposition of organic compounds. *Proceedings of the royal society of London. Series b, containing papers of a biological character*, *84*(571), 260-276.

Prasad, J., & Tripathi, R. K. (2020). Voltage control of sediment microbial fuel cell to power the AC load. *Journal of Power Sources*, *450*, 227721.

Rabaey, K., Lissens, G., Siciliano, S. D., & Verstraete, W. (2003). A microbial fuel cell capable of converting glucose to electricity at high rate and efficiency. *Biotechnology letters*, *25*(18), 1531-1535.

Rabaey, K., Ossieur, W., Verstraete, W., & Verhaege, M. (2004). Continuous microbial fuel cells convert carbohydrates to electricity.

Rabaey, K., & Verstraete, W. (2005). Microbial fuel cells: novel biotechnology for energy generation. *TRENDS in Biotechnology*, *23*(6), 291-298.

Rahimnejad, M., Ghoreyshi, A. A., Najafpour, G., & Jafary, T. (2011). Power generation from organic substrate in batch and continuous flow microbial fuel cell operations. *Applied Energy*, *88*(11), 3999-4004.

Ramadass, Y. K., & Chandrakasan, A. P. (2010). A battery-less thermoelectric energy harvesting interface circuit with 35 mV startup voltage. *IEEE Journal of Solid-State Circuits*, *46*(1), 333-341.

Ramos, R., Biel, D., Fossas, E., & Guinjoan, F. (2009). Sliding-mode control design applied to parallel-connected modular inverters through FPGA-based implementation. *IET control theory & applications*, *3*(12), 1611-1624.

Recio-Garrido, D., Perrier, M., & Tartakovsky, B. (2016). Modeling, optimization and control of bioelectrochemical systems. *Chemical Engineering Journal*, *289*, 180-190.

Rehman, K., Fatima, F., Waheed, I., & Akash, M. S. H. (2018). Prevalence of exposure of heavy metals and their impact on health consequences. *Journal of cellular biochemistry*, *119*(1), 157-184.

Ren, S., Xia, X., Yuan, L., Liang, P., & Huang, X. (2013). Enhancing charge harvest from microbial fuel cells by controlling the charging and discharging frequency of capacitors. *Bioresource technology*, *146*, 812-815.

Rittmann, B. E. (2008). Opportunities for renewable bioenergy using microorganisms. *Biotechnology and bioengineering*, *100*(2), 203-212.

Spiazzi, G., & Mattavelli, P. (2018). Sliding-mode control of switched-mode power supplies. In *The Power Electronics Handbook* (pp. 8-1-8-24). CRC press.

Spiazzi, G., Mattavelli, P., & Rossetto, L. (1997). Sliding mode control of DC-DC converters. *system*, *2*(1).

Sung, S. W., & Lee, I.-B. (1996). Limitations and countermeasures of PID controllers. *Industrial & engineering chemistry research*, *35*(8), 2596-2610.

Trapero, J. R., Horcajada, L., Linares, J. J., & Lobato, J. (2017). Is microbial fuel cell technology ready? An economic answer towards industrial commercialization. *Applied energy*, *185*, 698-707.

Ucar, D., Zhang, Y., & Angelidaki, I. (2017). An overview of electron acceptors in microbial fuel cells. *Frontiers in microbiology*, *8*, 643.

Utkin, V. (1977). Variable structure systems with sliding modes. *IEEE Transactions on Automatic control*, *22*(2), 212-222.

Vora, N. D., Patel Priyanshu Harishbhai, Soni Ruchit. (2020). Comparative Assessment of Multi modular DC-DC Boost converter's Calculated and Circuitry output. *International Research Journal of Engineering and Technology (IRJET)*.

Wang, H., Park, J.-D., & Ren, Z. (2012). Active energy harvesting from microbial fuel cells at the maximum power point without using resistors. *Environmental science & technology*, *46*(9), 5247-5252.

Wang, Y.-H., Lin, S.-H., & Juang, R.-S. (2003). Removal of heavy metal ions from aqueous solutions using various low-cost adsorbents. *Journal of hazardous materials*, *102*(2-3), 291-302.

Watanabe, K. (2008). Recent developments in microbial fuel cell technologies for sustainable bioenergy. *Journal of bioscience and bioengineering*, *106*(6), 528-536.

Wilkinson, S. (2000). "Gastrobots"—benefits and challenges of microbial fuel cells in foodpowered robot applications. *Autonomous Robots*, *9*(2), 99-111.

Woodward, L., Perrier, M., Srinivasan, B., Pinto, R., & Tartakovsky, B. (2010). Comparison of real-time methods for maximizing power output in microbial fuel cells. *AIChE Journal*, *56*(10), 2742-2750.

Wu, S., Li, H., Zhou, X., Liang, P., Zhang, X., Jiang, Y., & Huang, X. (2016). A novel pilot-scale stacked microbial fuel cell for efficient electricity generation and wastewater treatment. *Water research*, *98*, 396-403.

Xia, C., Zhang, D., Pedrycz, W., Zhu, Y., & Guo, Y. (2018). Models for microbial fuel cells: a critical review. *Journal of Power Sources*, *373*, 119-131.

Yong, X.-Y., Feng, J., Chen, Y.-L., Shi, D.-Y., Xu, Y.-S., Zhou, J., Wang, S.-Y., Xu, L., Yong, Y.-C., & Sun, Y.-M. (2014). Enhancement of bioelectricity generation by cofactor manipulation in microbial fuel cell. *Biosensors and Bioelectronics*, *56*, 19-25.

Zeng, Y., Choo, Y. F., Kim, B.-H., & Wu, P. (2010). Modelling and simulation of two-chamber microbial fuel cell. *Journal of Power Sources*, *195*(1), 79-89.

Zhang, D., Yang, F., Shimotori, T., Wang, K.-C., & Huang, Y. (2012). Performance evaluation of power management systems in microbial fuel cell-based energy harvesting applications for driving small electronic devices. *Journal of Power Sources*, *217*, 65-71.

Zhang, X., He, W., Ren, L., Stager, J., Evans, P. J., & Logan, B. E. (2015). COD removal characteristics in air-cathode microbial fuel cells. *Bioresource technology*, *176*, 23-31.